Dosimetry for Low Energy X-rays

Efficiency of the Alanine Pellet Dosimeter

Hjørringgaard, Jakob Grünewald

Publication date:
2021

Document Version
Publisher's PDF, also known as Version of record

Dosimetry for Low Energy X-rays: Efficiency of the Alanine Pellet Dosimeter

Jakob Grünewald Hjørringgaard

Department of Health Technology
Technical University of Denmark

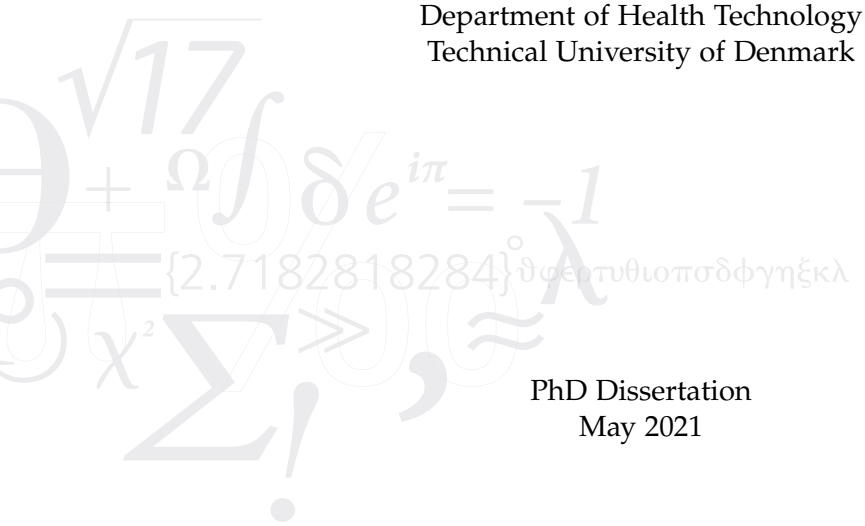

PhD Dissertation
May 2021

Supervised by:

Senior scientist Claus Erik Andersen, head of the dosimetry section at DTU Health Tech, Technical University of Denmark, Roskilde, Denmark.

Professor Arne Miller, head of the High Dose Reference Laboratory at DTU Health Tech, Technical University of Denmark, Roskilde, Denmark.

Scientist Christina Ankjærgaard, researcher at the dosimetry section at DTU Health Tech, Technical University of Denmark, Roskilde, Denmark.

This thesis was typeset with LaTeX and the `memoir` class by the author. The bibliography was typeset with `biber`. The figures were created with TikZ and `PGF` plots.

The enclosed publications have been reprinted with permission from Elsevier.

DTU Health Tech
Department of Health Technology
Technical University of Denmark
Risø Campus, Frederiksborgvej 399
DK-4000, Roskilde, Denmark

Preface

Due to an increasing demand for replacing radionuclide irradiators with the safer alternative that small self-shielded low energy x-ray irradiators provide, there is a need for developing a robust and traceable dosimetry system for low energy x-rays. However, commonly used dosimetry systems are energy dependent at low photon energies, resulting in large uncertainties on the measured dose. The objective of this PhD project is to explore methods for determining the energy deposition of low and medium energy x-rays, with the aim of establishing a traceable dosimetry system for use on a routine basis.

Work on the project was started in December 2017 at the Technical University of Denmark (DTU) Center for Nuclear Technologies (Nutech) High Dose Reference Laboratory (HDRL) under supervision by Lars R. Lindvold, Christina Ankjærgaard, and Arne Miller. The staff at Risø HDRL have assisted with laboratory measurements, and the general use of facilities, and a great thanks is due to Linda, Nina, Torben, and Mark. Initial work was carried out using a small x-ray irradiator located at Risø, however when useful results finally started to be compiled the x-ray tube broke down. Thus, experimental work for this project has been heavily dependent on access to x-ray beams by industrial collaborators and external research facilities.

Early in my project I had the great pleasure of working with Alan Tallentire, who taught me that *the spores never lie*. Alan helped me with the production of microbiological test filters, used for measuring the microbicidal effectiveness of low energy x-rays.

Access to x-ray facilities was granted from several collaborators for the duration of my project. At Aerial, France, Abbas Nasreddine was working on a similar PhD project, leading to a collaboration where we carried out irradiations together at both Aerial and at National Physical Laboratory (NPL), England. Here we had the pleasure to work with Anna Subiel who helped with the experiments. For irradiation of microbiological test filters access was granted to the x-ray facilities at e-beam technologies, COMET AG, Switzerland, where Dominique Cloetta and Willi Wandfluh was helpful with the experimental setup.

Moving into 2020 DTU Nutech was divided into three other departments, placing the ionizing radiation dosimetry section within the Department of Health Technology (Health Tech). With this, a change in my supervisor team was needed, since Lars' research obligations was moved elsewhere. The role as main supervisor was taken over by Claus E. Andersen who had already acted as a supervisor-in-spirit. Here I would to like express my gratitude towards the four supervisors who have guided me through the past three years. Four very different researchers and personalities, all overwhelmingly dedicated, patient, and helpful.

An external stay at the National Research Council Canada (NRC) was planned for the spring of 2020. Unfortunately, a global pandemic interrupted these plans. Instead, a shorter visit was scheduled for the beginning of 2021 at Direktoratet for Strålevern og Atomsikkerhet (DSA), Norway, however the pandemic roamed on and canceled that as well. Thanks are however still due to Malcolm McEwen, NRC, and Per-Otto Hetland, DSA, for their efforts regards granting access and organizing the planned visits.

Before I started work on my PhD project, I was teaching physics at a high school. One afternoon, in great despair over a particularly depressing set of lab reports I had to grade, I reached out for help. My good friend, and former PhD-colleague, Jeppe Brage Christensen, motivated me to abandon ship and apply for this PhD position. For that I owe him a Limfjordsporter.

Thanks goes to my fellow PhD students who have provided fruitful discussions and general motivation over the course of the past three years – Magdalena, Elaine, Martin, Grichar, Trine, Ashken, Mads, and Nicolo.

This work is dedicated to Luna and Pernille, for always putting a smile on my face.

Risø, May 3, 2021
Jakob Grünewald Hjørringgaard

Abstract

kilovoltage (kV) x-rays are used extensively in several aspects of radiation processing and radiotherapy. For applications, such as irradiation of blood products before transfusion, where irradiators using the radionuclide cesium-137 has traditionally been used, a demand for replacement with small self-shielded low energy x-ray irradiators has occurred in recent years. However, the response of commonly used routine dosimeters, such as alanine pellets, show an increasing energy dependence for low energy x-rays.

The present work investigates the energy dependence of the alanine pellet dosimeter. The alanine/electron paramagnetic resonance (EPR) dosimetry system is commonly used for reference and routine dosimetry, typically with traceability to national standards through calibration in a cobalt-60 reference field. Here the relative response, and efficiency, of the alanine pellet dosimeter is experimentally determined for irradiation at different kV x-ray qualities. The dependence of the relative efficiency of the dosimeter on spectral distribution of the x-ray beam is investigated using a microdosimetric one-hit detector model (OHDM). The results indicate that for medium energy x-rays there is little variation in the relative efficiency for a specific effective energy, while a more significant variation is observed for low energies.

Based on the conclusions from the application of the microdosimetric OHDM a general approach for determining quality correction factors, from literature data on the relative response, for cobalt-60 based calibrations is proposed.

Finally, the microbicidal effectiveness of kV x-rays is investigated using a specially designed test piece comprised of spores of *Bacillus pumilus*. The radiation response for irradiation with a 150 kV x-ray beam has been measured, and the response is shown to be identical to the radiation response for irradiation in cobalt-60, high energy x-ray, and low and high energy electron beams.

Resumé (Danish)

Lav- og medium-energetisk røntgenstråling anvendes ved flere aspekter af radioterapi og industriel strålebehandling. Det bruges bl.a. til bestråling af blodprodukter før transfusion, hvor strålekilden traditionelt har bestået af radionuklidet cæsium-137. Der er i de seneste år opstået et øget ønske om at udskifte disse radionuklide anlæg med små selvafskærmede lav-energetiske røntgenkilder. Almindeligt anvendte rutine-dosimetre, eks. alaninpiller, udviser dog en øget energiafhængighed i dette energiområde.

Alanine/elektron paragmagnetisk resonans (EPR) dosimetrisystemet anvendes til både reference og rutine dosimetri. Sporbarhed til nationale standarder opnås typisk via kalibrering i et kobolt-60 referencefelt. I denne afhandling undersøges energiafhængigheden af alaninpilledosimeteret ved både eksperimentel bestemmelse af den relative respons, og effektivitet, samt ved anvendelse af en mikrodosimetrisk model i kombination med Monte Carlo (MC) beregninger. Resultaterne indikerer, at der for røntgenkilder med medium energi kun er en lille variation i den relative effektivitet for en specifik effektiv energi, mens en mere signifikant variation observeres for lave energier.

Med udgangspunkt den mikrodosimetriske model, og konklusionerne fra anvendelsen af denne, foreslås en generel tilgang til bestemmelse af kvalitetskorrektionsfaktorer til kobolt-60 baserede kalibreringer, bestemt fra litteraturdata om den relative respons.

Desuden undersøges den mikrobicide effektivitet af lav-energetisk røntgenstråling, ved anvendelse af et specialdesignet test filter indeholdende sporer af *Bacillus pumilus*. Testfiltrene bestråles i et 150 kV røntgenfelt, og den observerede overlevelsesrate af sporer sammenlignes med bestrålinger ved tilsvarende doser i et kobolt-60 referencefelt.

List of Publications

Publications in peer-reviewed journals constituting the basis of this thesis:

I **Hjørringgaard JG**, Ankjærgaard C, Bailey M, and Miller A (2020).
Alanine pellet dosimeter efficiency in a 40 kV x-ray beam relative to cobalt-60
Published in: Radiation Measurements: **136** 106374
DOI: 10.1016/j.radmeas.2020.106374

II **Hjørringgaard JG**, Miller A, Andersen CE, Cloetta D, Wandfluh W, and Tallentire A (2021).
Comparison of the microbicidal effectiveness of 150 kV x-rays and cobalt-60 gamma rays
Submitted to: Radiation Physics and Chemistry

III **Hjørringgaard JG** and Nasreddine A (2021).
Comparison of detector efficiency for different alanine pellet dosimetry systems in kilovoltage x-ray fields
In preparation

IV **Hjørringgaard JG**, Ankjærgaard C, and Andersen CE (2021).
The microdosimetric one-hit detector model for calculating the relative efficiency of an alanine pellet dosimeter in low energy x-ray beams
Submitted to: Radiation Measurements

Oral presentations at conferences and workshops related to the content:

- International Symposium on Standards, Applications and Quality Assurance in Medical Radiation Dosimetry, Vienna 2019

List of Abbreviations

ABS	Acrylonitrile butadiene styrene
BIPM	Bureau International des Poids et Mesures
CPE	charged particle equilibrium
DS	donor suspension
DSA	Direktoratet for Strålevern og Atomsikkerhet
DTU	the Technical University of Denmark
EPR	electron paramagnetic resonance
GC	Gammacell
GVHD	graft-versus-host disease
HDRL	High Dose Reference Laboratory
Health Tech	Department of Health Technology
HV	high-voltage
HVL	half-value layer
IAEA	International Atomic Energy Agency
IC	ionization chamber
ICRU	The International Commission on Radiation Units and Measurements
IMS	International Measurement System
KV	kilovoltage
LE	low energy
LET	linear energy transfer
MC	Monte Carlo
ME	medium energy
NIST	National Institute of Standards and Technology
NPL	National Physical Laboratory
NRC	National Research Council Canada
Nutech	Center for Nuclear Technologies

OHDM	one-hit detector model
PMMA	polymethyl methacrylate
PSDL	primary standard dosimetry laboratory
PTB	Physikalisch-Technische Bundesanstalt
SAR	stable alanine radical
SIT	Sterile Insect Technique
SSD	source to surface distance
SSDL	secondary standard dosimetry laboratory

Contents

Part I

Summary Report

Chapter 1

Introduction

Ionizing radiation has been used for countless beneficial applications since the discovery of x-rays in 1895 by Wilhelm Conrad Röntgen (Röntgen 1895), with gamma rays and subatomic particles being discovered the subsequent years. The first use for treatment of cancer was carried out just a few months after the initial discovery of x-rays (Bernier et al. 2004). The idea of using ionizing radiation for inactivation of microorganism was formulated over the following years (Prescott 1904), resulting in widespread use of ionizing radiation for preservation of food products and sterilization of e.g. medical equipment. Later applications of ionizing radiation in an industrial setting include alteration of material properties (cross-linking, curing, grafting etc.), purification of gas effluents from power plants, and many more.

1.1 The Need for Dosimetry

Identical for all applications of ionizing radiation is the importance of accurate knowledge of the dose deposition in the irradiated material. The beneficial effect of irradiating the material, e.g. tumor control, microbial inactivation, etc., requires some specific dose to the material. However, harmful effects of ionizing radiation occur for exceedingly large doses. These harmful effects could be damage to healthy tissue during radiotherapy, destruction of material properties during irradiation of medical products and polymers.

The lower and upper limit required to obtain the beneficial effect, while avoiding harmful effects, leaves the user with a *treatment window* describing the optimal dose to be delivered to the material. The situation is sketched in Figure 1.1, where the cumulative probability of beneficial and harmful effects are shown as a function of dose. The treatment window depicted illustrates the probability of obtaining the beneficial effects without the harmful effects. Introducing an uncertainty on the delivered dose to the material results in a greater dose being required to ensure the beneficial effects while a smaller dose sets the limit of acceptance regarding the harmful effects. This situation is illustrated in Figure 1.1 by the dashed lines representing a 5 % uncertainty on the delivered dose. The result of the added uncertainty is a narrowing treatment window, and

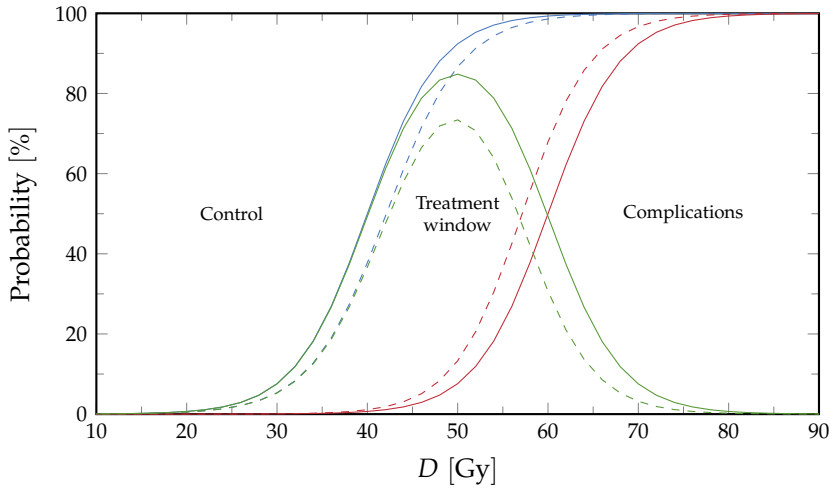

Figure 1.1: Sketch of the probability for radiation effects to occur after a given dose of ionizing radiation to a material. The optimal dose is determined by maximizing the probability of beneficial effects (blue) while reducing the probability of harmful effects (red). This optimization is illustrated by the treatment window (green). The effect of introducing a 5 % uncertainty in the dose is depicted by the dashed lines. The dose level on the abscissa is arbitrarily chosen for illustration purposes.

a reduced probability of beneficial effects without harmful effects even for the optimal dose. For some products, the difference between dose levels required to obtain beneficial effects relative to harmful effects may get quite small, requiring accurate dose determination in order to even have a significantly large probability of obtaining the beneficial effects without harmful effects. This narrowing treatment window highlights the need for accurate dosimetry in both radiotherapy and industrial applications of ionizing radiation.

1.2 X-ray Applications

Kilovoltage (kV) x-rays are used extensively in radiotherapy (Scrimger and Connors 1986; Niroomand-Rad et al. 1987; Beatty et al. 1996; Verhaegen et al. 1999). Recently an increasing interest has emerged for applications of low energy x-rays in e.g. blood irradiation (Janatpour et al. 2005; Dodd and Vetter 2009), phytosanitary treatment (Follett 2014), and Sterile Insect Technique (SIT) (Mastrangelo et al. 2010; Mehta and Parker 2011), where cesium-137 or cobalt-60 have traditionally been used. Increasing difficulties related to purchasing and transportation of radioactive materials have motivated the interest in switching

from radioisotopes to small self-shielded kV x-ray irradiators for these purposes (Dodd and Vetter 2009).

For the case of blood irradiation, blood bags are irradiated before transfusion to help prevent transfusion-induced graft-versus-host disease (GVHD) in immunocompromised patients by inactivation of viable lymphocytes. The absorbed dose range required is typically between 25 Gy and 50 Gy (EDQM 2015). To ensure that the blood components have received an adequate dose, measurements of absorbed dose must be carried out on the product or in simulated product (ISO/ASTM 51939 2017).

1.3 Response of the Alanine Dosimeter

The introduction of these small kV x-ray irradiators has also renewed the interest in the applications of some commonly used transfer dosimetry systems for quality assurance at kV photon energies. Specifically, the photon energy dependence of the alanine pellet dosimeter has been under investigation in recent years (Zeng and McCaffrey 2005; Waldeland et al. 2010; Anton and Büermann 2015; Khoury et al. 2015) in order to characterize the relative response of the dosimeter in kV x-ray fields. A discrepancy has been reported between the experimentally determinations and Monte Carlo (MC) calculations of the relative response of the alanine pellet dosimeter at low x-ray energies. These results indicate that the relative efficiency of the dosimeter is also energy dependent and must be fully characterized in order to establish traceable dosimetry using these transfer dosimetry systems. An issue emerging is the difficulty of experimentally determining the relative response of the transfer dosimeters directly in the small self-shielded irradiators, due to the lack of practical access for ionization chambers.

The present work investigates the energy dependence of the alanine pellet dosimeter in kV x-ray fields, and explores methods for assessment of the energy dependence in non-standard geometries such as blood irradiators, where direct measurement of dose using ionization chambers are difficult. The aim of the work is to establish traceability to national standards through a cobalt-60 calibration of the alanine pellet dosimetry system. Finally, the use of the alanine pellet dosimeter as a proxy for the microbicidal effectiveness in kV x-ray beams is explored.

1.4 Thesis Outline

Part I contains the summary report:

Chapter 2 gives an introduction to dosimetry, including the fundamental physics of ionizing radiation, a general description of dosimeters, and traceabillity. Focus is then given on the alanine/electron paramagnetic resonance (EPR) dosimetry system.

Chapter 3 describes the energy dependence of the alanine pellet dosimeter. The description is based on experimental measurements of the relative response of the dosimeter, as well as Monte Carlo calculated dose ratios of alanine to water.

Chapter 4 presents the microdosimetric one-hit detector model (OHDM) for calculating the relative efficiency of the alanine pellet dosimeter. This chapter focuses on the calculation of microdosimetric distributions and fixing the free parameters of the model. The free model parameters are determined based on literature values of the relative efficiency.

Chapter 5 shows the applications of the microdosimetric OHDM to different irradiation conditions. First a characterization of the relative efficiency for monoenergetic photon beams are investigated, followed by an investigation of the influence of different spectral distributions of the x-ray beams on the relative efficiency.

Chapter 6 establishes a quality correction factor to be applied to dose to water measurements using a cobalt-60 calibration of the alanine pellet dosimeter. The chapter focus on the application in blood irradiators; however the same process is used for establishing traceable dosimetry in Chapter 7.

Chapter 7 investigates the microbicidal effectiveness of kV x-rays. Specially designed test filters containing spores of *Bacillus pumilus* are irradiated in a 150 kV x-ray beam, to study the radiation response of the spores compared to the response after irradiation in a cobalt-60 reference field.

Part II contains the published, submitted, and prepared manuscripts denoted Paper I through IV

Chapter 2

Basics of Dosimetry

The concept of radiation dosimetry can be boiled down to the determination of the *absorbed dose*. The determination of this quantity requires knowledge of the interaction mechanisms of different types of ionizing radiation with matter, as well as well characterized detectors for measuring the absorbed dose, referred to as *dosimeters*. There exists a multitude of different dosimeters most of which determine the absorbed dose *indirectly*. These dosimeters must therefore be calibrated with respect to an *absolute* dose measurement.

The following chapter outlines the basic concepts of dosimetry, from the fundamental interactions of ionizing radiation with matter to calibration of dosimeters to primary standards. The mechanisms for signal production in different dosimeters relevant to this thesis will be included with special attention paid to the alanine pellet dosimeter.

The definitions and descriptions of the basic quantities of dosimetry is based on The International Commission on Radiation Units and Measurements (ICRU) definitions in ICRU Report 85 (2011). Dose refers throughout this thesis to *absorbed dose to water* if nothing else is specified.

2.1 X-rays

X-rays are a type of ionizing radiation consisting of uncharged particles, *photons*, generated by either electronic transitions in the atom, *characteristic x-rays*, or an inelastic collision of two charged particles (typically an electron and a nucleus), termed *bremsstrahlung x-rays*. The energy distribution of generated x-rays depends on different parameters such as kinetic energy of the charged particles producing the x-rays, material of the medium where interactions occur, and geometrical considerations.

For controlled use of x-rays in for instance radiology, mammography, and blood irradiation, x-rays are generated using an x-ray tube. A classical design of an x-ray tube, or *cathode tube*, consists of vacuum contained by a glass envelope with a anode and cathode pair placed within. The cathode consists of a heated filament from which electrons are accelerated by applying a high-voltage (HV)

potential difference between the anode and cathode, towards the anode *target*. The target consists of a heavy element, typically tungsten, where the electrons are slowed down emitting both characteristic and bremstrahlung x-rays.

The applied HV determines the maximum energy of generated x-rays but the distribution of x-rays in energies lower than the maximum energy varies depending on target material, incident angle, external filtration etc. Therefore, the applied HV is not enough to characterize a specific x-ray beam. Typically an x-ray beam *quality* is expressed on the basis of the half-value layer (HVL) – the thickness of attenuating material, typically aluminum or copper, required to reduce the air-kerma rate by 50 % of its value without the presence of the attenuating material (Ma et al. 2001).

An *effective energy* E_{eff} associated with the x-ray beam, defined as the energy of a monoenergetic photon beam having the same HVL as the x-ray beam, can be determined from the HVL. This is done by calculating the *effective mass attenuation coefficient* $(\mu/\rho)_{\text{eff}}$ (see Section 2.2.1) of the beam

$$\left(\frac{\mu}{\rho}\right)_{\text{eff}} = \frac{\ln 2}{\rho \text{HVL}}. \tag{2.1}$$

The effective energy can then be estimated from tabulated values of the mass attenuation coefficients and the relation to photon energies available from National Institute of Standards and Technology (NIST) (Hubbell and Seltzer 1995).

2.2 Interactions with Matter

The primary quantity of interest in dosimetry is the absorbed dose D with the formal definition

$$D = \frac{\mathrm{d}\bar{\varepsilon}}{\mathrm{d}m}, \tag{2.2}$$

where $\mathrm{d}\bar{\varepsilon}$ is the mean energy imparted by ionizing radiation to mass $\mathrm{d}m$. The mean energy imparted is determined by the interactions in the target medium and how frequently they occur.

An interaction between radiation and matter is said to occur when the energy or direction of the radiation particle is altered, or the particle is completely absorbed by the medium. The probability of a specific interaction occurring is described by *interaction coefficients*, which depend on both radiation particle type and energy, and the material of the medium in which the particle is propagating. The most fundamental interaction coefficient is the *cross section* σ, which is associated with the material. A general definition of the cross section for interactions of a specific type j is the mean number of interactions N_j per particle fluence ϕ

$$\sigma_j = \frac{N_j}{\phi}. \tag{2.3}$$

Since the radiation particles can typically undergo several different and independent interactions it is practical to introduce the *total cross section* σ_{tot} as the sum of independent cross sections

$$\sigma_{\text{tot}} = \sum_j \sigma_j = \frac{1}{\phi} \sum_j N_j. \tag{2.4}$$

Ionizing radiation is typically divided into two classes – *directly* and *indirectly* ionizing radiation. This is basically just a different way of expressing whether the ionizing radiation consist of charged (electrons, positrons, protons, alphas, ions) or neutral particles (neutrons, photons[1]). Even though photons directly ionize the medium they are considered indirectly ionizing particles since they liberate charged particles which then deposit energy to the medium. In this sense the terms directly and indirectly ionizing radiation can be better understood in terms of how the energy is deposited in the medium rather than how ionizations are produced.

2.2.1 Photon Interactions

The three primary photon interactions with matter, of interest to the work carried out in this thesis, is the photoelectric effect, Compton effect (incoherent scattering), and pair production. The relative importance of these three interaction types are depicted in Figure 2.1, where the dominant interaction is sketched for regions of atomic number Z of the absorbing medium and photon energy E. The lines displayed in Figure 2.1 represent corresponding values of Z and E where two types of interactions are equally probable. That is the cross sections for the Compton effect σ_{C} is equal to the cross section for photoelectric effect σ_{ph} or pair production σ_{pp}.

Photoelectric Effect

The photoelectric effect is an interaction of photons with matter, where the photon is completely absorbed in the process of liberating an atomic-shell electron. For an incident photon of energy E_γ interacting with an electron bound by a potential energy U_e, the electron is liberated with kinetic energy $E_e = E_\gamma - U_e$. The threshold photon energy for photoelectric effect to occur, assuming the target atom is at rest, is $E_\gamma > U_e$. The dependence of the cross section for photoelectric effect on atomic number of the medium and incident photon energy is roughly

$$\sigma_{\text{ph}} \propto \frac{Z^n}{E_\gamma^{7/2}}, \tag{2.5}$$

where n is dependent on the Z-value of the target material, and varies approximately between 4 for low-Z materials and 4.8 for high-Z materials.

[1] Here photons are included as particles.

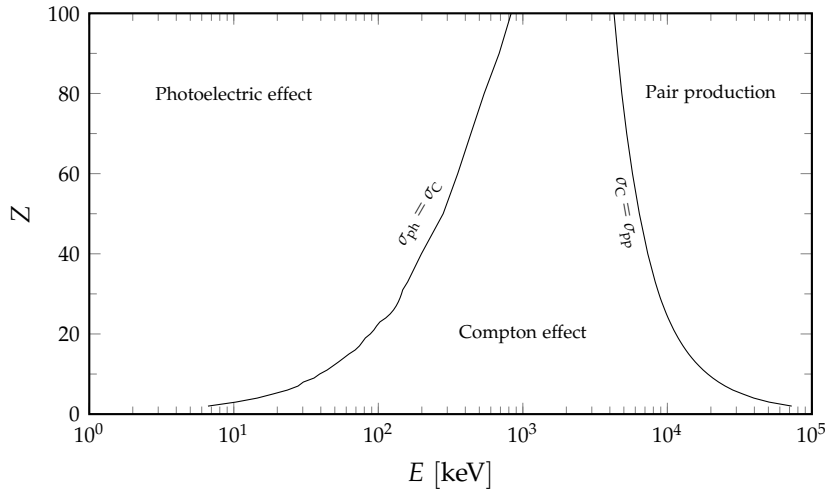

Figure 2.1: The relative importance of the three primary photon interactions. Solid lines represent combinations of material atomic number Z and photon energy for which two interaction probabilities are equal. Data from Berger (2010).

Photoelectric effect is the dominant photon interaction for low energies. In terms of total cross section and energy transferred to *secondary electrons*, photoelectric effect also dominates. Since the atomic-shell binding energies for most elements are in the order of a few eV to a few keV the energy of the liberated electron is close to the incident photon energy.

Compton effect

Compton effect (or incoherent scattering) is a process of inelastic scattering of a photon with a 'loosely' bound electron. The situation is often approximated by inelastic scattering of a photon with a free electron. Contrary to the photoelectric effect, the incident photon is not absorbed during the Compton interaction, but rather loose some of its energy and is deflected from its initial direction. The energy lost by the photon is transferred to the electron, which is liberated, thus ionizing the atom. The kinetic energy of the liberated electron E_e is dependent on the scattering angle θ of the photon by

$$E_e = E_\gamma - E'_\gamma, \tag{2.6}$$

$$= E_\gamma \left[1 - \frac{1}{1 + (E_\gamma / m_e c^2)\,(1 - \cos\theta)}\right], \tag{2.7}$$

where E_γ and E'_γ is the energy of the photon before and after scattering respectively, m_e is the electron mass, and c is the speed of light in vacuum. It is evident from Equation (2.7) that the maximum energy of the liberated electron $E_{e,\max}$ is obtained for photon scattering angle $\theta = \pi$ (full reflection of the photon), such that

$$E_{e,\max} = E_\gamma \left[1 - \frac{1}{1 + 2\,(E_\gamma / m_e c^2)}\right]. \tag{2.8}$$

The maximum energy of the liberated electron as a ratio of the incident photon energy is depicted in Figure 2.2 for incident photon energies from 1 keV to 10 MeV. It is evident from Figure 2.2 that the maximum energy of the liberated

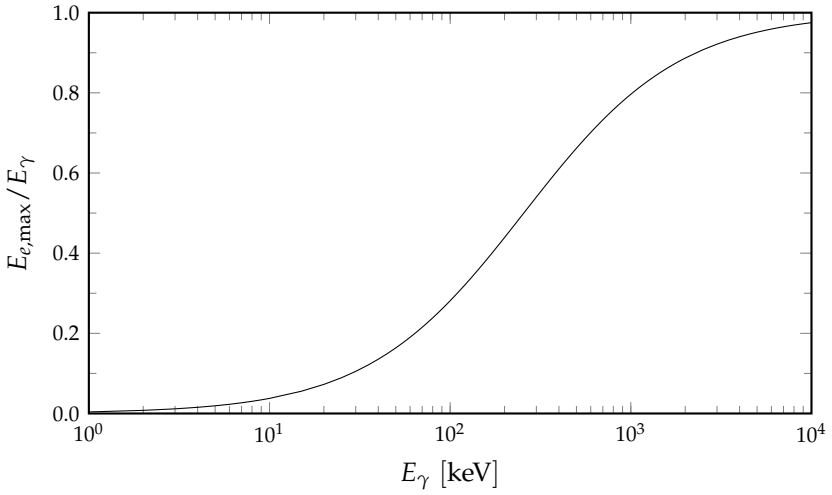

Figure 2.2: The maximum energy of Compton electrons $E_{e,\max}$ as a ratio of the incident photon energy E_γ, see Equation (2.8).

electrons by Compton scattering of low and medium energy photons significantly lower than the energy of the incident photon. Thus, the Compton effect contributes to quite low-energy secondary electrons.

For energies greater than the rest mass of the electron, the dependence of the cross section for Compton scattering on atomic number of the medium and incident photon energy is (from the Klein-Nishina formula)

$$\sigma_C \propto \frac{Z}{E_\gamma}. \tag{2.9}$$

However, for low incident photon energies, where the photon energy becomes comparable to the binding energy of inner-shell electrons of the target material this dependence does not hold. In reality, the Compton cross sections decrease rapidly for incident photon energies below the electron rest mass.

Pair Production

Pair production refer to an absorption process of photons in the presence of a coulomb field (of the atomic nucleus). Here the incident photon is transformed into a electron-positron pair. Pair production has a lower threshold energy $E_{\gamma,\mathrm{th}}$ equal to the combined rest mass of the produced particles, $E_{\gamma,\mathrm{th}} = 2m_e c^2 = 1.022\,\mathrm{MeV}$. Above this threshold energy the dependence of the cross section of pair production is

$$\sigma_{\mathrm{pp}} \propto Z^2 \cdot \ln(E_\gamma), \tag{2.10}$$

while becoming completely independent of photon energy for very large energies. Pair production is obviously only an important interaction for photon energies above the threshold energy, and thus only little focus is given to the process here.

Photon Attenuation

The interaction cross sections is the microscopic description of interaction probabilities. It is convenient to express the interaction probabilities for photons in terms *attenuation coefficients*. The *linear attenuation coefficient* μ is defined as the mean faction $\mathrm{d}N/N$ of photons that undergo some interaction after traversing a distance $\mathrm{d}l$ in a material

$$\mu = \frac{1}{\mathrm{d}l}\frac{\mathrm{d}N}{N}. \tag{2.11}$$

Since μ will be heavily dependent on the density ρ of the material it is customary to express μ relative to the material density. Defining the *mass attenuation coefficient* μ/ρ in this way

$$\frac{\mu}{\rho} = \frac{1}{\rho\,\mathrm{d}l}\frac{\mathrm{d}N}{N}, \tag{2.12}$$

does in part eliminate this large dependence. The mass attenuation coefficient and cross sections are related by

$$\frac{\mu}{\rho} = \frac{N_\mathrm{A}}{M}\sigma_{\mathrm{tot}}, \tag{2.13}$$

where N_A is the Avogadro constant and M is the molar mass of the material.

Since dose is defined from the energy deposited in the material and, as we have seen previously in this chapter, different photon interactions lead to different energy distributions of secondary electrons, it is relevant to assess the energy transferred to charged particles. Equivalent to the mass attenuation coefficient describing the mean fraction of photons undergoing interactions after traversing some distance in a material, the *mass energy-transfer coefficient* μ_{tr}/ρ is introduced to describe the mean energy transferred to kinetic energy of secondary electrons by photon interactions $\mathrm{d}R_{\mathrm{tr}}/R$ after traversing a distance $\mathrm{d}l$

of material

$$\frac{\mu_{\text{tr}}}{\rho} = \frac{1}{\rho\,\mathrm{d}l}\frac{\mathrm{d}R_{\text{tr}}}{R}. \tag{2.14}$$

Some fraction g of the kinetic energy transferred to secondary electrons will be lost, on average, to radiative processes such as emission of *bremsstrahlung* photons. The *mass energy-absorption coefficient* is therefore introduced to describe the mean fraction of the energy transferred to kinetic energy of secondary electrons which gets absorbed in the material

$$\frac{\mu_{\text{en}}}{\rho} = \frac{\mu_{\text{tr}}}{\rho}\left(1-g\right). \tag{2.15}$$

The fraction g is material specific and depends on the movement and energy deposition of electrons in the material. A general description of charged particle interactions with matter is however outside the scope of this thesis.

2.2.2 Dosimetric Quantities

Fluence

For relating the interaction probabilities of individual particles to dosimetric quantities, such as absorbed dose, the number of particles entering a volume of interest is considered. The *fluence* ϕ is defined as the number of particles $\mathrm{d}N$ that enters a spherical volume of cross-secional area $\mathrm{d}a$ by

$$\phi = \frac{\mathrm{d}N}{\mathrm{d}a}. \tag{2.16}$$

Kerma

The kinetic energy released per unit mass, *kerma* K, is defined as the sum of kinetic energy of all charged particles transferred from primary uncharged particles (e.g. photons) $\mathrm{d}E_{\text{tr}}$ in a medium of mass $\mathrm{d}m$

$$K = \frac{\mathrm{d}E_{\text{tr}}}{\mathrm{d}m}. \tag{2.17}$$

Since kerma is a quantity that describes the total energy transferred from uncharged to charged particles, and the mass energy-transfer coefficients are a measure of the probabilities for these kinds of interactions to occur, these quantities are closely related

$$K = E\phi\frac{\mu_{\text{tr}}}{\rho}, \tag{2.18}$$

for monoenergetic photons of energy E. Similar to the mass energy-absorption coefficients only accounting for the fraction of generated secondary electrons not lost to radiative processes, so can the *collision kerma* K_{col} be defined as the

fraction of the kerma not lost to radiative processes, and thus contributing to local energy deposition, by

$$K_{\text{col}} = K\,(1-g)\,, \tag{2.19}$$

$$= E\phi\frac{\mu_{\text{en}}}{\rho}, \tag{2.20}$$

again, for monoenergetic photons. Kerma is particularly used in dosimetry protocols for calibration of dosimeters in low and medium energy x-ray beams (Aukett, Harrison, et al. 1996; Ma et al. 2001)

Absorbed Dose

The absorbed dose to a material is, according to Equation (2.2), a measure of the energy deposited in an infinitesimally small region of the medium. A combination of information on the incident photons with the mass energy-absorption coefficients of the material will therefore be sufficient for calculating the absorbed dose. Assuming charged particle equilibrium (CPE), the dose in a medium is exactly the collision kerma

$$D \overset{\text{CPE}}{=} K_{\text{col}}. \tag{2.21}$$

The relationship between absorbed dose D to a medium and the mass energy-absorption coefficient can then be expressed as

$$D \overset{\text{CPE}}{=} E\phi\frac{\mu_{\text{en}}}{\rho}, \tag{2.22}$$

for monoenergetic photons, and more generally as

$$D \overset{\text{CPE}}{=} \int_0^{E_{\max}} E\phi\frac{\mu_{\text{en}}}{\rho}\,\mathrm{d}E, \tag{2.23}$$

for a distribution of primary photon energies with maximum energy $E_{\max}$. Here both the photon fluence and the mass energy-absorption coefficient is of course functions of photon energy.

2.3 Radiation Dosimeters

A *dosimeter* is in principle any detector which undergo some quantifiable reaction (heat, charge, chemical change, emission of light, etc.) after being subject to some incident radiation, producing a *detector response* r which is a measure of the absorbed dose D. The detector response is typically affected by several factors such as radiation type, radiation energy, environmental influences (temperature, humidity, ...) etc. Calibrations in terms of some reference conditions is therefore crucial for the standardization of use of such dosimeters.

The approach for dose measurements is thus to establish a *calibration coefficient* $N_{D_{\mathrm{w}},Q}$ for converting dosimeter response to dose to water in radiation beam quality Q as

$$N_{D,\mathrm{w},Q} = \frac{D_{\mathrm{w},Q}}{r_Q}, \tag{2.24}$$

under reference conditions. Correction factors k_i for any influence factor i can then be applied for the use of the calibration coefficient in non-reference conditions. Note that the calibration coefficient is not necessarily a independent of dose. The absorbed dose to water can then be determined from the dosimeter response as

$$D_{\mathrm{w}} = rN_{D,\mathrm{w},Q}\prod_i k_i. \tag{2.25}$$

The calibration coefficient is, for the end user, typically obtained over a series, or *chain*, of calibrations between different dosimeter types and irradiation facilities. Also, it is clear that at some initial point in this calibration chain the absorbed dose must be determined by *absolute* measurements. Classification of different levels of dosimetry is therefore introduced.

Absolute dosimetry is where the dose measurement is done with a *primary measurement standard*. A primary measurement standard is of the highest metrological quality and allows for the determination of the unit of a quantity from its definition. That is, a direct measurement of the dose from its definition. Dosimeters used for this purpose include water and graphite based calorimeters, ionization chambers (ICs), and chemical dosimeters (particularly the Fricke dosimeter) (ICRU Report 64 2001). The absolute measurement of dose can be utilized to determine calibration coefficients for other dosimeters according to Equation (2.24).

Reference dosimetry is where the dose is measured at the user beam under well-established reference conditions, using a dosimeter which is calibrated at a standards laboratory under matching reference conditions. The dose in the user beam is the determined according to Equation (2.25). ICs are typically used as reference dosimeters.

Relative dosimetry is when the dose measurement in the user beam is carried out under non-reference conditions. The deviations from reference conditions can be accounted for by use of relevant ratios (mass energy-absorption coefficients, stopping powers, etc.) and other appropriate corrections (Andreo, Burns, Nahum, et al. 2017).

2.4 Traceabillity

The absolute dosimetry carried out at primary standard laboratories around the world are transferred to the end user (hospitals, laboratories, etc.) by a series of calibrations. A *secondary standard* is calibrated directly against the primary standard and is used for calibration of user instruments. This chain of

calibrations ensure that the dosimeter applied at the end user has a calibration that is *traceable* to a primary standard.

Primary standards must, on the other hand, be validated by comparison with other primary standards to ensure agreement and consistency on doses determined by calibrations traceable to different primary standards. An international framework for traceability in dosimetry, centered around the Bureau International des Poids et Mesures (BIPM), was established in 1958 enabling international comparisons and traceability to the SI. The BIPM works with primary standard dosimetry laboratories (PSDLs) to arrange international comparisons. The PSDLs supply calibrations for national secondary standard dosimetry laboratories (SSDLs), who further supplies tertiary standards and end users with calibrations, elongating the calibration chain but conserving traceability to the primary standard.

The BIPM also provides calibrations to the International Atomic Energy Agency (IAEA) to extend traceability worldwide, and to countries without access to the ionization dosimetry standards at BIPM. The international arrangement of traceability, the International Measurement System (IMS), is sketched in Figure 6.2.

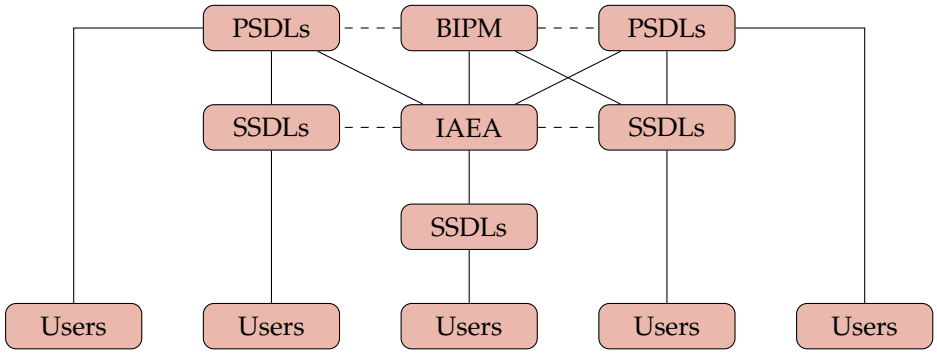

Figure 2.3: The IMS for traceability in radiation dosimetry. Solid lines represent calibrations and dashed lines represent comparisons. The figure is reproduced from Andreo, Burns, Hohlfeld, et al. (2000).

As the calibrations continue on downwards in Figure 6.2, the accumulated uncertainties on the calibrations increase. To ensure reasonable uncertainties at the user level it is therefore crucial to minimize the added uncertainty to the calibration chain in each step.

2.5 The Alanine Dosimeter

The dosimeter under investigation in the present thesis is the alanine/EPR dosimetry system. Alanine is one of the simplest amino acids. The L isomer L-

α-alanine has been used extensively as a dosimeter since the early 1960's when its use was first described by Bradshaw et al. (1962). Dosimetry using alanine is based on the generation of stable free radicals by ionizing radiation, see Figure 2.4, and a measurement of the EPR-response is related to the free radical concentration by EPR spectroscopy. For some time, the stable alanine radical (SAR) shown in Figure 2.4 was considered the sole contributor to the EPR signal (Malinen et al. 2003). The EPR signal obtained is, however, not due to a single

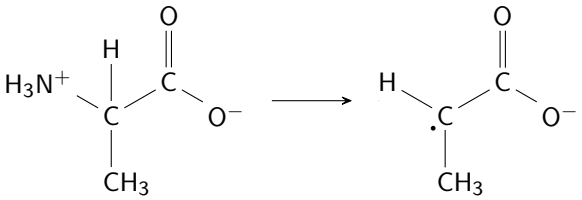

Figure 2.4: Chemical formula for L-α-alanine with SAR production by radiation induced ionization. The SAR was for some time believed to be the only contributor to the EPR signal.

free radical species, as could be falsely interpreted from Figure 2.4, but rather several stable free radical species occur in varying relative amounts (Sagstuen et al. 1997; Malinen et al. 2003).

Alanine can be used as a dosimeter in its powder form, however, for most common applications the powder is mixed with a binder material such as paraffin wax, polyethylene, cellulose, etc. (Hansen 1984; Arber and Sharpe 1993; Gall et al. 1996) to form pellets or films. The alanine dosimeter is used for many applications as both transfer and reference standard dosimeter, as well as secondary standard dosimetry system (Anton 2005; ICRU Report 80 2008).

The principle behind EPR spectroscopy is utilization of the splitting of the electron energy levels due to an external magnetic field (the Zeeman effect) to quantify the number of radicals in a sample. In an external magnetic field B_0 the magnetic moment of the free electrons align either parallel or antiparallel to the magnetic field, resulting in an energy difference ΔE between the two spin states of

$$\Delta E = \mu_{\mathrm{B}} g_{\mathrm{e}} B_0, \tag{2.26}$$

where μ_{B} is the Bohr magneton and g_{e} is the Landé factor of an electron. Since electrons are Boltzmann distributed, more electrons will occupy the lower energy states. However, the electrons can switch between energy states by either emission or absorption of photons with energy equal to the energy difference ΔE. Exposing the sample to a fixed microwave frequency with energy ΔE results in a net absorption of the microwave energy. The EPR spectrum is generated by sweeping across a range of magnetic field strengths measuring this absorption, typically by reflection. For the present work using EPR spectroscopy

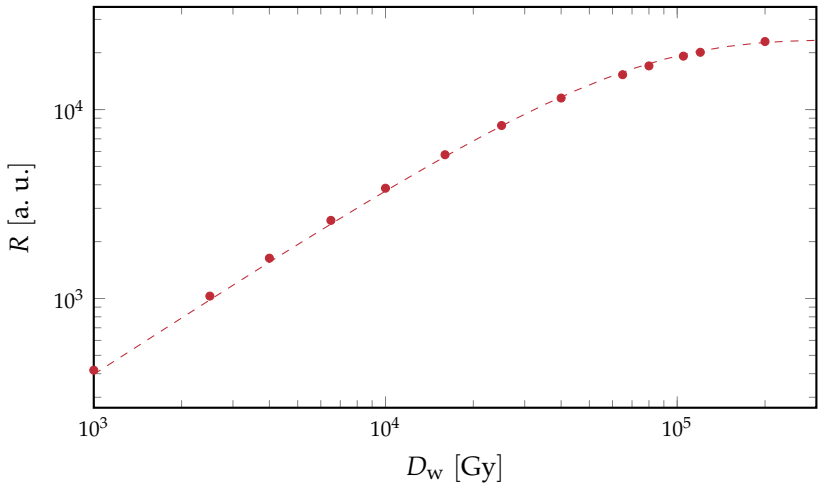

Figure 2.5: Typical EPR-response R of an alanine pellet dosimeter as a function of dose. The dashed line is a fit of Equation (2.27) to the experimental data.

for alanine pellet dosimeters, the EPR response R refers to the peak-to-peak amplitude of the first derivative of the measured absorption spectrum normalized to the mass of individual pellets.

A typical relation between EPR-response of alanine pellet dosimeters as a function of dose is shown in Figure 2.5. This response curve is measured for alanine pellet dosimeters purchased from Harwell Dosimeters (Batch BX608) irradiated at the Risø High Dose Reference Laboratory (HDRL) cobalt-60 Gammacell (GC) 3. The alanine pellets are cylindrical with height 2.7 mm and diameter 4.8 mm, and composition of 91 % L-α-alanine and 9 % paraffin wax binder. The EPR measurements were carried out using a Bruker EMXmicro spectrometer, operating at 9.53 GHz, setting microwave power to 2.23×10^{-2} mW with magnetic sweep width 15.0 G and modulation amplitude 2.0 G. The general dependence of the EPR-response of alanine pellet dosimeters on the dose is linear at low doses and exponentially saturating at high doses following the expression

$$R(D) = R_0 \left[1 - \exp\left(-\frac{D}{D_0}\right)\right], \tag{2.27}$$

where R_0 is the maximum detector response at full saturation, and D_0 is the *characteristic dose* of the detector. For the data presented in Figure 2.5 the characteristic dose is determined to be $D_0 = 57.9$ kGy with maximum detector response $R_0 = 2.3 \times 10^4$.

A response function like the one depicted in Figure 2.5 can be used for traceable dose measurements using alanine pellet dosimeters, provided that the dose measurements used to establish the response curve are traceable to

national standards or the same beam quality. Since the response of the alanine pellet dosimeter is dependent on different environmental conditions such as irradiation temperature, humidity, and general fading of signal over time, a correction to reference conditions will need to be applied.

The response of the alanine dosimeter is linearly dependent on the irradiation temperature, with temperature coefficients typically in the range $0.1\,^{\circ}\mathrm{C}^{-1}$ to $0.3\,^{\circ}\mathrm{C}^{-1}$ for irradiation temperatures in the range $-10\,^{\circ}\mathrm{C}$ to $50\,^{\circ}\mathrm{C}$. For temperatures above $50\,^{\circ}\mathrm{C}$ and below $-10\,^{\circ}\mathrm{C}$ the temperature coefficient deviates significantly from the linearity (Nagy et al. 2000; Desrosiers et al. 2004; Sharpe et al. 2009). The variation in temperature coefficients in the literature implies that temperature coefficients need to be determined for individual alanine pellet dosimetry systems, including EPR-spectrometers with corresponding settings. For instance, measurements at Risø HDRL show that the temperature coefficient takes values of $0.11\,^{\circ}\mathrm{C}^{-1}$, $0.13\,^{\circ}\mathrm{C}^{-1}$, and $0.18\,^{\circ}\mathrm{C}^{-1}$ for the same alanine pellet dosimeters, irradiated in a cobalt-60 GC with dose 10 kGy in the temperature range $15\,^{\circ}\mathrm{C}$ to $55\,^{\circ}\mathrm{C}$, for EPR-response measured on a Bruker e-scan, Bruker EMS-104, and Bruker EMX micro spectrometer, respectively. The induced signal in the alanine dosimeter fades a few percent during the first few hours after irradiation, and over longer durations of storage, in the order of years, the relative decrease in signal due to fading is heavily dependent on storage conditions like temperature and relative humidity (Sleptchonok et al. 2000). The impact of fading due to humidity can however be significantly reduced by storing the dosimeters under equal conditions pre- and post-irradiation (Arber and Sharpe 1993).

Alanine dosimeters, in the shape of pellets and films, are used for dose measurements for a wide variety of beam qualities. Since a typical calibration of the alanine EPR-response per dose is performed for irradiation of dosimeters in a cobalt-60 reference field with traceability to national standards, it is important to characterize the *relative response* F_{Q,Q_0} of the alanine dosimeters in the different beam qualities where the dosimeters are used. The relative response of the alanine dosimeter in a beam quality Q compared to a reference beam quality Q_0 is described by

$$F_{Q,Q_0} = \frac{(R/D)_Q}{(R/D)_{Q_0}}. \tag{2.28}$$

Several studies of alanine pellet dosimeters irradiated in high energy ($\geq 6\,\mathrm{MeV}$) electron beams have shown a sub-unity relative response ranging from 0.95 to 0.99 (Bergstrand, Bjerke, et al. 2005; Zeng, McEwen, et al. 2005; McEwen, Sephton, et al. 2006; Vörös et al. 2012; Anton, Kapsch, Krauss, et al. 2013; McEwen, Sharpe, et al. 2015). Recently, a consensus paper was published carrying out an analysis of the available literature data, recommending a correction factor $f_{\mathrm{Co}\to e} = 1.014$ to be applied to the dose measured using a cobalt-60 calibration independent of electron energy (McEwen, Miller, et al. 2020). Similar studies for irradiations in high energy x-ray fields show a smaller decrease in detec-

tor response per dose compared to high energy electrons. On average a 0.5 % decrease in detector response relative to cobalt-60 irradiations is observed independent of energy (Bergstrand, Shortt, et al. 2003; Anton, Kapsch, Krystek, et al. 2008; Anton, Kapsch, Krauss, et al. 2013).

The decrease in relative detector response is much more pronounced for x-rays with HV $\lesssim$ 300 kV. This is expected due to the rather large decrease in the ratio of mass energy-absorption coefficients of alanine to water for monoenergetic photon energies $\lesssim$ 100 keV. The energy dependence of the alanine pellet dosimeter for low and medium energy x-rays will be discussed in more detail in Chapter 3.

Chapter 3

Energy Dependence

Several studies concerning the energy dependence of the alanine pellet dosimetry system have been published in recent years (Zeng and McCaffrey 2005; Waldeland et al. 2010; Anton and Büermann 2015; Khoury et al. 2015). The energy dependence has been known for several decades (Coninckx et al. 1989; Hansen et al. 1989). However, renewed interest in replacing radioactive sources for industrial purposes with self-shielded low energy x-ray irradiators has increased the demand for a full characterization of this energy dependence (Dodd and Vetter 2009). More recent studies have suggested that the energy dependence is partly due to a shift in dose-to-detector to dose-to-water ratio for low energy x-rays relative to a reference field (typically cobalt-60), and partly due to a decrease in intrinsic detector efficiency.

In the following chapter the current status of the characterization of the energy dependence of the alanine pellet dosimeter will be presented. The process of determining the energy dependence is illustrated by an experimental approach in low and medium energy x-ray fields. Issues regarding translating the energy dependence from idealized experimental setups to practical use in more complex geometries, e.g. small self-shielded irradiators, will be discussed, including what characterization is required for use in traceable dosimetry.

The results presented in this chapter, based on paper I and III, are used to highlight the issues concerning alanine pellet dosimetry at low x-ray energies. All uncertainties listed, in writing or illustrations, in the following chapter are stated at $k = 1$.

3.1 Dosimeter Response

3.1.1 General Considerations

A reduction in the generation of stable free radicals per dose to water for alanine pellets irradiated with low energy x-rays relative to a cobalt-60 reference is expected from simple considerations of the mass energy absorption coefficients. For monoenergetic photons the deposited dose in a medium D_{med} can

be calculated by

$$D_{\text{med}} = E\phi(E) \left(\frac{\mu_{\text{en}}}{\rho} \right)_{\text{med}}, \tag{3.1}$$

where E is the photon energy, $\phi(E)$ is the photon fluence in the medium, and $[\mu_{\text{en}}/\rho]_{\text{med}}$ is the mass energy absorption coefficient for the medium. Assuming large detector volume compared to the range of secondary electrons the ratio of dose to a detector D_{det} to D_{med} can be expressed as (Andreo, Burns, Nahum, et al. 2017)

$$\frac{D_{\text{det}}}{D_{\text{med}}} = \frac{(\mu_{\text{en}}/\rho)_{\text{det}}}{(\mu_{\text{en}}/\rho)_{\text{med}}} \equiv \left(\frac{\mu_{\text{en}}}{\rho} \right)^{\text{det}}_{\text{med}}. \tag{3.2}$$

The alanine to water ratio of mass energy absorption coefficients relative to the value for a cobalt-60 reference beam quality Q_0 is shown in Figure 3.1. The

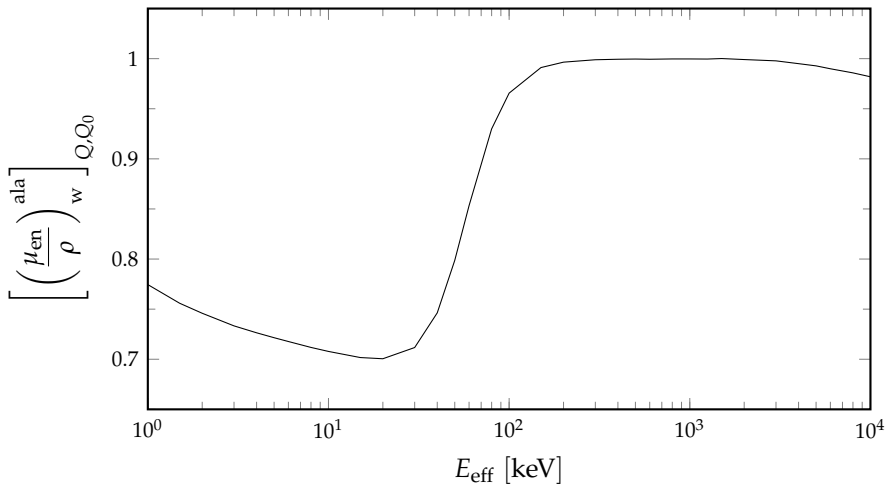

Figure 3.1: Alanine to water mass energy absorption coefficients relative to the value at for a cobalt-60 reference beam Q_0. Data from Hubbell and Seltzer (1995).

subscript 'Q, Q_0' on the ordinate-label refers to the ratio of monoenergetic value Q to cobalt-60 reference value Q_0. By comparing Equation (3.2) with Figure 3.1 it is observed that the relative D_{ala} to D_{w} ratio decreases significantly for photon energies below approximately 100 keV. This indicates a lower dose to alanine compared for the same dose to water when irradiated at low energy x-rays relative to cobalt-60 irradiations. A smaller dose to the alanine pellet results in a lower generation of stable free radicals, and thus the response per dose to water decreases.

The effect sketched out here is obviously not the full story. Firstly, we are not encountering monoenergetic photon beams when using x-ray generators.

Secondly, the derivation of Equation (3.2) requires that secondary electrons deposit their energy locally, and that the photons fluence at the detector position is identical for the medium and the detector. This section does, however, illustrate the energy dependence introduced by the variation in interaction probabilities between detector material and medium. For a full determination of the dose ratios MC calculations are the optimal approach.

3.1.2 Experimental Determination of the Relative Response

An experimental determination of the relative response F_{Q,Q_0} is obtained by examination of the EPR response R per dose to water D_w delivered to the alanine pellet dosimeter at kV x-ray beam qualities Q relative to a cobalt-60 reference quality Q_0

$$F_{Q,Q_0} = \frac{(R/D_w)_Q}{(R/D_w)_{Q_0}}. \tag{3.3}$$

In this thesis the relative response was determined for three x-ray beam qualities obtained using two different x-ray tubes and geometries.

The first x-ray beam quality considered was a low filtered 40 kV beam with a first HVL of 0.08 mm of aluminum, corresponding to an effective energy of 9 keV. This set of irradiations was carried out at the Center for Nuclear Technologies (Nutech) – now Department of Health Technology (Health Tech) – at the Technical University of Denmark (DTU) using a Varian VF-50J x-ray tube. A detailed description of the x-ray field and irradiation geometry can be found in Andersen et al. (2003) and Paper I. Measurement of D_w was performed using a PTW 23344 parallel plate ionization chamber with a designated PTW 2962 polymethyl methacrylate (PMMA) slab phantom, designed for use in soft x-ray beams. For irradiations of alanine pellet dosimeters, the ionization chamber and designated PMMA slab, were interchanged with an Acrylonitrile butadiene styrene (ABS) holder containing four alanine pellets with front face at the phantom surface. The irradiation geometries are sketched in Figure 3.2. The ionization chamber measures the dose at the surface position, while the EPR readout of the irradiated alanine pellets corresponds to the average value over the pellet dimensions. The EPR response must be corrected to the surface value to obtain comparable quantities. A correction factor k_{vol} for this purpose was determined by the ratio of homogeneous surface dose D_0 deposition to actual dose $D(z)$ as a function of depth in the pellet z

$$k_{vol} = \frac{z_p \cdot D_0}{\int_0^{z_p} D(z)\,\mathrm{d}z}, \tag{3.4}$$

where z_p is the pellet thickness. The depth dose curve inside the pellet volume is obtained by MC calculation, and a correction factor of $k_{vol} = 1.84 \pm 0.03$ is obtained. The measured EPR response, both corrected and uncorrected, of the

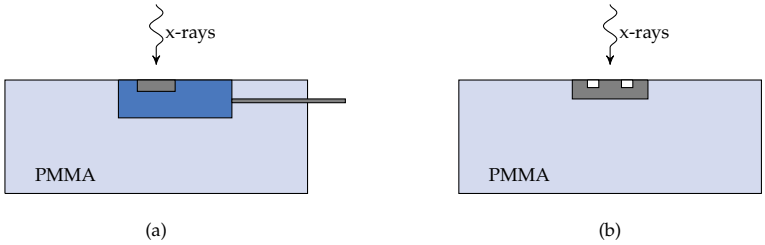

Figure 3.2: Sketch of the irradiation geometry used for the Varian VF-50J x-ray tube irradiations, showing ionization chamber placement (a) and alanine pellet dosimeter placement (b) in the PMMA phantom. Figure adopted from Paper I. Dimensions are not to scale.

irradiated alanine pellets normalized to the mass of individual pellets is shown in Figure 3.3. The relative response of the alanine pellet dosimeter in this kV x-

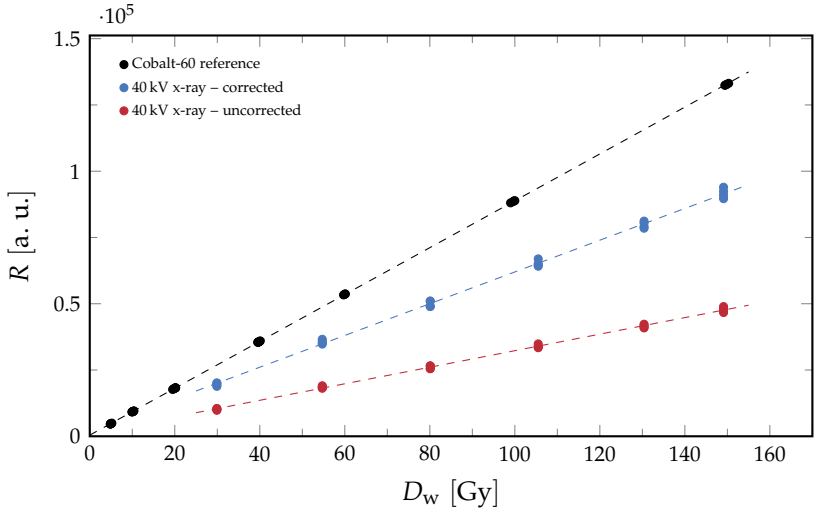

Figure 3.3: Measured EPR response R per mass of individual alanine pellets irradiated in a 40 kV x-ray field. For the EPR response after irradiation in the 40 kV x-ray field, also values corrected for dose gradient in the alanine pellet are shown.

ray field is obtained, according to Equation (3.3), by the ratio of the slopes of the response functions. Using the dose gradient corrected EPR response function for the x-ray field a value of $F_{Q,Q_0}^{40\,\mathrm{kV}} = 0.650 \pm 0.024$ is obtained.

A second set of irradiations was carried out at National Physical Laboratory (NPL) using two beam qualities with HVs 135 kV and 280 kV and HVLs

0.50 mm and 4.0 mm of copper, respectively, corresponding to effective energies 59 keV and 168 keV. Here a PTW 30012 Farmer type ionization chamber was used to obtain the D_w at 2 cm water equivalent depth. Measurements was carried out in a solid water phantom, and an ionization chamber dummy made of solid water was used to place the alanine pellets with central position at the effective point of measurement of the ionization chamber. The geometry is sketched in Figure 3.4. A more detailed description of beam qualities and irradiation conditions are given in Paper III.

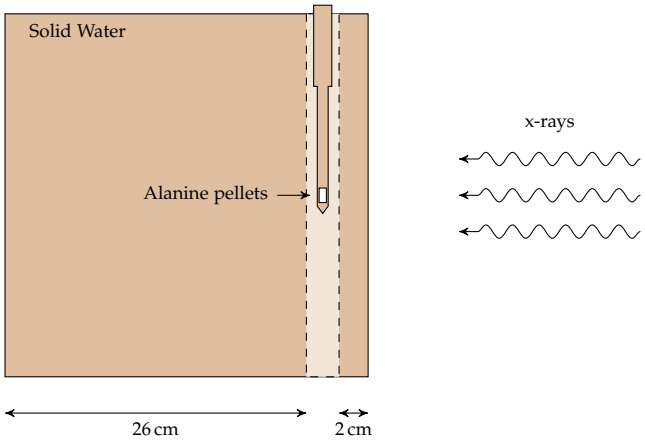

Figure 3.4: Side view of solid water geometry with ionization chamber dummy containing alanine pellets at the effective point of measurement of the actual ionization chamber.

MC calculations of the depth dose curve inside the alanine pellet volume showed a constant dose gradient for both beam qualities. The EPR readout corresponds directly to the D_w value at the central point of the pellet (Anton, Hackel, et al. 2015). Therefore, a correction for the dose gradient similar to Equation (3.4) is not necessary in this case. The measured EPR response normalized to individual pellet mass is shown in Figure 3.5 as a function of D_w. The relative response obtained for the 135 kV and 280 kV NPL x-ray beam qualities was determined, as the ratio of slopes, to $F_{Q,Q_0}^{135\,\mathrm{kV}} = 0.762 \pm 0.021$ and $F_{Q,Q_0}^{280\,\mathrm{kV}} = 0.941 \pm 0.025$ respectively.

The relative responses determined for the three x-ray beam qualities are shown in Figure 3.6 together with literature values for the relative response for comparison introduced in Section 3.1.3.

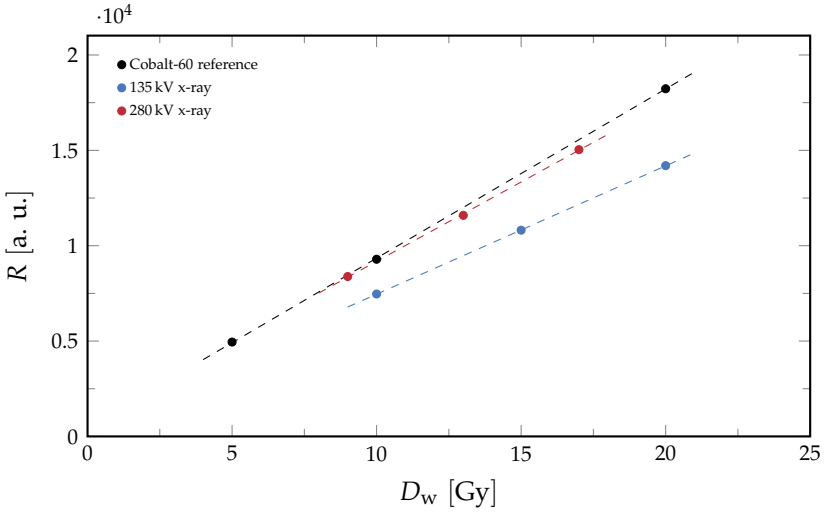

Figure 3.5: Measured EPR response R per mass of individual alanine pellets irradiated at the NPL 135 kV and 280 kV beam qualities.

3.1.3 Literature Overview of Relative Response

Several experimental studies of alanine exposed to kV x-rays have been conducted in the previous decades. Table 3.1 show the most relevant literature references where the relative response of alanine pellet dosimeters are investigated, either as the primary scope of the paper or as a biproduct for other studies. The beam quality identifiers HV and effective energy E_{eff} is listed to give an idea of the energy regime under investigation. Common for these studies is that the relative response F_{Q,Q_0} of x-ray beam quality Q is listed as EPR response R per D_{w} relative to a cobalt-60 reference quality Q_0 according to Equation (3.3).

Hansen et al. (1989) measured the relative response of alanine pellet dosimeters in a single 250 kV x-ray beam with effective energy of approximately 90 keV. The relative response was determined to be 0.82 ± 0.03 and 0.82 ± 0.06 for two different alanine pellet compositions (95 % L-α-alanine and 5 % binder and 75 % L-α-alanine and 25 % binder, respectively).

Coninckx et al. (1989) investigated the alanine dosimetry system as potential reference dosimetry system for use in accelerator radiation environments at CERN. The energy dependence of the alanine dosimeter was measured at four x-ray qualities with effective energies between 40 keV to 120 keV displaying a relative response in the range 0.75 to 0.95. The method for establishing the reference dose to water is, however, not described in detail, and the values for the relative response, and associated uncertainty, are therefore estimated from

Table 3.1: Overview of literature data on the relative response of the alanine pellet dosimeter in kV x-ray fields.

Reference	HV, kV	E_{eff}, keV	Note
Hansen et al. (1989)	250	90	
Coninckx et al. (1989)	-	40-120	Values extracted from graph.
Zeng and McCaffrey (2005)	150	71.5	Air kerma reference.
Chen et al. (2008)	80-250	32-145	Values extracted from graph.
Waldeland et al. (2010)	50-200	32-99	
Khoury et al. (2015)	125	-	In blood irradiator RS-2400.
Anton and Büermann (2015)	30-280	15-151	Very low uncertainties. Compared directly to water calorimeter primary standard.
Nasreddine et al. (2020)	50-100	27-43	Values obtained through private communication.

Figure 2 of their publication.

Zeng and McCaffrey (2005) measured the relative response of alanine pellet dosimeters in a 150 kV x-ray beam with effective energy 71.5 keV obtaining a value of 0.839 ± 0.007. Here, the response of alanine is in terms of air kerma instead of dose to water making direct comparison difficult.

Chen et al. (2008) studied the enhanced sensitivity of alanine pellet dosimeters doped by iodine atoms, as well as the energy dependence of non-doped alanine pellet dosimeters as a reference. They report a similar decrease in detector response as the other publications but does not specify exact values. The values depicted in Figure 3.6 and other figures in the present thesis are extracted from Figure 3 of their publication.

Waldeland et al. (2010) presented the first larger study of the energy dependence of the alanine pellet dosimeter, using x-ray beam qualities in the range 50 kV to 200 kV, with effective energies ranging from 32 keV to 99 keV. An almost linear dependence on the effective energy was observed for this range of beam qualities.

Anton and Büermann (2015) presented a detailed study of the alanine response for two series of x-ray qualities. A low energy TW series ranging from 30 kV to 100 kV and a medium energy TH series ranging from 70 kV to 280 kV. A very low uncertainty was achieved by using the Physikalisch-Technische Bundesanstalt (PTB) water calorimeter primary standard for determining the refer-

ence dose to water. Results were presented as a function of the mean energy of the x-ray beam with respect to photon fluence. For better comparison with other published data the effective energy is used when depicting their obtained data in the present study (the effective energy is here calculated from their listed HVLs).

Recently Nasreddine et al. (2020) added to the existing literature data by investigating the response of alanine detectors irradiated at x-ray beam qualities in very close resemblance to each other, using multiple instances of the same HV but with varying filtration. Some variation was observed, however, within experimental uncertainties, results was in agreement with the somewhat well-defined relation between the relative response and effective energy observed by Waldeland et al. (2010) and Anton and Büermann (2015).

The relative responses reported in these studies are shown in Figure 3.6 as a function of the effective energy (or equivalent energy as stated by Coninckx et al. 1989), together with experimentally determined values described in Section 3.1.2. A general trend is apparent in the data, somewhat in agreement with

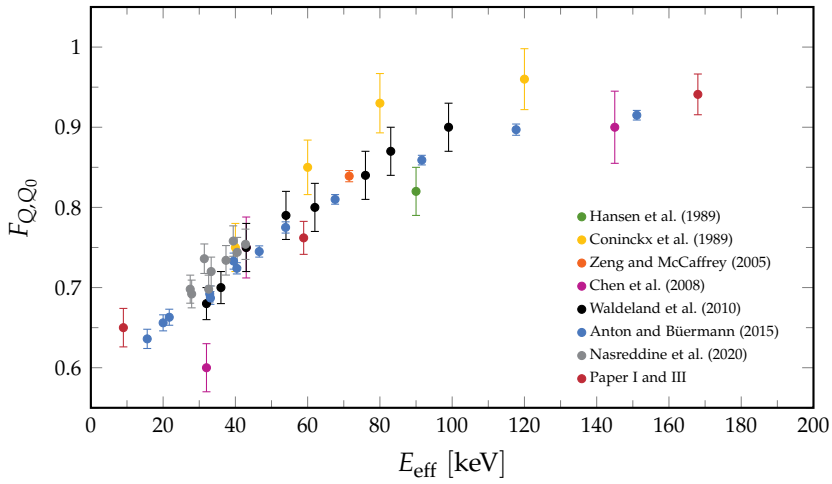

Figure 3.6: Literature values for the relative response F_{Q,Q_0} of the alanine pellet dosimeter in kV x-ray fields, quantified by their effective energy E_{eff}, relative to a cobalt-60 reference field.

the energy dependence of the ratios of mass energy absorption coefficients in Figure 3.1 – the relative response is decreasing for lower values of the effective energy and converging towards unity as the effective energy increases above 100 keV. For the very low end of the energy range the data is scarce, and below 30 keV only Anton and Büermann (2015) are contributing. For larger energies more individual studies are available, introducing a significant spread in the experimentally determined values for the relative response.

It is not obvious that the effective energy (or equivalently the HVL) of the x-ray beam should be sufficient characterization to unanimously determine the relative response of the alanine pellet dosimeter. Different data sets show different slopes and 'convergence rate', e.g. Coninckx et al. (1989), Waldeland et al. (2010), and Anton and Büermann (2015). This effect may just be within measurement uncertainties, but it could also indicate that knowledge of the effective energy (or HVL) of the x-ray beam is not sufficient information to accurately determine the relative response.

The experimentally determined values for relative response are all[1] obtained under well-defined laboratory conditions. This includes well characterized beams in a suitable irradiation geometry (phantom size and material, source to surface distance (SSD), low scatter conditions, etc.). If and how the relative efficiency is affected when translated to more complex irradiation conditions (e.g. blood irradiators where several x-ray sources may be present) is not clear. The most practical tool for investigating the influence of changing geometry is by MC calculations. This kind of investigation requires validation of the MC calculations ability to reproduce the observed relative response.

3.2 Monte Carlo Calculation of Dosimeter Response

Direct experimental determination of the relative response of dosimeters in complex fields like commercially available small self-shielded x-ray irradiators is a difficult task. Assuming the use of ionization chambers for D_w measurements, issues concerning the shift from reference conditions in which the chamber is calibrated, placement in irradiation cavity including wiring between ionization chamber and electrometer, etc. are introduced.

A practical alternative to direct measurements is the use of MC calculations. Assuming well known geometries, field size, and spectral distribution of photons, the relative ratio of doses H_{Q,Q_0} can be calculated as

$$H_{Q,Q_0} = \frac{(D_{ala}/D_w)_Q}{(D_{ala}/D_w)_{Q_0}}. \tag{3.5}$$

If the decrease in relative response of the detector at low photon energies is solely an effect of varying dose ratios, then the relative response is simply

$$F_{Q,Q_0} = H_{Q,Q_0}. \tag{3.6}$$

For the beam qualities investigated in the present study calculation of the relative ratio of doses was carried out by constructing the irradiation geometries sketched in Figure 3.2 and Figure 3.4 with the `cavity` usercode of the `EGSnrc`

[1] For all listed studies where detailed information on the irradiation geometry is given.

MC toolkit (Kawrakow et al. 2000). The reader is referred to Paper I and Paper III for a detailed description of calculations. For modeling of the alanine pellet dosimeters, a material data file with a mixture of alanine and paraffin wax, by ratio specified by the manufacturer, was constructed using bulk density. For calculations using alanine in high energy beams, both electron and x-ray, care should be taken when applying a density correction to the electron stopping powers, as the bulk density is considerably lower than the crystalline density (Zeng, McEwen, et al. 2005; Anton, Kapsch, Krauss, et al. 2013; ICRU Report 90 2016). The calculated value for the relative ratio of doses for the 40 kV beam quality is $H^{40\,\mathrm{kV}}_{Q,Q_0} = 0.707 \pm 0.017$, and for the irradiations carried out at NPL the calculated values are $H^{135\,\mathrm{kV}}_{Q,Q_0} = 0.863 \pm 0.020$ and $H^{280\,\mathrm{kV}}_{Q,Q_0} = 0.990 \pm 0.023$. The calculated relative ratio of doses overestimates the measured relative response by 8.1 %, 11.0 %, and 4.6 %, indicating an additional contribution to the decrease in relative response not accounted for in the MC calculations.

Calculated H_{Q,Q_0} values for two large sets of primary x-ray spectra (see Section 5.3 for a description of the spectra) are shown in Figure 3.7, together with the experimentally determined F_{Q,Q_0} values. The H_{Q,Q_0} values shown in

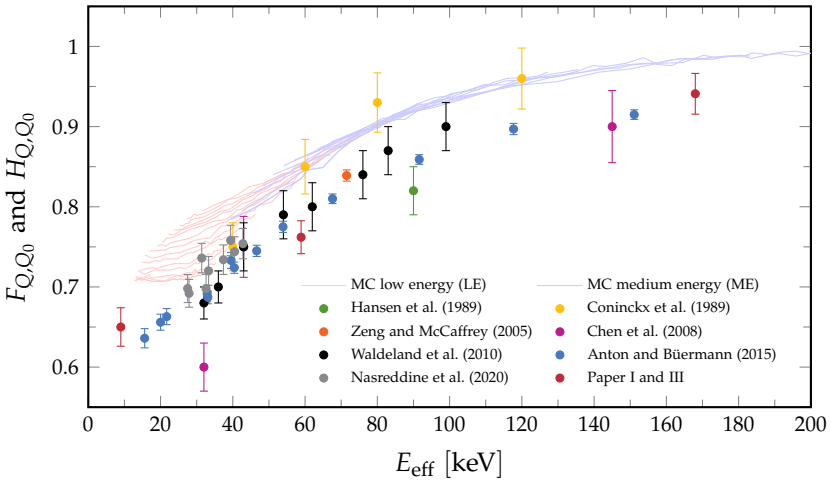

Figure 3.7: MC calculated relative dose ratios H_{Q,Q_0} using sets of low (red lines) and medium (blue lines) energy x-ray spectra, see Section 5.3 for details. Data points represent literature values of the relative response F_{Q,Q_0}.

Figure 3.7 are calculated for an alanine pellet placed at 2 cm depth in a water phantom with a parallel x-ray beam. Therefore it does not necessarily represent identical geometries as used to obtain the experimental F_{Q,Q_0} values. However, it does illustrate the general tendency of overestimating the relative response of the dosimeter as is observed for the three beam qualities studied here, and

which is also reported by Zeng and McCaffrey (2005), Waldeland et al. (2010), and Anton and Büermann (2015).

The interpretation of this discrepancy is that Equation (3.6) does not hold. The underlying assumption of Equation (3.6) is that the induced response in the detector per dose to detector material is independent of photon energy – that is the relative efficiency G_{Q,Q_0} is unity. The relative efficiency can be written as

$$G_{Q,Q_0} = \frac{(r/D_{\text{ala}})_Q}{(r/D_{\text{ala}})_{Q_0}}. \tag{3.7}$$

The relation between the relative response and the two contributors is then

$$F_{Q,Q_0} = G_{Q,Q_0} \cdot H_{Q,Q_0}, \tag{3.8}$$

$$\frac{(r/D_{\text{w}})_Q}{(r/D_{\text{w}})_{Q_0}} = \frac{(r/D_{\text{ala}})_Q}{(r/D_{\text{ala}})_{Q_0}} \cdot \frac{(D_{\text{ala}}/D_{\text{w}})_Q}{(D_{\text{ala}}/D_{\text{w}})_{Q_0}}. \tag{3.9}$$

From Equation (3.8) it is clear that the relative efficiency can be determined by the ratio of F_{Q,Q_0} to H_{Q,Q_0}. The experimental determination of G_{Q,Q_0} requires sufficiently detailed information about x-ray field and irradiation geometry to reliably perform MC calculations of H_{Q,Q_0}.

3.3 Experimental Determination of Relative Efficiency

An experimental determination of the relative efficiency of the alanine pellet dosimeter subject to irradiation in the three LE x-ray beam qualities considered here can now be determined according to Equation (3.8). The determined values are $G_{Q,Q_0}^{40\,\text{kV}} = 0.919 \pm 0.040$, $G_{Q,Q_0}^{135\,\text{kV}} = 0.890 \pm 0.032$, and $G_{Q,Q_0}^{280\,\text{kV}} = 0.954 \pm 0.034$. These experimentally determined G_{Q,Q_0} values are shown as a function of the effective energy of the x-ray beam in Figure 3.8 together with literature values.

The literature values shown in Figure 3.8 are obtained from Zeng and McCaffrey (2005), Waldeland et al. (2010), and Anton and Büermann (2015). both Zeng and McCaffrey (2005) and Waldeland et al. (2010) directly compute the relative efficiency in their studies, while Anton and Büermann (2015) present experimentally determined values for the relative response and MC calculations of the relative ratio of doses for all beam qualities under investigation, and the G_{Q,Q_0} values listed for Anton and Büermann (2015) here is obtained by taking the ratio of these values.

It is difficult to conclude much about the energy dependence of the relative efficiency from the available data, other than a significant decrease is observed for low energy x-rays. Different trends in the energy dependence can be determined from Figure 3.8, such as a local increase around 20 keV to 30 keV. The Waldeland et al. (2010) data indicate a steadily increasing relation for effective energies between 30 keV and 100 keV, while the Anton and Büermann (2015)

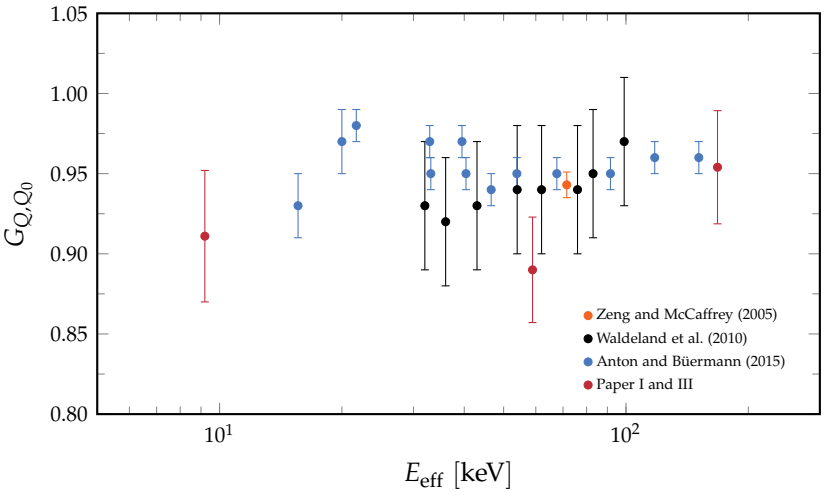

Figure 3.8: Experimentally determined values of the relative efficiency G_{Q,Q_0} as a function of effective energy of the primary x-ray beam.

data indicate almost constant value in the same energy range. The deviations between relative efficiency at specific energies determined in different studies can however be resolved by consideration of the experimental uncertainties. It may also be a consequence of the effective energy not being sufficient information to uniquely determine the relative efficiency.

3.4 Characterization of the Relative Efficiency

The experimental data on relative efficiency of the alanine pellet dosimeter in kV x-ray fields indicate an overall trend of decreasing efficiency for decreasing effective energy of the primary beam. Some variation in the determined values for G_{Q,Q_0} is observed for similar effective energies. However, since the experimental uncertainty is relatively large compared to the decrease in relative efficiency, the differences are not significant regarding uncertainties.

The deviations may however occur because of differences in irradiation geometry. The data obtained from Anton and Büermann (2015) consist of two distinct sets of irradiations. A low energy set where the pellets are placed at the surface of a PMMA phantom similar to the 40 kV irradiation of Paper I, and a medium energy set where the pellets are placed at 5 cm depth in a water phantom. In the study by Waldeland et al. (2010) the alanine pellets are placed in a solid water phantom at 2 cm depth, similar to the 135 kV and 280 kV irradiations of Paper III. Since the beam profile changes as it is attenuated through the phantom material, this may significantly affect the relative efficiency.

Even if all experimental data were obtained for similar geometries, it is not obvious that the effective energy should be sufficient to fully characterize the energy dependence of the relative efficiency, and thus of the relative response, of the dosimeter. Furthermore, it is not clear how the relative efficiency of the alanine pellet dosimeter is affected when transferred to non-standard x-ray fields.

The issue of determining the relative response of the alanine pellet dosimeter directly in a non-standard field, where ionization chambers can not easily or reliably be used, still stands. If the relative efficiency of the dosimeter placed in a specific geometry could be determined independently of a relative response measurement, then the relative response could be calculated by combination with a MC calculated relative ratio of doses according to Equation (3.8).

One approach for independently determining the relative efficiency of the alanine pellet dosimeter is the use of the microdosimetric one-hit detector model (OHDM). Olko (2002) applied the microdosimetric OHDM to calculate the relative response of alanine dosimeters irradiated by monoenergetic photons. The results showed a decrease in the relative efficiency comparable to the experimentally determined values.

Chapter 4

The Microdosimetric One-Hit Detector Model

Microdosimetry accounts for the discreteness of the dose deposition. The interactions of ionizing radiation (particles and photons) with matter can usually be treated by use of the mean values, e.g. average dose D to a given volume of material. This is the so-called *non-stochastic* version of dose (Rossi and Zaider 1996). Microdosimetry defines a volume of interest (target volume) where energy deposition events are considered. An ionizing particle passing through the target volume producing at least one ionization is called a single-event. When the single-event leads to the generation of a detector response (e.g. a free radical in alanine) this event is called a hit. The distribution of energy deposited inside the detector volume is not uniform since the energy transfer occurs in discrete events (Olko 2002).

The following chapter introduces the basics quantities of microdosimetry are introduced with a one-hit detector model (OHDM) for calculating a detector efficiency. The evaluation of microdosimetric distributions from MC calculated particle tracks is subsequently described, followed by an application of the OHDM calculation of the detector efficiency.

This chapter is based on the results of paper IV.

4.1 Microdosimetric Quantities

For interactions of ionizing radiation with matter, energy is transferred by ionizations and excitations. The stochastic quantity related to this transfer of energy is the *energy deposited* ε_i in a single interaction i, defined by (ICRU Report 36 1983)

$$\varepsilon_i = \varepsilon_{\text{in}} - \varepsilon_{\text{out}} + Q, \tag{4.1}$$

where ε_{in} is the energy of the incident particle, ε_{out} is the sum of the energies of all particles leaving the interaction, and Q is the total decrease in rest mass of the atom and all involved particles. ε_i is a stochastic quantity and is subject to random fluctuations for any given incident particle. The combined contribution

of energy depositions in a volume V is the *energy imparted* ε

$$\varepsilon = \sum_i \varepsilon_i. \tag{4.2}$$

For an *average energy expended per ionization produced*, W, in the medium the energy imparted can be expressed as

$$\varepsilon = j \cdot W, \tag{4.3}$$

where j is the total *number of ionizations* in the volume. Dividing the energy imparted by the mass m of the volume, the *specific energy* z is obtained

$$z = \frac{\varepsilon}{m}. \tag{4.4}$$

The mean value of the specific energy $\overline{z}$ is the mean energy imparted $\overline{\varepsilon}$

$$\overline{z} = \frac{\overline{\varepsilon}}{m}. \tag{4.5}$$

The mean specific energy is the stochastic equivalent of the non-stochastic quantity of absorbed dose D which is defined from the mean specific energy as

$$D = \lim_{m \to 0} \overline{z}. \tag{4.6}$$

For the definition of the energy imparted in Equation (4.2) the sum is of a finite number of discrete events. This would imply that the energy imparted is described by a non-continuous function. The specific energy can be approximated as a continuous random variable for sufficiently large number of interactions. In this case the probability that the specific energy produced in multiple energy transfer events in the interval $[z, z + \mathrm{d}z]$ is $f(z)\,\mathrm{d}z$. Usually only one track overlaps the target volume for low doses where $D \ll \overline{z}$, which motivates the consideration of a *single-event frequency distribution* $f_1(z)$ (Horowitz 2006). Here the subscript refers to the single-event consideration, rather than the general *multi-event frequency distribution* $f(z)$. The single-event frequency distribution measures the distribution of z with the restriction that all energy deposits occur as single events (Rossi and Zaider 1996).

The expectation value of $f_1(z)$ is the *frequency mean specific energy* $\overline{z_\mathrm{F}}$ which in turn is the first moment of the frequency distribution

$$\overline{z_\mathrm{F}} = \frac{\int_0^\infty z f_1(z)\,\mathrm{d}z}{\int_0^\infty f_1(z)\,\mathrm{d}z}. \tag{4.7}$$

Typically $f_1(z)$ is normalized to a single event and the denominator in Equation (4.7) is unity. Single event distributions are independent of the dose, but do depend on the characteristics of the ionizing particle track and the target shape, size, and composition. $\overline{z_\mathrm{F}}$ is the average dose deposited in the target volume by single events.

4.2 Detector Response in Microdosimetry

The microdosimetric OHDM is applied in the present study to explore the relative efficiency of the alanine pellet detector. The OHDM is a phenomenological model based on the multi-hit and multi-target theories originally applied to describe inactivation of microorganisms. Here it is assumed that a detector contains a single type of target which can tolerate a certain amount of hits (energy deposition events) before it is affected (cell death in the microbiological case or signal production for ionizing radiation detectors). The hits in the target are assumed to be independent of each other and as such, the process can be described by Poisson statistics. The probability that no effect occurs (survival S) after n hits can be described as a function of D by (Kellerer 1985; Horowitz 2006)

$$S(D) = \sum_{\nu=0}^{n-1} \frac{\mathrm{e}^{-\alpha D} (\alpha D)^{\nu}}{\nu!}, \tag{4.8}$$

where α is a saturation parameter.

As the name suggests, one-hit detectors are the special case of $n = 1$. Here the probability of survival reduces to the simple, purely exponential function

$$S(D) = \mathrm{e}^{-\alpha D}. \tag{4.9}$$

In this case α can be interpreted as the mean number of hits in the target per unit absorbed dose. For $n > 1$ Equation (4.8) describes the survival function for some biological systems (see for instance the survival curves presented in Chapter 7).

The probability of survival can be expressed in terms of the microdosimetric single-event frequency distribution as (Zaider 1990)

$$S(D) = \exp\left[-\frac{D}{\overline{z_{\mathrm{F}}}} \int_0^{\infty} \left(1 - \mathrm{e}^{-\alpha z}\right) f_1(z)\, \mathrm{d}z\right]. \tag{4.10}$$

The physical interpretations of the different parts of Equation (4.10) are

- $\overline{z_{\mathrm{F}}}$: The average dose deposited by single energy deposition events.
- $D/\overline{z_{\mathrm{F}}}$: The average number of events taking place in the target volume after irradiation of dose D.
- $1 - \exp(-\alpha z)$: The probability of an effect occurring after deposition of specific energy z.
- $\int_0^{\infty} \left(1 - \mathrm{e}^{-\alpha z}\right) f_1(z)\, \mathrm{d}z$: The probability that an effect occurs in the target volume per energy deposition event.
- $\frac{D}{\overline{z_{\mathrm{F}}}} \int_0^{\infty} \left(1 - \mathrm{e}^{-\alpha z}\right) f_1(z)\, \mathrm{d}z$: The number of effective hits after irradiation of dose D.

The probability that a detector response $R(D)$ is produced is the complement probability of the probability of survival

$$R(D) = 1 - S(D) \tag{4.11}$$

$$= 1 - \exp\left[-\frac{D}{\overline{z_F}} \int_0^\infty \left(1 - e^{-\alpha z}\right) f_1(z)\, dz\right]. \tag{4.12}$$

This is the normalized response function of a one-hit detector. The characteristic dose D_0 in

$$R(D) = 1 - \exp\left(-\frac{D}{D_0}\right), \tag{4.13}$$

can be estimated as

$$D_0 = \frac{\overline{z_F}}{\int_0^\infty \left(1 - e^{-\alpha z}\right) f_1(z)\, dz}, \tag{4.14}$$

assuming that Equation (4.13) is the characteristic response function of one-hit detectors (see Figure 2.5).

For low doses $D \ll \overline{z_F}$ the response function can be further simplified by the truncated Taylor expansion of the exponential function ($e^x \approx 1 + x$), obtaining

$$R(D) = \frac{D}{\overline{z_F}} \int_0^\infty \left(1 - e^{-\alpha z}\right) f_1(z)\, dz. \tag{4.15}$$

The relative efficiency of a one-hit detector defined by

$$G_{Q,Q_0} = \frac{(R/D)_Q}{(R/D)_{Q_0}}, \tag{4.16}$$

can then be expressed with the microdosimetric OHDM as

$$G_{Q,Q_0} = \frac{\frac{1}{\overline{z_F^Q}} \int_0^\infty \left(1 - e^{-\alpha z}\right) f_1^Q(z)\, dz}{\frac{1}{\overline{z_F^{Q_0}}} \int_0^\infty \left(1 - e^{-\alpha z}\right) f_1^{Q_0}(z)\, dz}, \tag{4.17}$$

where the superscript Q and Q_0 refer to the relevant beam qualities. The calculation of the relative detector efficiency using the microdosimetric OHDM depends on the free parameters of the model. These parameters are the target diameter d (assuming a spherical target) and the saturation parameter α. The target diameter does not appear directly in Equation (4.17) but the frequency distribution of specific energy depends on the target size and shape.

4.3 Monte Carlo Approach for Calculating Microdosimetric Distributions

The scoring of microdosimetric distributions is based on the evaluation of MC calculated ionizing particle track structures. The `Geant4-DNA` MC toolkit is used here in order to track particles to very low energies in water (Incerti 2010a; Incerti 2010b; Bernal et al. 2015; Incerti et al. 2018). Figure 4.1 shows three 1 keV electron tracks generated at the origin with momentum in the positive z-direction. Each dot represents ionization positions.

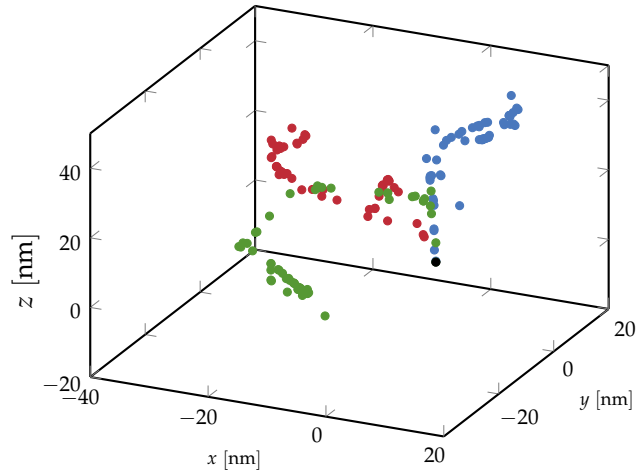

Figure 4.1: (x, y, z)-coordinates for ionizations produced by three 1 keV electrons in water calculated using the `Geant4-DNA` Monte Carlo code. Each color represents a single electron track. The black dot represents the origin.

The calculation of microdosimetric single-event frequency distribution from particle tracks is done according to the method described by Kellerer and Chmelevsky (1975), Kellerer (1985), and Rossi and Zaider (1996). The direct method for calculating the frequency distribution considers randomly placed target volumes of diameter d in the region of interest (detector volume) for individual particle tracks, and scoring the specific energy in this region. The region of interest can be interpreted as the bounding box of the particle track. A two-dimensional sketch of this method of analysis is shown in Figure 4.2a. This direct approach calculates accurate microdosimetric frequency distributions, but for large particle tracks the number of misses (randomly selected target volumes with $z = 0$) increases dramatically and the computations get very time consuming.

An alternative approach is using a weighted sampling procedure. Here only the *associated volume*, where $z > 0$, is sampled. This can be obtained by

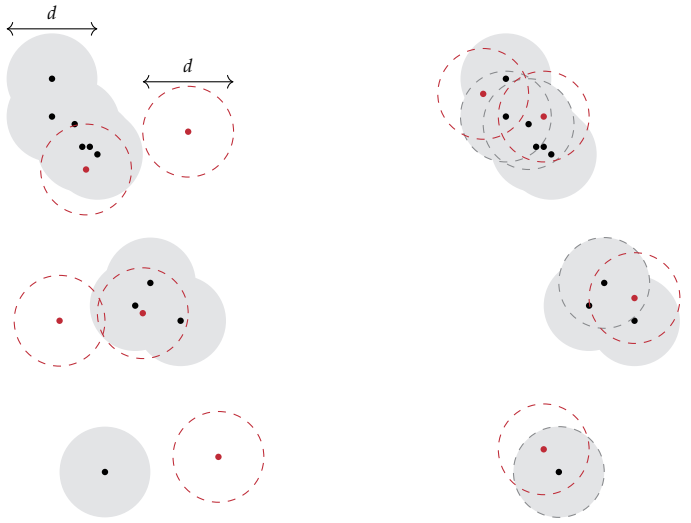

a) Uniform sampling – $f(z)$ b) Weighted sampling – $d(z)$

Figure 4.2: A two-dimensional illustration of the process for obtaining microdosimetric distributions. a) Uniform sampling resulting in the frequency distribution $f(z)$. b) Weighted sampling resulting in the dose distribution $d(z)$. Filled gray circles represent the associated volume of the particle track, red dashed circles represent a set of sampled target volumes, and gray dashed circles represent randomly selected energy transfer points for the weighted sample procedure. Illustration inspired by Famulari et al. (2017).

randomly selecting an energy transfer point (ionization position) in the particle track, and a randomly selected sampling point in the sphere of radius $r = d/2$ around the energy transfer point. A two-dimensional sketch of the situation is shown in Figure 4.2b. Using this weighted sampling procedure regions of high ionization density is favored by the choice of random energy transfer point with a weight factor proportional to z, and the *dose distribution* of specific energy $d(z)$ is obtained rather than the frequency distribution. Like for the frequency distribution, the probability that the specific energy produced in the interval $[z, z + \mathrm{d}z]$ is $d(z)\,\mathrm{d}z$ if this weighted sampling procedure is used (Kellerer and Chmelevsky 1975). As for the frequency distribution, the *single-event dose distribution* $d_1(z)$ can be considered when only single particle track can be assumed to overlap the target volume.

The frequency distribution and dose distribution of specific energy are related by

$$d_1(z) = \frac{z}{\overline{z}_\mathrm{F}} f_1(z), \tag{4.18}$$

and equivalently (Kellerer and Chmelevsky 1975; Kellerer 1985)

$$f_1(z) = \frac{z^{-1} d_1(z)}{\int_0^\infty z^{-1} d_1(z)\,\mathrm{d}z}. \tag{4.19}$$

Since the weighted sampling procedure, per definition, ensures at least one ionization present per target volume ($z > 0$) the computation time is heavily reduced relative to the uniform sampling method.

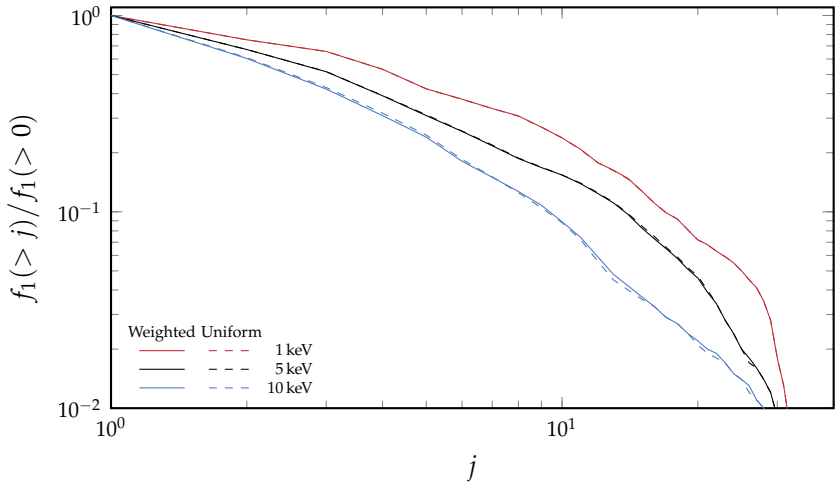

Figure 4.3: Cumulative frequency distribution of ionizations for single tracks obtained using the weighted sampling procedure (solid lines) and the uniform sampling procedure (dashed lines) for target diameter $d = 20\,\mathrm{nm}$.

To validate the equality of the two procedures, a set of single-event frequency distributions were calculated using the respective procedures. The obtained distributions of ionizations are shown in Figure 4.3 presented in cumulative form. The cumulative distributions shown in Figure 4.3 are for a single particle track at 1 keV, 5 keV, and 10 keV with target diameter $d = 20\,\mathrm{nm}$. This low energy and single track sample is chosen to reduce computation time, while the equality of the single-event frequency distributions obtained through the two procedures can still be confirmed.

In order to convert the number of ionizations j into specific energy z, an arbitrary value for the average energy expended per ionization produced of $W = 30\,\mathrm{eV}$ is chosen similar to Olko (2002). This scaling is not critical since, for the response of the alanine pellet dosimeter, the signal is induced by ionizations

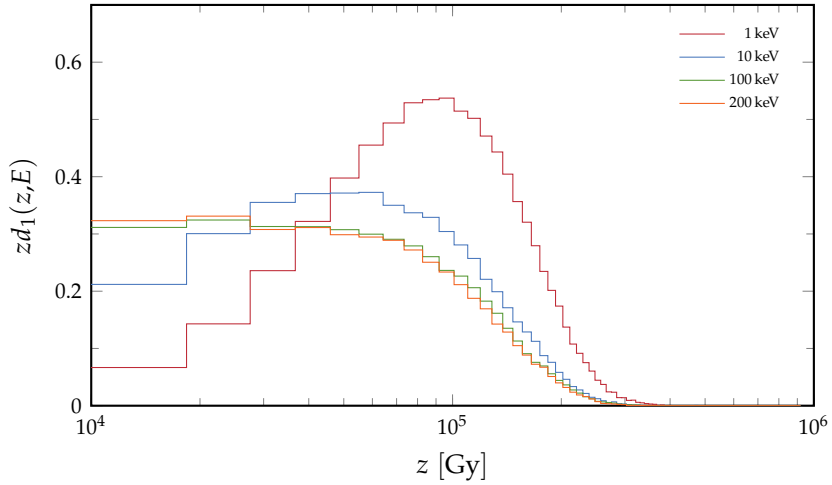

Figure 4.4: Microdosimetric single-event dose distribution of specific energy for 1 keV, 10 keV, 100 keV, and 200 keV electrons in water, using target diameter $d = 10\,\text{nm}$.

and not the overall energy deposition. The specific energy is then

$$z = \frac{6Wj}{\rho_{\text{target}}\pi d^3}, \tag{4.20}$$

where ρ_{target} is the density of the target volume. The calculated normalized single-event dose distribution of specific energy for 1 keV, 10 keV, 100 keV, and 200 keV electrons with target diameter $d = 10\,\text{nm}$ are shown in Figure 4.4. Here multiple particle tracks are analyzed individually to obtain a general microdosimetric spectrum for each energy. A general characteristic of the dose distribution, evident from Figure 4.4, is that increasing electron energy results in a shift in the distribution towards lower specific energies, as well as a convergence towards a specific dose distribution for higher energies. This would imply that composite microdosimetric spectra e.g. from photon spectra with a range of secondary electron energies, is quite sensitive to the fraction of low to high energy secondary electrons. The greater mean specific energy for lower energies is obtained by an increased mean number of ionizations occurring in the target volume, implying a greater ionization density.

4.4 Microdosimetric Distributions for Photons

Photons interact with matter via the usual processes (photoelectric effect, Compton effect, pair production, etc.) transferring energy to secondary electrons. The distribution of secondary electrons propagates through the detector,

depositing their energy along the way, producing the response (detector signal, cell death, etc.). The microdosimetric distributions for a primary beam of photons can thus be obtained by considering the secondary electrons produced in the medium. If the initial energy distribution of secondary electrons $\phi(E)$ produced in the medium by the primary photon beam is known, then the microdosimetric dose distribution of specific energy can be calculated by folding in the dose distribution of electrons (Figure 4.4) in with the secondary electron spectrum (**olko2006**)

$$d_1(z) = \frac{\int d_1(z,E)\phi(E)E\,\mathrm{d}E}{\int \phi(E)E\,\mathrm{d}E}. \tag{4.21}$$

For energies below approximately 1000 keV only photoelectric and Compton effect are relevant processes for ionizations in the medium. In the present study the initial energy distribution of photo- and Compton electrons are calculated using the `Geant4` MC toolkit (Agostinelli et al. 2003) using the `G4EmDNAPhysics_option2` electromagnetic model.

4.4.1 Cobalt-60 Reference Field

A cobalt-60 reference beam is used as an example of the calculation of microdosimetric distributions in photon fields. The microdosimetric single-event frequency distribution of a reference beam quality Q_0 is required for the calculation of the relative efficiency of a dosimeter according to Equation (4.17). The reference beam quality used here is a Nordion GC220 Gammacell located at the Risø HDRL. The spectral distribution of photons at the central region in a reference geometry with dose to water measurements with alanine pellet dosimeters traceable to NPL is shown in Figure 4.5.

The initial energy distribution of photo- and Compton electrons produced in an alanine pellet placed in the irradiation geometry by the primary photon beam is also shown. The two peaks in the secondary electron spectrum at approximately 0.96 MeV and 1.12 MeV corresponds to the maximum energy of Compton electrons produced by primary photons with energies in the two peaks in the cobalt-60 spectrum.

The dose distribution of specific energy obtained by folding the secondary electron spectrum with the dose distribution for monoenergetic electron beams according to Equation (4.21) is shown in Figure 4.6 for target diameter 10 nm, 20 nm, and 30 nm. The shape and position of the dose distributions in Figure 4.6 are affected by the target diameter in two ways – greater target diameter entails that more ionizations, and thus greater energy deposition, occurring in the target volume, and at the same time the increase in target diameter result in a greater mass of the target volume. The combined effect is evident in Figure 4.6, where an increase in target diameter shifts the dose distribution towards lower mean specific energies. The mean specific energy follows a power function of

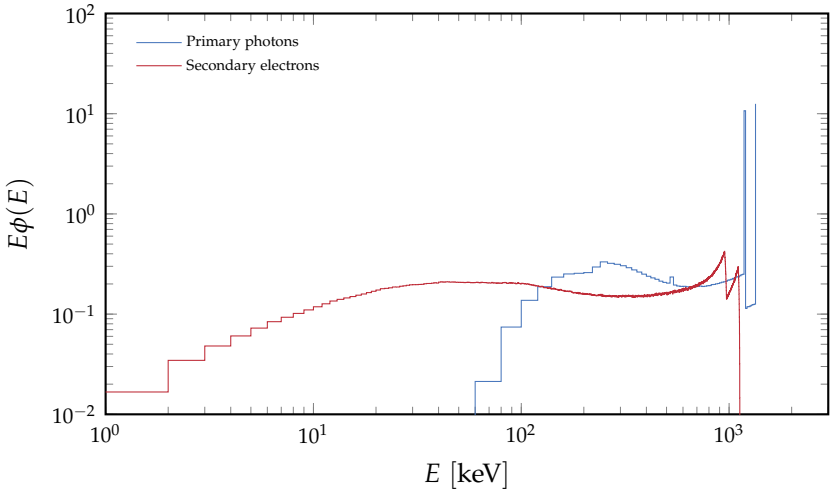

Figure 4.5: Primary photon energy spectrum at the central region of the HDRL cobalt-60 Gammacell (blue) and secondary electron energy spectrum produced in an alanine pellet irradiated in the central position (red) calculated using the `Geant4` MC toolkit. Both spectra are normalized to unit area under the curve.

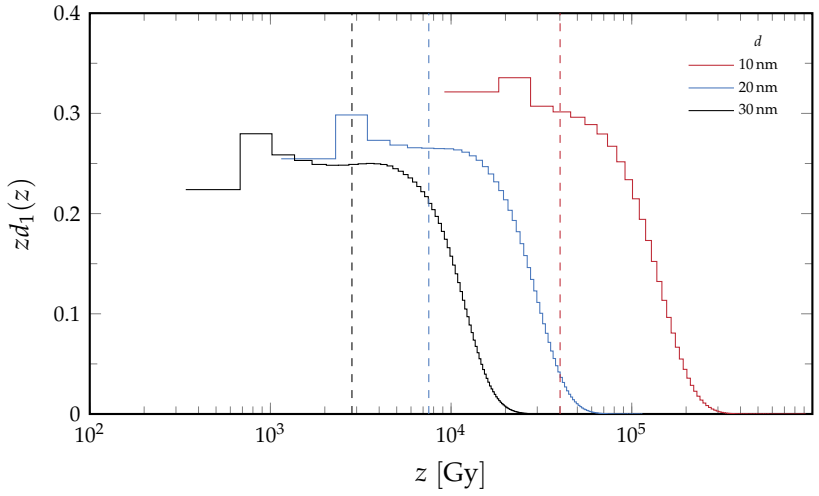

Figure 4.6: Microdosimetric single-event dose distribution of specific energy for alanine pellets in the HDRL cobalt-60 Gammacell. Different distributions are shown, illustrating the dependence of the microdosimetric distributions on target volume. Target volumes shown are $d = 10\,\text{nm}$ (red), $d = 20\,\text{nm}$ (blue), and $d = 30\,\text{nm}$ (black). The vertical dashed lines represent the first moment of each dose distribution.

the diameter of the spherical water targets (see Figure 4.7) of the form

$$\frac{\overline{z_F}}{\mathrm{Gy}} = c_0 \cdot \left(\frac{d}{\mathrm{nm}}\right)^{c_1}, \tag{4.22}$$

where the parameters c_0 and c_1 can be determined by regression analysis. For

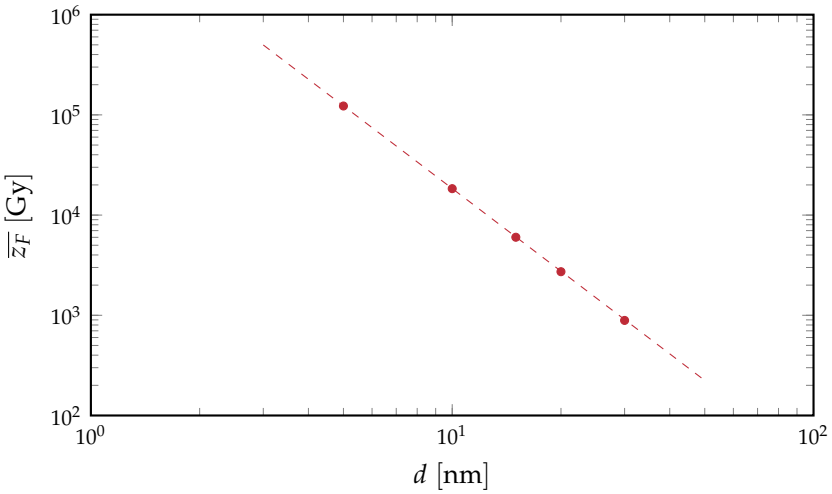

Figure 4.7: Mean specific energy $\overline{z_F}$ in a spherical water target of varying diameter d for irradiations in the HDRL cobalt-60 gammacell (dots), and a regression of the form Equation (4.22) (dashed line).

the microdosimetric distributions obtained for the cobalt-60 Gammacell the coefficients are $c_0 = 1.01 \times 10^7$ and $c_1 = -2.74$.

4.5 Free Model Parameters

The microdosimetric OHDM, with relative efficiency described by Equation (4.17), depends on the free model parameters α and d. For the model to best describe the relative efficiency of the alanine pellet dosimeter irradiated in kV x-ray fields, experimental data for the relative efficiency in well-known fields is used to determine the optimal set of model parameters. Several studies of the relative response and efficiency of the alanine pellet dosimeter in kV x-ray fields are available in the literature (Zeng and McCaffrey 2005; Waldeland et al. 2010; Anton and Büermann 2015). For fixing the free model parameters detailed knowledge of the x-ray spectra and irradiation geometry is required in addition to the experimentally determined values for the relative efficiency. For this purpose, the data published by Waldeland et al. (2010) is chosen. Here

a detailed description of dosimeter, irradiation geometry, and the generation of x-ray spectra is given. The beam modalities used in their study, as well as the measured relative efficiency of the alanine pellet dosimeter, are listed in Table 4.1. In their work x-ray spectra were calculated using the `SpekCalc` software

Table 4.1: List of beam modalities produced based on the work of Waldeland et al. (2010), with their corresponding, experimentally determined, relative efficiency G^{exp}_{Q,Q_0}.

Potential [kV] Nominal	E_{eff} [keV]	Filtration [mm]		HVL [mm]		G^{exp}_{Q,Q_0}
		Al	Cu	Al	Cu	
50	32	4.2	-	2.6	-	0.93 ± 0.04
70	36	4.0	-	3.4	-	0.92 ± 0.04
100	43	4.4	-	5.0	-	0.93 ± 0.04
120	54	7.0	-	-	0.39	0.94 ± 0.04
135	62	10.5	-	-	0.58	0.94 ± 0.04
150	76	4.0	0.53	-	0.94	0.94 ± 0.04
180	83	6.0	0.53	-	1.16	0.95 ± 0.04
200	99	6.0	0.99	-	1.73	0.97 ± 0.04

(Poludniowski 2007; Poludniowski and Evans 2007). The same method was applied here, using the specifications of the filtration, SSD, and HVL used in their study.

The input potential of the beam modalities was adjusted to match the HVL as described by Waldeland et al. (2010). Initial secondary electron spectra produced in an alanine pellet by the primary photon beams was calculated for the irradiation geometry in `Geant4`, similarly to the procedure described in Section 4.4. The microdosimetric distributions associated with the respective beam modalities is then calculated by folding of the secondary electron spectrum with the monoenergetic electron distributions according to Equation (4.21).

The optimal set of model parameters α and d can now be determined by comparison of experimentally determined values of the relative efficiency G^{exp}_{Q,Q_0} with model calculated values G^{calc}_{Q,Q_0} for a wide range of of beam parameters. The choice of saturation parameter α is evaluated for any given target diameter d by minimizing the relative least squares M

$$M = \sum_{Q} \left(\frac{G^{\text{exp}}_{Q,Q_0} - G^{\text{calc}}_{Q,Q_0}}{G^{\text{exp}}_{Q,Q_0}} \right)^2 , \tag{4.23}$$

where the sum over Q represent the inclusion of all beam modalities listed in Table 4.1. As an additional constraint a secondary electron spectrum for a primary cesium-137 field, with unity relative efficiency, is also included in the

analysis. The calculated relative least squares for a wide range of model parameters are shown in Figure 4.8. The value of the saturation parameter which

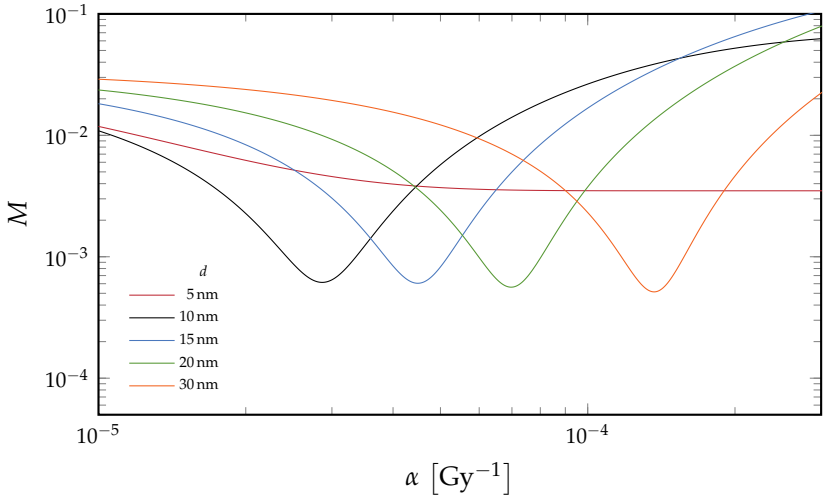

Figure 4.8: Parameter M (see Equation (4.23)) as a function of the saturation parameter α for different target diameters d in water.

best reproduce the literature data is then determined by locating the minimum of M for each target diameter. From Figure 4.8 it appears that target diameters in the range 10 nm to 30 nm are all able to reproduce the set of experimentally determined relative efficiencies equally well (the minimum values of M are roughly equal). Therefore, the minimization of M is not sufficient to determine the best value for the target diameter, and its associated saturation parameter, only optimal saturation parameter for each target diameter.

To establish a single optimal set of model parameters the ability of each set to predict response function and linearity index in the HDRL cobalt-60 Gammacell was examined. The detector response as a function of dose can be calculated by Equation (4.12), using the single-event frequency distribution for alanine pellets irradiated in the Gammacell for different target diameters, with saturation parameter determined from Figure 4.8. The calculated response functions are shown in Figure 4.9 together with measured response of alanine pellets irradiated in the Gammacell shown in Figure 2.5. The linearity index $f(D)$ is the response per dose normalized to a specific dose point is defined as

$$f(D) = \frac{(R/D)_{\text{dose}}}{(R/D)_{\text{ref. dose}}}. \tag{4.24}$$

The calculated and measured linearity index are shown in Figure 4.10, with the reference dose chosen at 1 kGy.

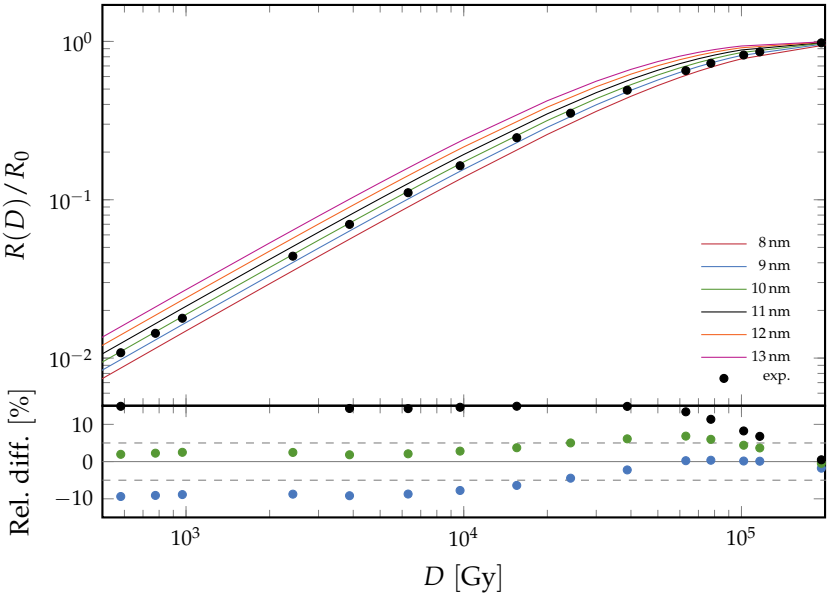

Figure 4.9: *Top:* Measured (black dots) and calculated (solid lines) response function of alanine pellets irradiated in the HDRL cobalt-60 Gammacell. *Bottom:* Relative difference between measured and calculated response. Colors match the legend in the top part of the figure.

The relative difference between measured and calculated response function and linearity index is shown in the bottom parts of Figure 4.9 and Figure 4.10. In both cases model calculations using the parameter set $d = 10\,\text{nm}$ and $\alpha = 2.86 \times 10^{-5}\,\text{Gy}^{-1}$ show the best agreement with experimental data. This set of parameters is therefore adopted for use in the model for further calculations.

The comparison between measured and calculated response, and linearity, curves for the alanine pellet dosimeter assumes that the measured saturation of EPR-response is purely due to an intrinsic effect of the dosimeter. That is, that the peak-to-peak height of the first derivative of the EPR spectrum is directly proportional to the concentration of stable free radicals. Different factors such as spectrometer settings (specifically the microwave power) and beam quality, altering the ratio of free radical species, may influence the response curve (Wieser and Girzikowsky 1996; Malinen et al. 2003). In the present work the comparison is used to settle on a specific choice of model parameters, from a set which all, according to Figure 4.8, appear to reproduce literature values of the relative efficiency equally well.

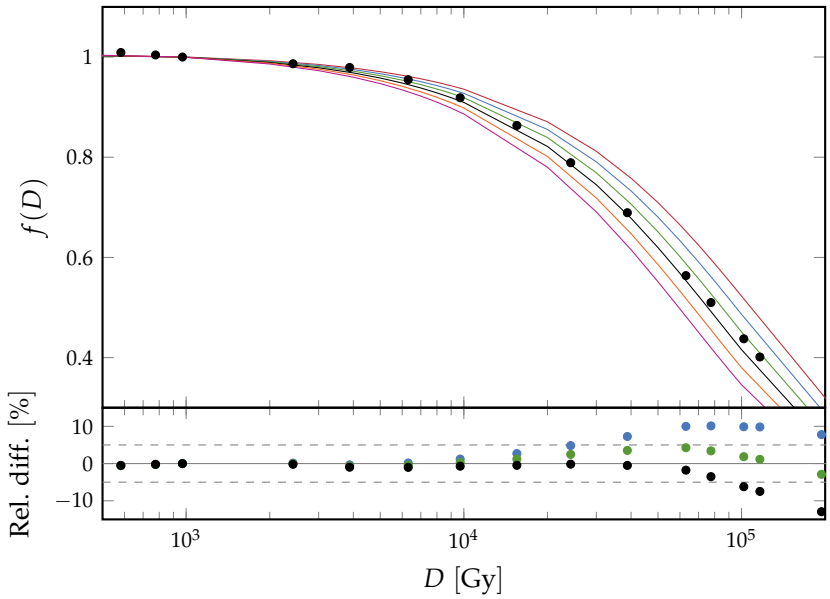

Figure 4.10: *Top:* Measured (black dots) and calculated (solid lines) linearity index of alanine pellets irradiated in the HDRL cobalt-60 Gammacell. *Bottom:* Relative difference between measured and calculated response. Color coding is identical to Figure 4.9.

4.6 Evaluation of Model Uncertainty

To evaluate the uncertainty of model calculations a sensitivity analysis was carried out concerning the uncertainty of the literature values of the relative efficiency used to determine the optimal parameter set. Random values for the relative efficiency, within the uncertainty bounds listed in Table 4.1, was generated for each beam quality and used in the process for determining the optimal parameter set described in the previous sections. This was done for 4×10^3 iterations. Figure 4.11 show the resulting distribution of optimal saturation parameter for target diameter $d = 10\,\text{nm}$. A Gaussian fit to the distribution was performed to determine the standard deviation of the saturation parameter for this particular target diameter, and a value of $\sigma_\alpha = 5.97 \times 10^{-6}\,\text{Gy}^{-1}$ was obtained.

The standard deviation appears to be large relative to the determined optimal value ($\approx 21\,\%$), however, the actual uncertainty on the resulting model calculation is not necessarily as large.

In order to evaluate the model uncertainty, only the variation in saturation parameter for a specified target diameter is considered. Doing a full analysis

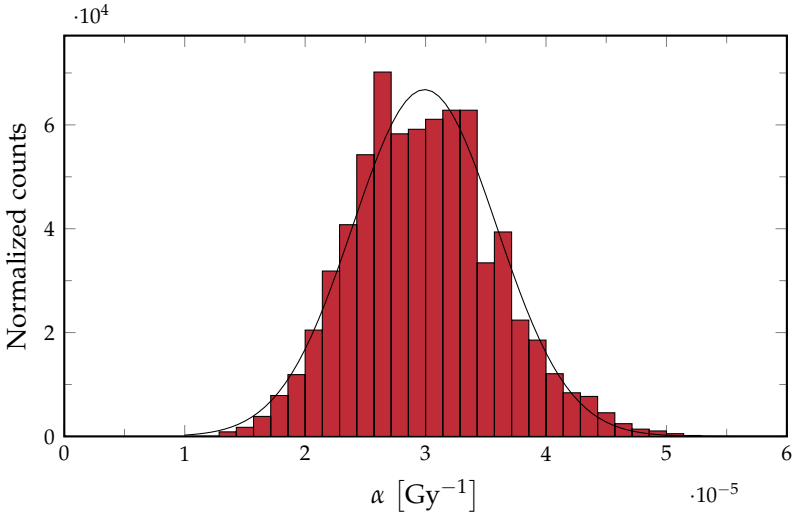

Figure 4.11: Distribution of saturation parameter α for target diameter $d = 10\,\text{nm}$ for a random sample of relative efficiency for evaluation of optimal parameter sets. The black line represents a Gaussian fit to the distribution.

of optimal model parameter sets results in a distribution of target diameters as well. This is not included in the uncertainty evaluation here, since the transition from a mix of distributions to a single standard deviation is not feasible.

For the applications of the microdosimetric OHDM presented in the next chapter, the evaluated uncertainty on the saturation parameter will be used to estimate the uncertainty on the model predictions.

Chapter 5

Application of the Microdosimetric Model

The microdosimetric OHDM for calculations of the relative efficiency of alanine pellet dosimeters is sensitive to the distribution of initial secondary electrons created in the detector volume by the primary photon beam. The model can therefore be applied to study the effect on the relative efficiency of the dosimeter from changes in external properties, e.g. beam quality, filtration, and attenuation. A characterization of how the dosimeter response changes due to these external properties are of importance when dosimetry is needed in non-standard geometries where dosimetry using ionization chambers, which are usually considered as the golden standard, are not possible.

In the following chapter the microdosimetric OHDM is applied to different x-ray fields to evaluate the dependence of the alanine pellet dosimeter relative efficiency on photon energy, beam quality, and external factors.

This chapter is based on the results in paper IV.

5.1 Monoenergetic Photons

As a first application of the model the energy dependence of the relative efficiency is investigated by considering a set of monoenergetic photon primaries. A test geometry consisting of a box of crystalline alanine with density $\rho_{\text{ala}} = 1.42\,\text{g}\,\text{cm}^{-3}$ irradiated with monoenergetic photons was created in `Geant4`. For each energy, the energy distribution of initial secondary electrons produced in the test detector was scored for 10^6 primary photons. This utilized geometry is somewhat unrealistic, however the computation time for scoring of secondary electrons is significantly lower than for a more realistic geometry, like the ones considered in Section 4.4 and Section 4.5. To test the agreement between this idealized geometry and a more realistic version, the initial energy distribution of secondary electrons was also calculated for some monoenergetic primary photons in the geometry used in Section 4.5, described by Waldeland et al. (2010). The number of primary photons used was increased to 10^8 for these calculations to get comparable statistics. Calculated secondary electron energy spectra for photon energies 50 keV, 100 keV, and 110 keV for both ge-

ometries are shown in Figure 5.1. Included in the figure is also the relative

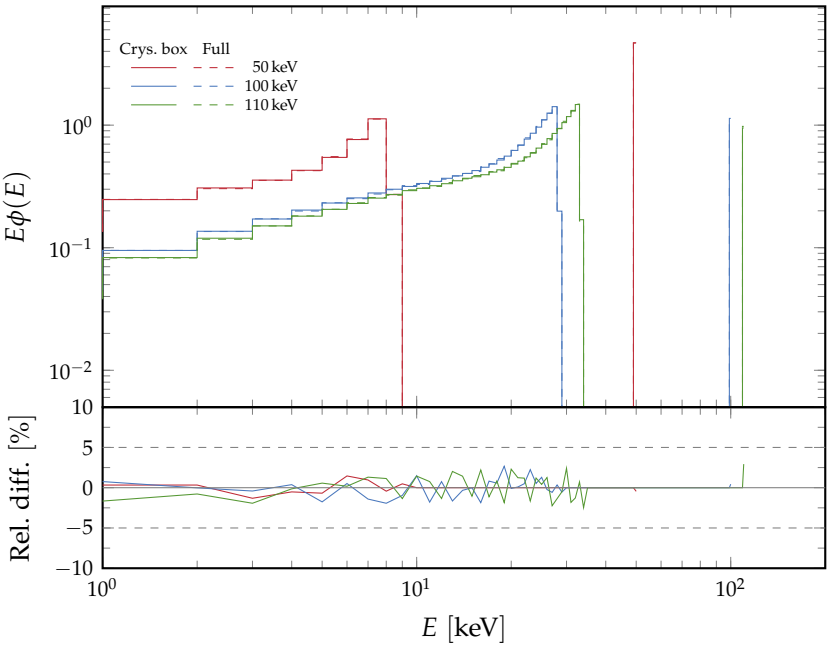

Figure 5.1: Calculated secondary electron energy spectra for monoenergetic photon primaries in a test geometry consisting of a box of crystalline alanine and a more realistic 'full' geometry. See body text for details.

difference between the energy distribution from the two applied geometries. Excellent agreement is observed between the two cases, implying that the contribution to the secondary electron spectrum from electrons produced in the surrounding material is negligible for these energies. The general appearance of the spectra is a bit peculiar compared to what is observed for primary x-ray spectra. The single peak in each spectrum located at the primary photon energy is due to electrons produced by photoelectric effect. The peak intensity decreases for higher energies as the Compton effect becomes the more dominant process for ionization of the medium. The sharp edge of the lower energy part of the spectra correspond to the maximum allowed energy of Compton electrons, 8.2 keV, 28.1 keV, and 33.1 keV for the 50 keV, 100 keV, and 110 keV photons, respectively. The empty region between the Compton edge and the photoelectrons is typically not present in secondary electron spectra produced by primary photon spectra, since the continuous primary photon energy distribution allows for different locations of the Compton edges and photoelectron peaks. However, for hard-filtered x-ray and/or low energy x-ray beams, this effect may still be present (see e.g. Figure 7 in Paper IV).

The calculated secondary electron spectra for monoenergetic photons were folded with the microdosimetric distributions for monoenergetic electrons as described in Section 4.4, and the relative efficiency is calculated according to Equation (4.17). The calculated relative efficiency of an alanine pellet dosimeter, with $2\sigma_\alpha$ model uncertainty, as a function of the primary photon energy is shown in Figure 5.2.

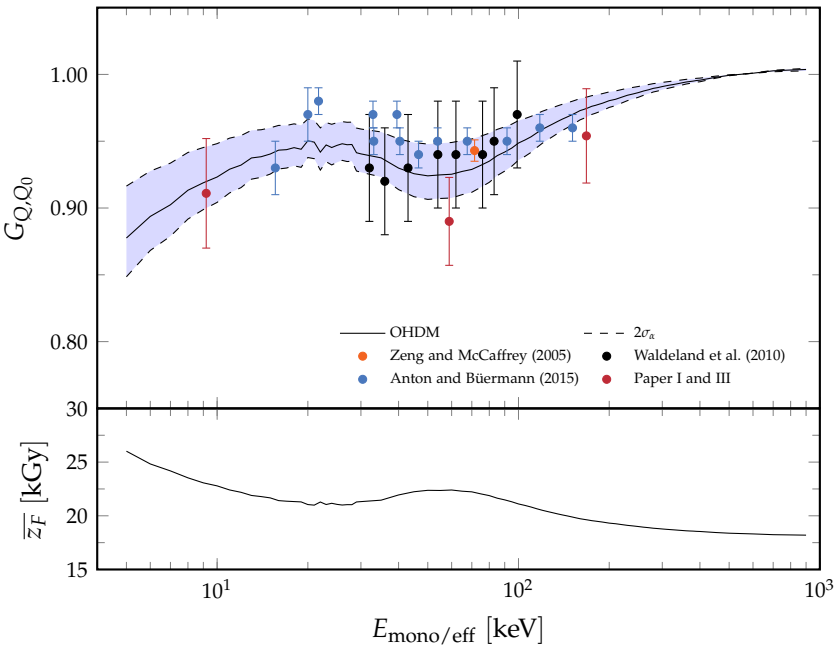

Figure 5.2: *Top:* Relative efficiency G_{Q,Q_0} calculated with the microdosimetric OHDM for monoenergetic primary photons. Calculations done using model parameters $d = 10\,\mathrm{nm}$ and $\alpha = 2.86 \times 10^{-5}\,\mathrm{Gy}^{-1}$. Dashed lines represent $2\sigma_\alpha$ model uncertainty. *Bottom:* The mean specific energy for target diameter $d = 10\,\mathrm{nm}$.

Also shown is the mean specific energy calculated according to Equation (4.7). All model calculations are done using the optimal parameter set determined in Section 4.5. The mean specific energy is a measure for how localized the dose deposition occurs, and as such it may not come as a surprise that it is directly correlated to the relative detector efficiency. Local and opposite extrema are observed for the relative efficiency and the mean specific energy at roughly 20 keV and 50 keV. These local extrema occur as the fraction of secondary electrons produced by Compton effect increases. These electrons have much lower energies than photoelectrons for the same primary photon

energy. The low energy electrons have higher linear energy transfer (LET) and thus exhibit a more localized dose deposition.

Literature values for experimentally determined relative efficiency are shown on top of the model calculations as a function of the effective energy of the primary photon beam (Zeng and McCaffrey 2005; Waldeland et al. 2010; Anton and Büermann 2015; Hjørringgaard et al. 2020). Unpublished data from Paper III is also included. The literature data obtained from Anton and Büermann (2015) is not listed directly in their paper, but is determined by taking the ratio of the relative response to the MC calculated dose ratios (Table 6 and Table 7 of their paper). In general, good agreement is obtained between the model calculations and literature data for this somewhat simplified comparison – the overall trend in the experimental data is reproduced by the model calculations, as well as the local extrema of the model appear to be present in the experimental data also.

As discussed before, it is not obvious that a single beam qualifier like the effective energy of the x-ray beam is sufficient to characterize the variation of the relative efficiency of the dosimeter. Therefore, some of the discrepancies between model calculations and experimental data may simply be due to the fact that other beam parameters have to be taken into account.

5.2 Linearity Index

The calculated response function $R(D)$ and linearity index $f(D)$ of an alanine pellet dosimeter irradiated in the HDRL cobalt-60 Gammacell and by monoenergetic 10 keV photons is shown in Figure 5.3. As discussed previously, the relative efficiency of a dosimeter irradiated in beam quality Q with respect to reference beam quality Q_0 is, for low doses, the ratio of the slopes of the respective response functions, see e.g. Equation (4.16). It is important to note that the dose considered here is the dose to detector material, not water. The ratio of slopes for the two response functions, in the linear low dose region, is therefore exactly the the relative detector efficiency shown in Figure 5.2.

The decrease in induced response per dose for low energy photons directly results in an increase in dose to detector required for saturation of response, as shown in the bottom part of Figure 5.3. The effect is however small and should not be of importance for most routine applications.

5.3 Set of X-ray Spectra

A variety of x-ray tube HVs can have the same HVL (and thus effective energy according to Equation (2.1)) depending on the filtration thickness and materials, anode material and angle, etc. Despite the identical HVL the spectral distributions are thus different, resulting in different secondary electron spectra as well. The dependence of the relative dosimeter efficiency on other beam characteris-

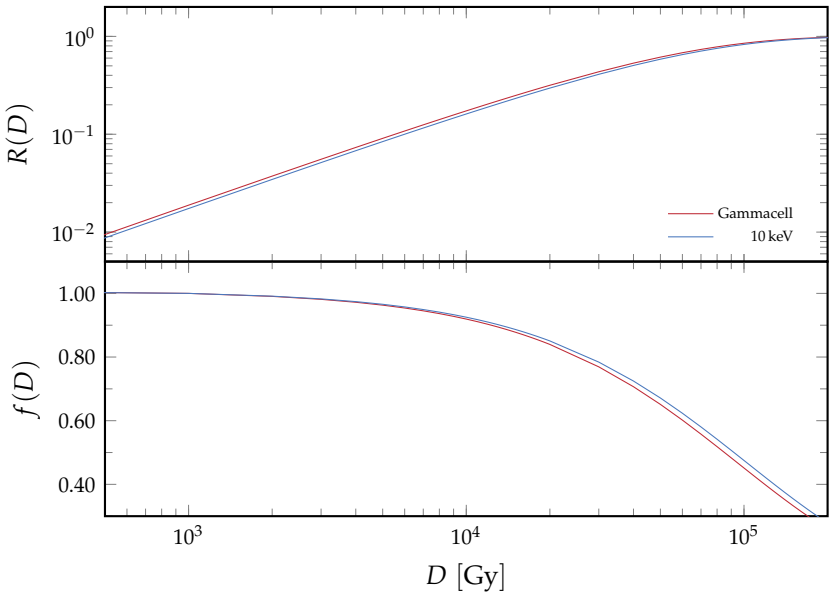

Figure 5.3: *Top:* Calculated response function $R(D)$ for an alanine pellet dosimeter in the HDRL cobalt-60 Gammacell (red) and in a monoenergetic 10 keV photon field (blue). *Bottom:* Linearity index $f(D)$. Calculattions are done using the microdosimetric OHDM with model parameters $d = 10\,\text{nm}$ and $\alpha = 2.86 \times 10^{-5}\,\text{Gy}^{-1}$.

tics should therefore be characterized. For this purpose, a set of x-ray spectra with HV in the range 40 kV to 300 kV with varying filtration was produced using the `SpekCalc` software. The range of the HVs and HVLs was chosen to cover the range of variations in these parameters reported by North American clinics (see Figure 2 of Ma et al. 2001). This range is chosen since it gives an indication of the beam quality range for which a characterization of the relative detector efficiency would be of importance.

In general, the x-ray spectra were calculated using anode angle 30°, 1 mm beryllium filtration, and 1000 mm of air. The variation in HVL was obtained by varying the thickness of an additional aluminum or copper filtration of the beam. The set of x-ray spectra was divided into two groups – an LE set ranging from 40 kV to 170 kV, where the additional filtration added was aluminum, and an ME set ranging from 100 kV to 300 kV where the additional filtration was copper.

Initial secondary electron spectra was calculated using the same irradiation geometry and alanine pellet size and composition as was used for fixing the free parameters of the model in Section 4.5. This geometry is based on the

information from Waldeland et al. (2010). The calculated relative efficiency of the alanine pellet dosimeter for these beam quality ranges are shown in Figure 5.4 and Figure 5.5 respectively.

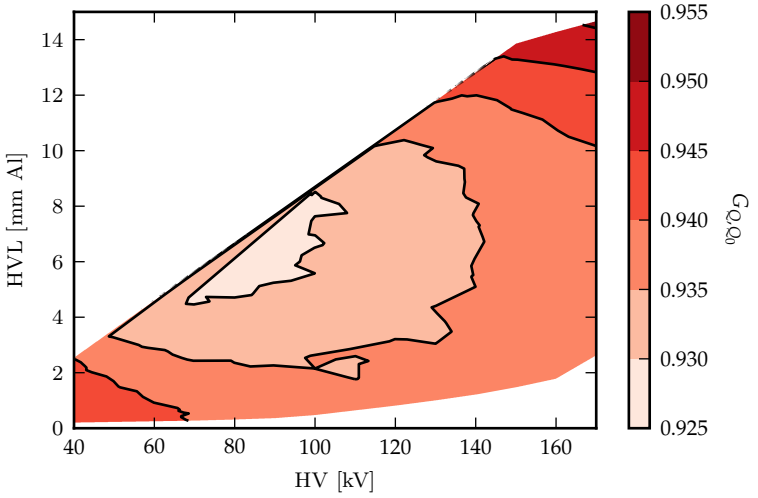

Figure 5.4: Relative efficiency calculated using the microdosimetric OHDM for a set of LE x-ray spectra obtained using the `SpekCalc` software. The model parameters used for the calculation is $d = 10\,\text{nm}$ and $\alpha = 2.86 \times 10^{-5}\,\text{Gy}^{-1}$.

For the LE set in Figure 5.4 the relative efficiency varies between roughly 5.0 % and 7.0 %, with a local minimum around HV 100 kV and HVL 8 mm of aluminum. An HVL of 8 mm of aluminum corresponds to an effective energy of approximately 50 keV, which is exactly the location of the local minimum of relative efficiency for monoenergetic photons shown in Figure 5.2. Overall, the range of HVLs shown in Figure 5.4 correspond to effective energies in the range of 15 keV to 90 keV.

For the ME set in Figure 5.5 the relative detector efficiency is steadily increasing for increasing HV and HVL. For HVLs above 2 mm of copper the variation in relative efficiency is practically determined by the HVL. The effective energies corresponding to the range in HVLs in the medium energy set is between 45 keV to 200 keV corresponding to the steadily increasing part of Figure 5.2 for energies above the local minimum.

The relative efficiency calculated for the two sets of x-ray spectra shown in Figure 5.4 and Figure 5.5 is presented as a function of the HVL for all HVs in Figure 5.6. A third order polynomial is fitted to each set respectively, and the residuals is shown in the bottom part of Figure 5.6. In general the residuals are within 0.5 %, however for the low HVL part of the medium energy set the residuals increase to around 1 %, due to a variation in the calculated relative

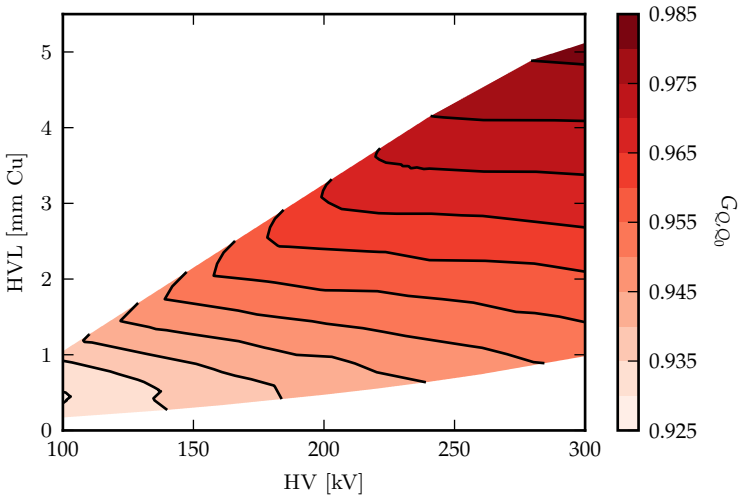

Figure 5.5: Relative efficiency calculated using the microdosimetric OHDM for a set of ME x-ray spectra obtained using the `SpekCalc` software. The model parameters used for the calculation is $d = 10\,\text{nm}$ and $\alpha = 2.86 \times 10^{-5}\,\text{Gy}^{-1}$.

Table 5.1: Fit to the relative response as a function of HVL for the two sets of primary x-ray beam qualities. The fit is of the form $G_{Q,Q_0} = \sum_{i=0}^{n} a_i \cdot \text{HVL}^i$.

Energy range	HVL unit	a_0	a_1	a_2	a_3
Low	mm Al	0.943	-3.21×10^{-3}	2.73×10^{-4}	-1.19×10^{-6}
Medium	mm Cu	0.927	1.90×10^{-2}	-2.40×10^{-3}	1.51×10^{-4}

efficiency of 2 % for the same HVL. The polynomial regression thus be used to estimate the relative efficiency of the alanine pellet dosimeter in kV x-ray fields with known HVL. The coefficients of the polynomial regression is listed in Table 5.1.

5.4 Relative Response Calculation

It is important to keep in mind that the decrease in relative detector efficiency is not the only factor to affect the response of the dosimeter in kV x-ray fields relative to cobalt-60 reference fields. As discussed in Chapter 3 the ratio of dose to dosimeter material D_{dos} to dose to water D_{w} is also energy dependent. A full characterization of the energy dependence of the response of the alanine pellet dosimeter in kV x-ray fields should therefore include both effects.

Taking the two sets of x-ray spectra discussed in the previous section as a

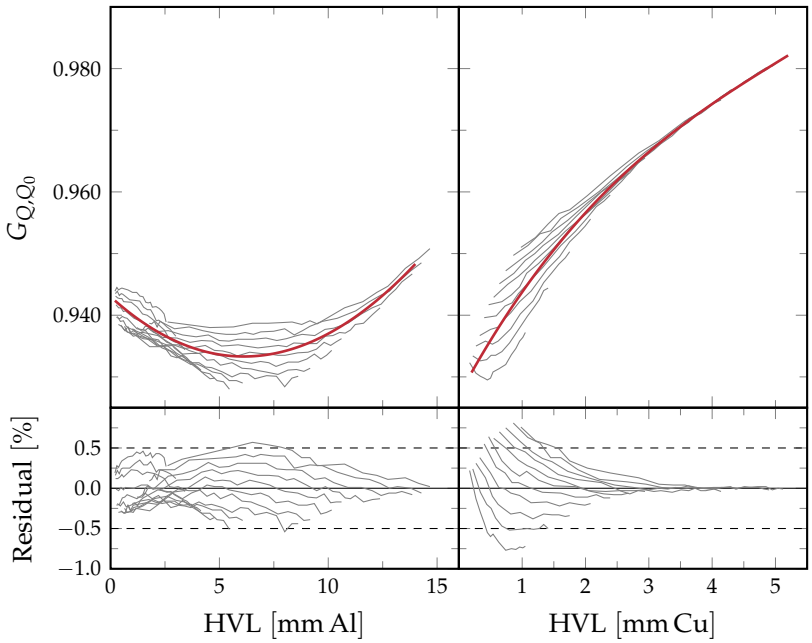

Figure 5.6: *Top:* Model calculated relative detector efficiency as a function HVL (gray) for the LE (left) and ME (right) sets of x-ray spectra. A third order polynomial fit to each set is carried out (red). *Bottom:* Residuals of the polynomial fit.

starting point, the ratio of doses in the x-ray qualities relative to a cobalt-60 reference H_{Q,Q_0} can be MC calculated. For this purpose, the `dosrznrc` usercode of the `EGSnrc` MC software is used (Kawrakow et al. 2000). Here a standard geometry consisting of an alanine pellet (based on the Harwell pellet dimension and composition) placed at 2 cm depth in a water phantom is constructed for calculating D_{dos}. D_{w} is obtained by changing the dosimeter material to water and scoring the dose in the same volume. For dose ratio calculation for the cobalt-60 Gammacell the `g` usercode was used (see e.g. Paper I). For all x-ray calculations a parallel beam was used. The calculated H_{Q,Q_0} values for the low and medium energy set of x-ray spectra in this generic MC geometry is shown in Figure 5.7 against the effective energy of the x-ray spectra. Also shown is literature data for the relative response of alanine pellet dosimeters in kV x-ray fields, plotted as a function of the effective energy of the beam. The literature values for relative response is included to illustrate the discrepancy between between pure dose ratio considerations and the observed energy dependence of the dosimeter response.

Combining the effects of dose ratio energy dependence and relative effi-

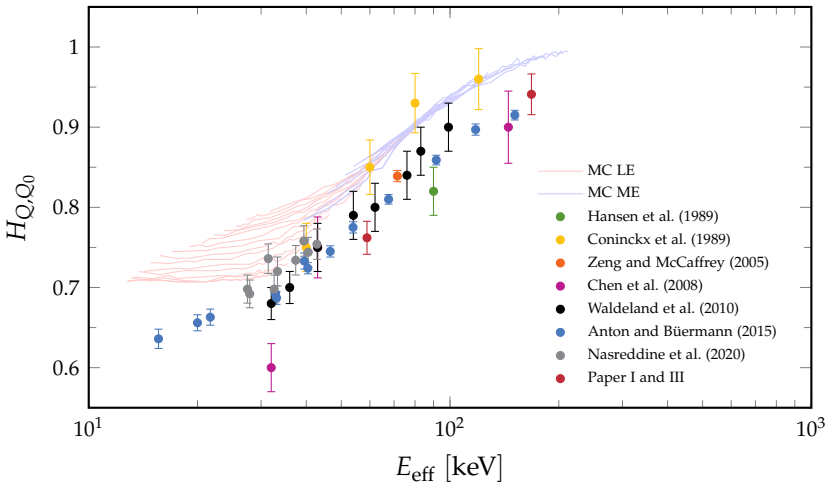

Figure 5.7: MC calculated relative dose ratios H_{Q,Q_0} using sets of low (red lines) and medium (blue lines) energy x-ray spectra. Data points represent literature values of the relative response F_{Q,Q_0}.

ciency of the dosimeter, see Equation (3.8), a model predicted value of the relative response for the two sets of x-ray spectra can be obtained. The calculated relative response for the LE and ME x-ray sets are shown in Figure 5.8 as a function of effective energy. Also shown is literature values for the relative response for comparison. In the same manner as in Figure 5.6 a polynomial regression is done for each set of calculated F_{Q,Q_0} values. Good agreement between model calculation and experimental data is observed for effective energies above 30 keV. In the very low energy regime the model calculation overestimates the relative response, and the discrepancy is not resolved by the spread in relative response introduced by the variation in beam quality in the model calculations.

A factor that could conceivably resolve this discrepancy is the fact that dose gradients are not necessarily constant for these low energy irradiations, as was seen for the 40 kV irradiation in Chapter 3. If dose gradients are constant then the EPR response measured corresponds to the dose in the center of the pellet Anton, Hackel, et al. (2015). MC calculations of the dose distribution within the alanine pellet dimensions were carried out for identical geometry as was used for the calculation of H_{Q,Q_0} for the two sets of x-ray spectra. No significant deviation from the assumption of constant dose gradient was however observed for any of the individual LE beam qualities. Anton and Büermann (2015) assumes constant dose gradient for their low energy measurements, however, does not specify how this is validated.

Another factor that may influence the discrepancy is the choice of geometry

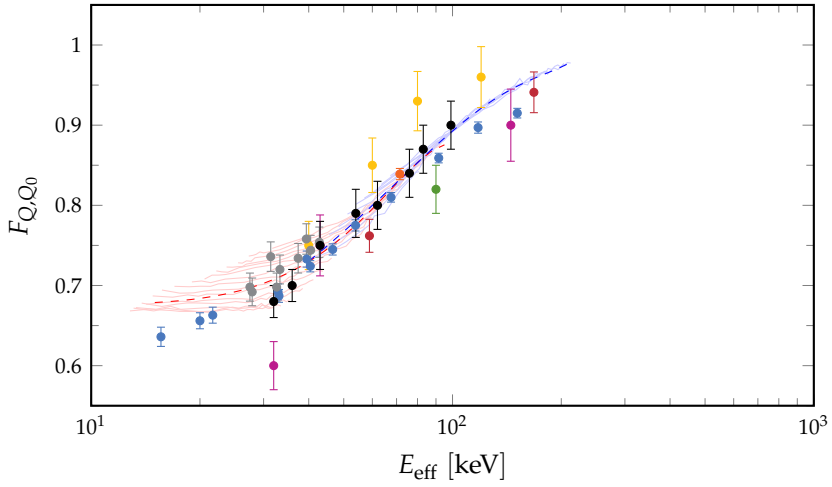

Figure 5.8: The relative response F_{Q,Q_0} of an alanine pellet dosimeter irradiated in kV x-ray fields calculated by combining the relative efficiency G_{Q,Q_0} from Figure 5.6 and the relative ratio of doses H_{Q,Q_0} from Figure 5.7. Data points represent literature values for F_{Q,Q_0} (see 5.7 for legend).

for the model calculations. The low energy (TW) set of Anton and Büermann (2015) is measured at the phantom surface, while the model calculations depicted in Figure 5.8 is for alanine pellets positioned at 2 cm depth in a water phantom.

Chapter 6

Alanine Dosimetry for Low Energy X-rays

With the increasing demand for replacement of radioactive sources by small self-shielded low energy x-ray irradiators, and taking into account the energy dependence of commonly used transfer dosimetry systems, a consensus on the dosimetric approach is needed. A general approach for using alanine dosimetry in industrial low energy x-ray fields, taking blood irradiators as a starting point, is described in this chapter. The goal is to determine a quality correction factor k_Q to be applied to dose measurements based on a dose-to-water calibration obtained by cobalt-60 irradiation. It is desirable that laboratories offering dose measurements and calibration services for low energy x-ray facilities use the same k_Q factor for the same effective energies in order that traceable dose measurements from these laboratories are based on the same correction.

In the following chapter specifications of commercially available blood irradiators will be described, with focus on the difficulties that lack of information on the x-ray field entails on the application of an alanine pellet dosimetry system. A general approach for the application of literature data on the relative response of alanine pellet dosimeters will be described including estimation of uncertainty. Furthermore, a schematic traceability chain and associated uncertainty budget for this approach are shown and discussed.

Further work towards a consensus on the k_Q factor for low energy x-ray dosimetry using alanine is needed, and a collaboration on this subject between DTU Health and NPL has been initiated.

6.1 Blood Irradiation

Before transfusion involving certain immunocompromised patients, blood products are irradiated for inactivation of viable lymphocytes. This process helps prevent transfusion associated graft-versus-host disease (GVHD). While GVHD is rare, it is fatal in approximately 90 % of cases (Greenbaum 1991; EDQM 2015). Traditionally gamma irradiators consisting of sealed cesium-137 radionuclides have been used, but the potential of misuse of radionuclides and the corresponding increase in price and difficulty of purchasing has encouraged

an increasing demand for x-ray alternatives (Dodd and Vetter 2009).

Guidelines for the irradiation of blood products state a typical required dose range of 25 Gy to 50 Gy, where 50 Gy is an upper limit to avoid damaging other cell components (EDQM 2015). Measurements of absorbed dose are typically carried out within a blood equivalent volume with the intent of determining the distribution of absorbed dose within the irradiated volume. Measurements of dose distribution is typically carried out in a polystyrene phantom, which is considered blood equivalent for cesium-137 photon energies (ISO/ASTM 51939 2017). Different approaches are used to ensure uniform dose delivery to the product, mainly rotation of the product or multiple radiation sources placed around the product.

Commercial self-shielded x-ray blood irradiators are available from several manufacturers, however information on x-ray tube specifications is not easily available. In Europe and North America, the most notable blood irradiators are manufactured by Rad Source Technologies and Best Theratronics. The Rad Source Technologies blood irradiator RS 3400 consists of six canisters that rotate a central x-ray source. The x-ray source consists of a long filament surrounded by a cylindrical target material, emitting photons in all directions orthogonal to the filament. Other irradiators from Rad Source Technologies use the same x-ray tube technology, for instance the RS 2400 designed for Sterile Insect Techniques (SITs). A characterization of the RS 2400 x-ray tube carried out by Wagner et al. (2009) indicated an effective energy of the x-ray tube of approximately 88 keV, for a HV of 150 kV, using aluminum as attenuating material. The HV is adjustable, and as such the effective energy is not a fixed value for the tube. Best Theratronics[1] have two available blood irradiators, the Raycell Mk1 and Mk2. The Raycell Mk2 consists of two opposing x-ray tubes with HV of 160 kV resulting in an average photon energy between 60 keV and 80 keV.

Alanine pellet dosimeters are recommended for both reference and routine dosimetry in blood irradiation by ISO/ASTM 51939 (2017). However, as discussed in Section 3.1.3, several experimental studies have been carried out during the last few decades, characterizing the energy dependence of the alanine pellet dosimeter in low energy x-ray fields. Therefore, for use of the alanine pellet dosimeter as a routine dosimetry system for blood irradiators, agreement on how to apply a quality correction factor to the cobalt-60 calibrated dose measured by alanine pellet dosimeters should be reached by institutes providing routine dosimetry services using alanine pellet dosimeters.

6.2 Application of Literature Data

Several authors have investigated the energy dependence of the alanine pellet dosimeter in low energy x-ray fields. A brief description of the available literature data was given in Section 3.1.3. For the evaluation of applicable values of

[1] www.theratronics.ca/

the relative response for use in dosimetry for x-ray blood irradiators different approaches concerning inclusion of literature data may be considered. A first approach would obviously be to include all available data. This approach would include a rather large spread in relative response, primarily due to the inclusion of data from Coninckx et al. (1989) and Chen et al. (2008) where the values for the relative response, and associated uncertainty, can only be estimated from graphs. Therefore, to filter the data, it is chosen to use only recent data, where exact values of the determined relative response with stated uncertainty, determined using dose to water in a cobalt-60 field as reference. Furthermore, only data sets including beam qualities in the relevant effective energy range energy range for dosimetry in this type of x-ray irradiator is applied. The relevant effective energy range is estimated to be between 50 keV and 100 keV. Excluding literature data on this basis leaves the more recent data by Waldeland et al. (2010), the TH-series from Anton and Büermann (2015), and the data presented in Paper III and described in Chapter 3, see Figure 6.1.

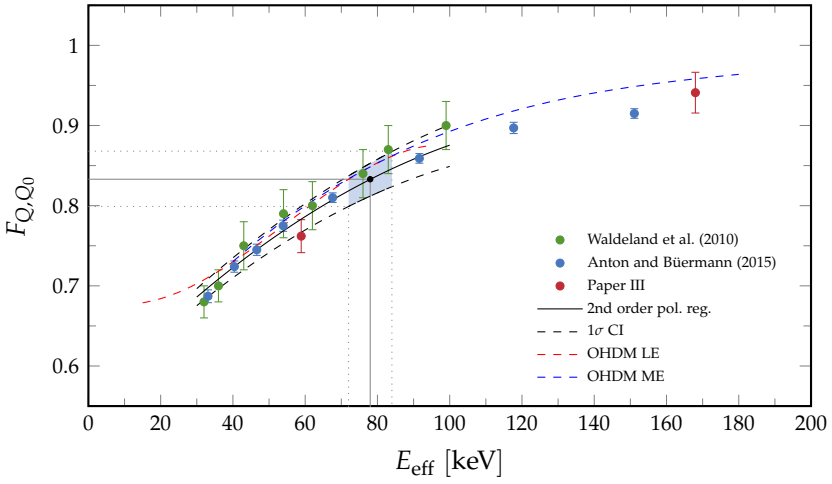

Figure 6.1: Selected literature values for the relative response of alanine pellet dosimeters irradiated in low energy x-ray fields.

The relationship between relative response and effective energy in the region of interest is determined from the literature data by performing a 2nd order polynomial regression, weighted by a factor of $1/u^2$ where u is the $k = 1$ uncertainty on the relative response, to the combined data. The uncertainty on the value of the relative response determined from the regression analysis is estimated by the 1σ-confidence bond. The regression and confidence band is also shown in Figure 6.1.

Also shown in Figure 6.1 are the calculated values of the relative response for the two sets of x-ray spectra from Figure 5.8 described in Chapter 5. The

fitted and model calculated curve follow the Anton and Büermann (2015) and Waldeland et al. (2010) data, respectively. This is hardly surprising since the fitting procedure includes weighting with the inverse of the uncertainties, favoring the Anton and Büermann (2015) data, while the free parameters of the model is determined using the Waldeland et al. (2010) data. The model calculations of the relative response shows very little variation for a specific effective energy. This prediction encourages the use of effective energy as the sole beam qualifier for determining the relative response from literature data. Based on these observations, it is assumed that traceable dosimetry can be established by using literature data on the relative response to determine a quality correction factor.

6.3 Estimating the Relative Efficiency

The main challenge in estimating the relative efficiency of alanine pellet dosimeters in these small self-shielded irradiators is the determination of effective energy of the x-ray beam. Information about the x-ray tubes is scarce, and thus estimation of the effective energy may be flawed. Wagner et al. (2009) measured the effective energy of the RS 2400 irradiator, for SIT, using both aluminum and copper as attenuating material. The details about how the measurements was performed is not clear, however values of 88.5 keV and 65.8 keV were obtained using the aluminum and copper filtration, respectively. Effective energies determined for x-ray beams of the same HV of 150 kV as used by Wagner et al. (2009) indicate a somewhat lower effective energy – $E_{\text{eff}} = 71.5$ keV by Zeng and McCaffrey (2005), $E_{\text{eff}} = 76$ keV by Waldeland et al. (2010), and $E_{\text{eff}} = 67.6$ keV by Anton and Büermann (2015).

Due to the lack of information regarding the beam specifications in these types of fields, a general effective energy can be chosen as the average of the limiting values of effective energies present in literature, with the lower limit $E_{\text{eff}}^{\text{L}} = 67.6$ keV and upper limit $E_{\text{eff}}^{\text{U}} = 88.5$ keV, obtaining a mean effective energy

$$\overline{E}_{\text{eff}} = \frac{E_{\text{eff}}^{\text{U}} + E_{\text{eff}}^{\text{L}}}{2} \approx 78\,\text{keV}. \tag{6.1}$$

Assuming a rectangular distribution between the limiting values an uncertainty $u_{\overline{E}_{\text{eff}}}$ can be estimated by

$$u_{\overline{E}_{\text{eff}}} = \frac{E_{\text{eff}}^{\text{U}} - E_{\text{eff}}^{\text{L}}}{2 \cdot \sqrt{3}} \approx 6.0\,\text{keV}, \tag{6.2}$$

with relative uncertainty

$$\frac{u_{\overline{E}_{\text{eff}}}}{\overline{E}_{\text{eff}}} = 7.7\,\%. \tag{6.3}$$

Using the polynomial regression in combination with the mean effective energy yields an value for the relative response of $F_{Q,Q_0} = 0.83$ with an uncertainty of 2.5 % estimated from the 1σ-confidence band. To include the uncertainty of the effective energy on the estimate of the relative response, the confidence band value at $\overline{E}_{\text{eff}} \pm u_{\overline{E}_{\text{eff}}}$ was evaluated, see Figure 6.1, to determine the lower and upper 1σ limiting values F^{L}_{Q,Q_0} and F^{U}_{Q,Q_0}. The combined uncertainty on the relative response is then determined by

$$u_{F_{Q,Q_0}} = \frac{F^{\text{U}}_{Q,Q_0} - F^{\text{L}}_{Q,Q_0}}{2}, \tag{6.4}$$

yielding an estimate on the relative response of

$$F_{Q,Q_0} = 0.83 \pm 0.034. \tag{6.5}$$

Due to the limited information available, the uncertainty presented here for the relative response is an informed estimate rather than a rigorous calculation. The corresponding quality correction factor k_Q is the inverse of the relative response, resulting in

$$k_Q = 1.20 \pm 0.049. \tag{6.6}$$

The dose to water in the low energy x-ray field $D_{\text{w},Q}$ can then be calculated from the dose to water determined from a cobalt-60 calibration D_{w,Q_0} by multiplying with the quality correction factor as

$$D_{\text{w},Q} = k_Q D_{\text{w},Q_0}. \tag{6.7}$$

The traceability of a dose measurement in a low energy x-ray field, for instance a blood irradiator, is established by including the quality correction factor and associated uncertainty in an established traceability chain for the dose to water of alanine pellet dosimeters in a cobalt-60 reference field. A schematic of the traceability chain, with accumulated uncertainties based on the traceability for the Risø HDRL gammacells, for dose to water measurements in low energy x-ray fields using alanine pellet dosimeters is shown in Figure 6.2.

It should be noted that the final uncertainty on $D_{\text{w},Q}$ is dependent on the x-ray quality, and the available information on beam characteristics. If the effective energy of the x-ray field is well known, then the uncertainty on the measured dose decreases. Also the value of the effective energy itself influences the final uncertainty on the dose measurement since the gradient of the relative response changes with effective energy, see Figure 6.1.

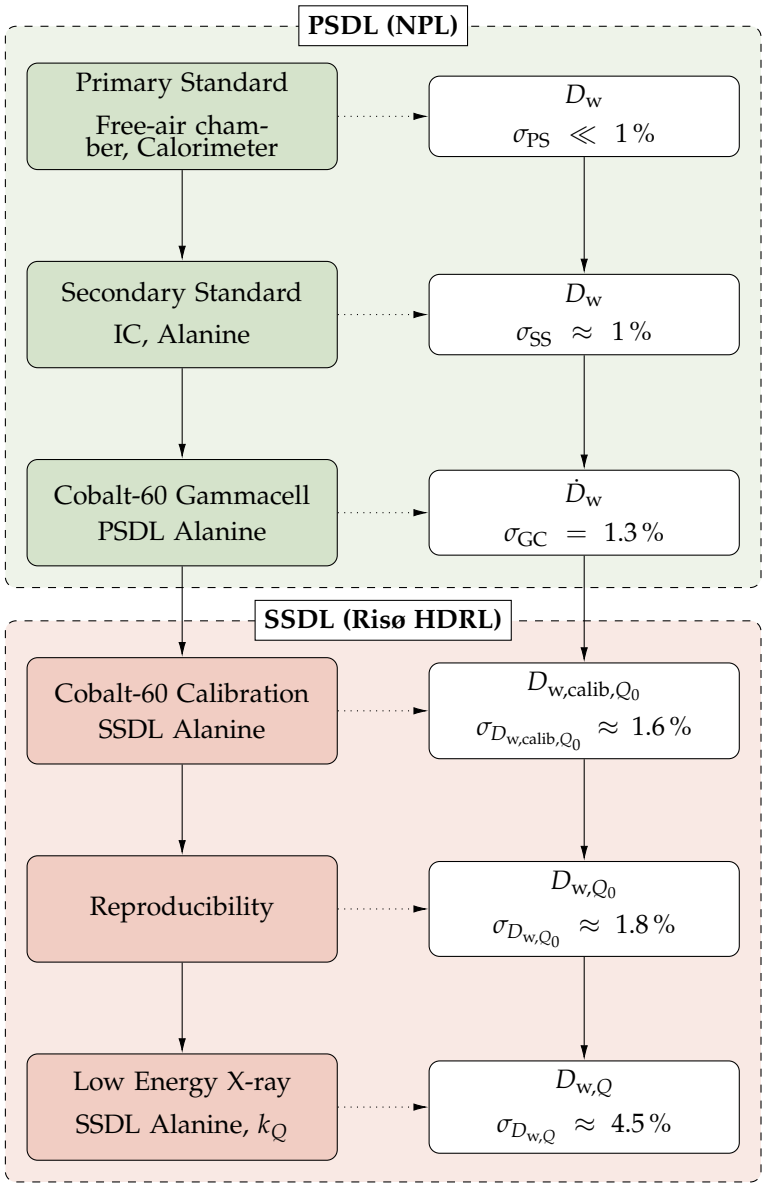

Figure 6.2: Schematic of a general traceability chain for dosimetry at low energy x-ray blood irradiation facilities with associated cumulated uncertainties. The stated uncertainties are related to the traceability chain for the Risø HDRL gammacells with traceability to the primary standard graphite calorimeter at NPL.

Chapter 7

Microbicidal Effectiveness of Low Energy X-rays

The radiation response, quantified by the dose-log survival curve, of spores of *Bacillus pumilus* subject to different radiation qualities have been studied in previous publications (Tallentire and Khan 1975; Tallentire, Miller, and Helt-Hansen 2010; Tallentire and Miller 2015). The beam qualities under investigation consisted of high and low energy electrons, high energy x-rays, and cobalt-60 gamma rays. Applications of low energy x-rays involving cell inactivation and potentially sterilization are being introduced to the market. An example is for decontamination of medicinal cannabis which is currently carried out using cobalt-60 gamma rays (Hazekamp 2016) while self-shielded x-ray units, similar to irradiators discussed in Chapter 6, are being made commercially available (for instance the Rad Source Technologies RS 420 emitter). It is therefore of interest to expand on the previous studies of the radiation response of *B. pumilus* spores to include low energy x-rays.

The radiation response of *B. pumilus* spores subjected to kV x-rays will be studied in the following chapter. Firstly, a description of the production of microbiological test filters, ensuring similar reference conditions for irradiations in all beam qualities, will be given, followed by the experimental procedure applied. Dose measurements were carried out by alanine/EPR dosimetry, following the procedure outlined in Chapter 6, assessing the validity of this approach.

The results presented in this chapter are based on Paper II.

7.1 Microbiological Test Filters

The microbiological test filters were produced in the same way as in the previous publications (Tallentire, Miller, and Helt-Hansen 2010; Tallentire and Miller 2015), with method based on the procedure described by Powers et al. (1957). A test filter consists of a known amount of microorganisms homogeneously placed on the surface of a cellulose acetate membrane. The exact procedure for the production of test filters is given in Tallentire, Miller, and Helt-Hansen

(2010), with a brief description of said procedure given below.

Spores was obtained from Crosstex as a suspension of *B. pumilus* spores (ATCC strain 27142 LOT PU140) in water containing 2.5×10^9 spores/cm^3. Extracts of the original suspension were used to produce diluted suspensions, so-called donor suspensions (DSs), containing concentrations of viable spores of *B. pumilus* ranging from 4×10^7 spores/cm^3 (DS 1) to 4 spores/cm^3 (DS 8). The spores were mounted on the cellulose acetate membrane using a sintered glass filter funnel, using 10 cm^3 of individual DSs, obtaining test filters containing number of spores ranging from 4×10^1 spores/filter to 4×10^8 spores/filter. The range of viable spores present on the test filters is chosen such that the dose-log survival curve will cover several log cycles of inactivation. After the spores have been mounted on the membrane, they were transferred to an open Petri dish, placed in a laminar flow bench for drying, and the spores were eventually stored in sealed Petri dishes in a refrigerator until use. An overview of the test filters is given in Table 7.1.

Table 7.1: Overview of test filters produced for x-ray irradiations, showing test filter name and suspension of *B. pumilus* spores, the number of spores present on the test filter, the desired log surviving fraction after irradiation, and the dose required for obtaining the desired log surviving fraction S (determined from Figure 7.1.

Test filter	Spores on filter	$\log S$	D [kGy]
DS 8	4×10^1	0	0.0
DS 7	4×10^2	-1	2.5
DS 6	4×10^3	-2	4.3
DS 5	4×10^4	-3	5.8
DS 4	4×10^5	-4	7.2
DS 3	4×10^6	-5	8.4
DS 2	4×10^7	-6	9.5
DS 1	4×10^8	-7	10.6

The DS 8 test filter is used as a reference point for calculating the surviving fraction S as

$$S = \frac{(\text{mean colony count})_{\text{DS}}}{(\text{mean colony count})_{\text{DS 8}}} \times \text{conc. factor}, \tag{7.1}$$

where the concentration factor is the ratio of spore concentration of reference DS 8 to the DS under investigation. The mean colony count is the number of colony forming units present on the test filters post irradiation, after 24 h incubation. The incubation is carried out by placing the test filters on the surface of a tryptic soy agar medium and keeping it at a stable temperature of 32 °C.

To allow for valid comparison of the microbicidal effectiveness of different beam qualities, it is important to ensure identical reference conditions for the

spores. This was obtained by placing individual test filters on top of a hydrated filter pad inside a sealed 9 cm polymer Petri dish. This combined geometry will be denoted a *test piece* in the following sections.

7.1.1 Test Filter Validity

Immediately following the production of test filters, and over the duration of a few weeks, a set of reference irradiations were carried out in the cobalt-60 gammacell 1 located at Risø HDRL to test the validity of the filter batch. Gammacell 1 has a dose rate of approximately 3.4 Gy min^{-1} at the reference position.

The dose rate to the test filters was measured using alanine pellet dosimeters placed in a similar geometry as is used for irradiation of test filters as test pieces. The geometry consisted of two stacked Petri dishes, each containing four alanine pellets placed on top of a filter pad. On top of the upper Petri dish was placed an additional alanine dosimeter (four pellets in a designated ABS holder). The Petri dishes were placed on top of a styrofoam cylinder to elevate them to the central vertical region of the gammacell sample chamber. Irradiation was performed with nominal dose of 2.0 kGy, and the measured dose was (2.20 ± 0.08) kGy (3.4 %) at $k = 2$. A 10 % correction to the nominal dose rate was therefore applied for determining the dose to test filters.

For irradiation of test pieces in the gammacell two test pieces were stacked on top of the same styrofoam cylinder used for the dose measurements. Exposure times were determined based on the survival functions from previous publications and the measured dose rate. Following irradiation, the test filters were incubated, and the number of colony forming units was counted. To estimate the uncertainty on the surviving fraction of spores, two test filters of equal DS were irradiated. The uncertainty is the evaluated based on the assumption that there is equal probability for the count of spores to be between the limiting values obtained by these two test filters. In this case the uncertainty is estimated by the average relative difference between the counts on the two filters divided by $\sqrt{3}$ (Sharpe et al. 2009).

The surviving fraction was calculated according to Equation (7.1), and the resulting dependence of the log surviving fraction on dose is shown in Figure 7.1, together with data obtained for irradiation in the gammacell for an old batch of *B. pumilus* test filters. The agreement between the two batches of test filters is well within the associated uncertainties on both dose and the surviving fraction of spores. It was therefore concluded that the produced batch of test filters were valid for comparison with data from the previous publications.

18 months elapsed from production of test filters until irradiation in an appropriate x-ray field was possible. Therefore, a separate set of irradiations at the Risø HDRL gammacell 3 were carried out, to ensure that the test filters were still reacting as intended. Gammacell 3 is a Nordion GC-220 with dose rate of approximately 85 Gy min^{-1} at the reference position. The dosimetric procedure carried out was identical to what was done for the irradiations in Gammacell 1.

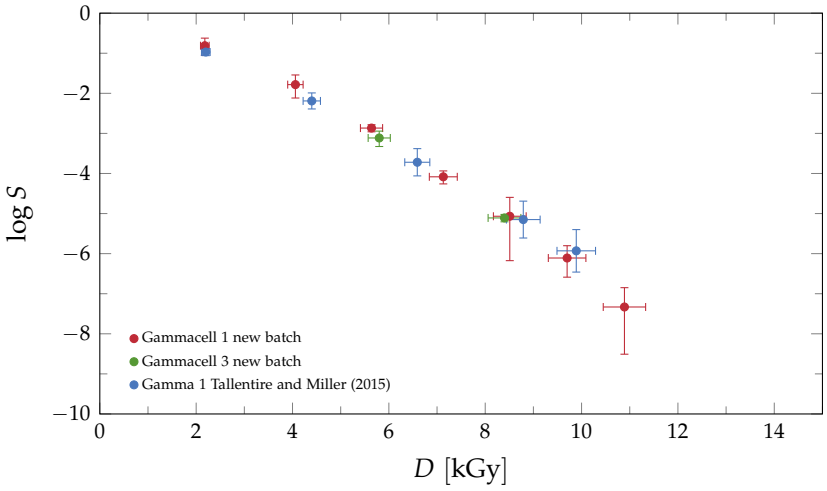

Figure 7.1: Surviving fraction of water hydrated *B. pumilus* spores subjected to radiation dose in a cobalt-60 gammacell. The surviving fraction from the new batch of test filters is compared to the surviving fraction of the gamma irradiations presented in Tallentire and Miller (2015). The error bars represent uncertainties at $k = 2$.

Only three test pieces (DS 3, DS 5, and DS 8 for reference) were used to verify the validity of the test filters. The survival curve for these irradiations is also shown in Figure 7.1. Good agreement is again observed, verifying the validity of the batch of test filters 18 months after production. Furthermore, it is noted that no effect due to differences in dose rate seems to be present.

7.2 X-ray Irradiations

X-ray irradiation of test pieces was carried out at ebeam Technologies, Comet, Flamatt Switerland, using a XBA-200/270H x-ray tube. This x-ray tube is a large surface emitter having an exit window width 40 mm and height 270 mm. The large window size allows for irradiation of several test pieces simultaneously – a great advantage since low energy x-ray emitters typically produce lower dose rates compared to e.g. electron beams. The design of the x-ray tube is based on the e-beam emitter available from ebeam Technologies, but with a tantalum transmission target replacing the titanium-foil window.

Little information was available concerning dose rates, homogeneity of the field, and HVL so a characterization of relevant beam parameters was necessary for evaluating the absorbed dose to test filters. The geometry used for irradiation of test pieces was as part of a stack of Petri dishes placed on a

turntable with central axis at 10 cm distance from the exit window of the x-ray tube. The turntable was used to ensure homogeneity of dose distribution across the test filters. The irradiation geometry will be described in greater detail in Section 7.2.2.

7.2.1 X-ray Beam Characterization

The characterization of the x-ray field relevant for the present experiment consisted on the determination of effective energy by measurement of the HVL and measurement of the homogeneity of dose distribution across test filters.

The homogeneity of dose distribution was investigated by measurements using Gafchromic HD-V2 film in a geometry simulating the irradiation of test filters. The geometry consisted of a stack of 14 Petri dishes, each with a sheet of Gafchromic HD-V2 film covering the bottom, placed on the turntable at 10 cm distance of the exit window of the x-ray tube. Analysis of the irradiated films was carried out using the RisøScan software (Helt-Hansen and Miller 2004). The result was an average variation in dosimeter response of 1.5 % across the dimensions of the test pieces.

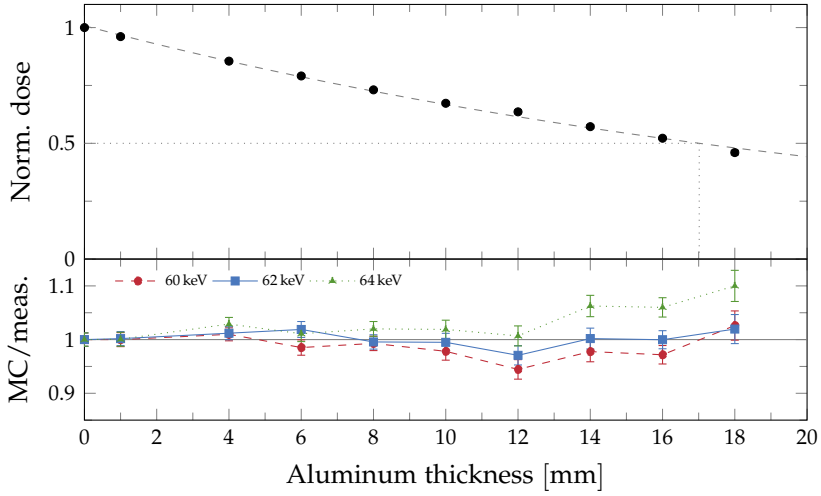

Figure 7.2: *Top:* Ionization chamber measurements of the attenuation of the x-ray beam by insertion of aluminum plates between the detector and source. *Bottom:* Ratio of MC calculated to measured attenuation for monoenergetic photon beams.

HVL measurements in the x-ray field was carried out using a PTW 23344 soft x-ray plane parallel ionization chamber. The ionization chamber was placed at the surface of a PTW 2962 PMMA phantom, with a 0.82 mm PMMA slab placed in front of the ionization chamber for build-up, with surface to exit window

distance 10 cm. Aluminum plates were placed between the ionization chamber and the x-ray tube to attenuate the beam. The normalized response measured as a function of the combined thickness of attenuating aluminum plates in this applied geometry is shown in Figure 7.2. The measured HVL in this geometry was approximately 17 mm of aluminum, which would correspond to an effective energy of roughly 120 keV by simple consideration of mass attenuation coefficients. The applied geometry does however differ significantly from the recommended approach for HVL measurements described in the AAPM TG-61 protocol for low energy x-ray dosimetry (Ma et al. 2001). Therefore the effective energy was instead estimated by MC calculation of the attenuation of monoenergetic photons using a calculation geometry approximating the actual irradiation geometry. The `flurznrc` usercode of the the `EGSnrc` MC software (Kawrakow et al. 2000) was used for the calculation. The irradiation geometry was approximated by by a cylindrical PMMA volume of diameter equal to the side length of the PTW 2962 phantom, with a air volume located at the position of the effective volume of the ionization chamber. Increasing thickness of aluminum was used to calculate the attenuation of the beam. The ratio of MC calculated to measured attenuation of the beam is shown in the bottom part of Figure 7.2 for three monoenergetic photon beams. Best agreement between calculated and measured attenuation is observed for photon energy $E_{\text{eff}} = 62\,\text{keV}$, having an average ratio of 1.002 with standard deviation 1.4 %. The determination of the effective energy by this approach is not ideal, and as such a conservative estimate of the uncertainty associated with this parameter of 5 % at $k = 1$ is adopted.

7.2.2 Irradiation Geometry and Dose Measurement Considerations

A geometry consisting of 14 Petri dishes stacked on the turntable was used for irradiation of test pieces in the 150 kV x-ray field. For each dose level two test pieces were irradiated and scored separately. Due to time considerations it was not feasible to irradiate the two sets of test filters containing the highest concentration of viable spores, and thus requiring the highest dose to obtain a countable number of colony forming units, DS 1 and DS 2. To ensure similar scatter conditions for all irradiated test pieces, only the central six Petri dishes of the stack were test pieces. The irradiation geometry is shown in Figure 7.3. Since the different test filters require different doses to obtain countable numbers of colony forming units, an irradiation schedule was planned in intervals to ensure dose levels in the order required. The required exposure times were estimated from measurements of the air kerma rate, using a NE2571 farmer type ionization chamber, at the reference 10 cm distance from the exit window. MC calculations of the ratio of dose to test filter to air kerma at the at reference position was then used to estimate the required exposure time.

The use of the NE2571 farmer type ionization chamber, having air kerma calibration traceable to PTB, was considered for dose measurements. However,

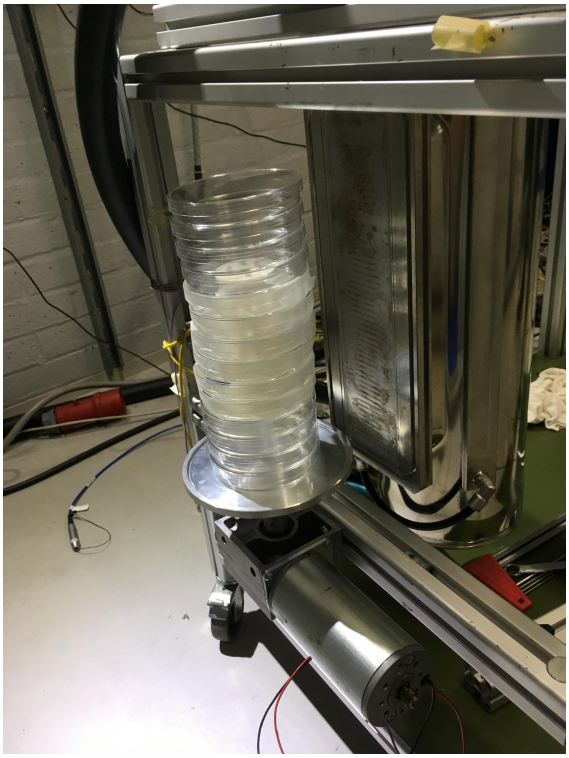

Figure 7.3: Picture of the irradiation geometry applied for x-ray irradiation of test pieces. A stack of 14 Petri dishes is placed on a turntable with central axis at 10 cm distance from the exit window of the x-ray tube. The content of the different Petri dishes in the stack is described in the text.

the available code of practices for ionization chamber dosimetry at low and medium energy x-rays (Aukett, Harrison, et al. 1996; Ma et al. 2001; Aukett, Burns, et al. 2005) deals with well-defined beams (typically circular field) for determining the dose to water at the surface of or 2 cm depth in a water phantom. The process of calculating the dose to water using the code of practices include determination of correction factors, e.g. backscatter factors, which are heavily dependent on field diameter and HVL. It is not clear how to appropriately and meaningfully select these correction factors from tabulated values.

7.2.3 Relative Response of Alanine Dosimeters

The dose to test filters was monitored during irradiation of test pieces by the use of both alanine film and pellet dosimeters, applying the approach described for kV x-ray dosimetry for blood irradiators using alanine pellet dosimeters

described in Chapter 6. The relative response of the alanine pellet dosimeter F^{P}_{Q,Q_0} determined based on literature data, for the effective energy $E_{eff} = 62\,keV$ of the x-ray beam, was determined to $F^{P}_{Q,Q_0} = 0.79 \pm 0.03$, resulting in a quality correction factor $k^{P}_{Q} = 1.26 \pm 0.04$ ($k = 1$).

No literature data on the relative response was available for the alanine film dosimeters. The quality correction factor to be applied to alanine film dosimeter measurements was determined by comparing the EPR response of alanine film and pellet dosimeters in the 150 kV x-ray field and the cobalt-60 reference field, respectively. Measurements in the 150 kV x-ray field were carried out by placing the pellet and film dosimeters, separately, at the surface of the PTW 2962 PMMA phantom, with surface to exit window distance 10 cm. The relationship between the EPR response measured by alanine film and pellet dosimeters, R^{F} and R^{P} respectively, is shown in Figure 7.4 for irradiation in the 150 kV x-ray field and the Risø HDRL gammacell 3. All irradiations are in the dose range 20 Gy to 200 Gy. The relative response of the alanine film dosimeter F^{F}_{Q,Q_0} is then

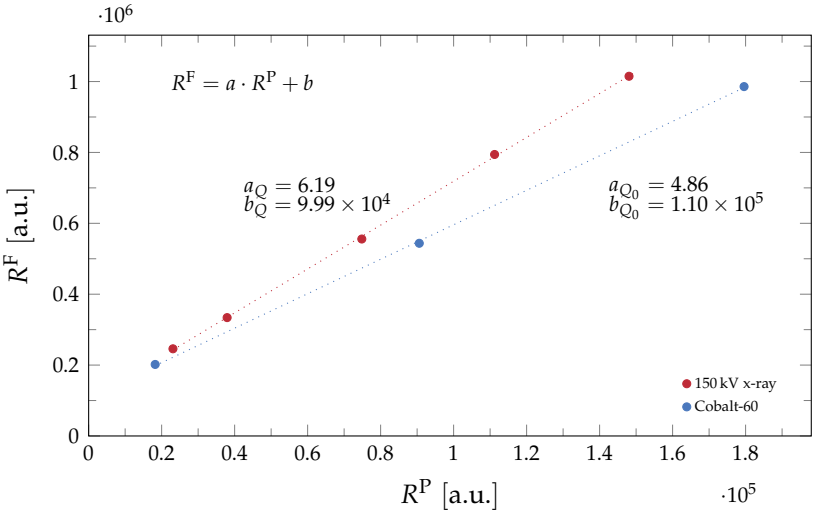

Figure 7.4: The EPR response of alanine film dosimeters R^{F} against alanine pellet dosimeters R^{P} for equal exposures in the 150 kV x-ray field and in a cobalt-60 reference field.

determined by correcting the relative response of the alanine pellet dosimeter by the ratio of the slopes a_{Q,Q_0}

$$F^{F}_{Q,Q_0} = a_{Q,Q_0} \cdot F^{P}_{Q,Q_0} = 1.01 \pm 0.05. \tag{7.2}$$

The corresponding quality correction factor is therefore $k^{F}_{Q} = 0.99 \pm 0.05$. The dose, to water, in the x-ray field $D_{w,Q}$ can then be determined from the product

of the quality correction factor and the cobalt-60 calibrated dose to water D_{w,Q_0} by

$$D_{w,Q} = k_Q \cdot D_{w,Q_0}, \tag{7.3}$$

for the alanine film and pellet dosimeters, respectively.

The use of alanine dosimeters during irradiation of test pieces allows for *in situ* dosimetry, directly monitoring the delivered dose to test pieces, not relying on dose rate measurements which may be vulnerable to fluctuations in the x-ray output. Furthermore, the alanine dosimeters are practical, and especially the film dosimeters can be placed at relevant positions in the irradiation geometry to monitor the dose.

7.2.4 Dose Measurement

Alanine dosimeters were added to the irradiation geometry for dose measurements during irradiation of test filters. The geometry consisted of 14 Petri dishes stacked on a turntable. Four alanine pellet dosimeters were placed on top of a dry filter pad in each of the two Petri dishes next to, on top and below, the central test pieces (see Figure 7.3). Three alanine film dosimeters were attached to the bottom of each of the test pieces to directly monitor the dose to each individual test piece. Only six test pieces could be irradiated simultaneously in this geometry, and since two test pieces of each suspension were included, irradiation of most test filters was fractionated. Between each fraction of dose, the alanine pellet dosimeters were replaced by blanks. The dose to test filters was then determined by the sum of dose measured with alanine pellet dosimeters from each fraction where the test piece was present in the stack. Since the alanine film dosimeters were attached to the test pieces individually, no summation of doses measured by film dosimeters was needed. A comparison of the measured dose by alanine film $D^{F}_{w,Q}$ and pellet dosimeters $D^{P}_{w,Q}$ during irradiation of test filters is shown in Figure 7.5. The doses measured by the alanine film dosimeters are on average 3.0 % lower than what was measured by the alanine pellet dosimeters. Within the uncertainties associated with individual dose measurements, the two dosimeters agree, however the discrepancy appears to be systematic.

An explanation for this small offset in dose is probably due to the difference in detector volume. For the determination of the relative response for the alanine film dosimeter in Section 7.2.3, the alanine films and pellets were irradiated with front face at equal distance from the x-ray tube exit window. The measured EPR response can be thought of as an average over the detector volume, and if there is a dose gradient through the dimensions of the dosimeter then the measured EPR response would not correspond to the surface dose. In the case of comparing alanine film and pellet dosimeter response, a dose gradient through the detector is expected, most notably for the pellet dosimeter having much greater dimensions. For proper comparison of EPR responses the

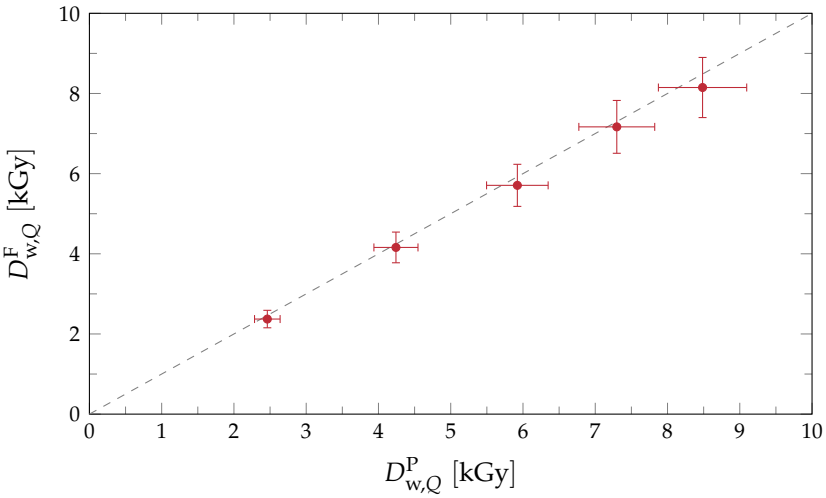

Figure 7.5: Doses to test filters measured by pellet $D^{P}_{w,Q}$ and alanine film $D^{F}_{w,Q}$ dosimeters. The error bars represent uncertainties at $k = 2$. The dashed gray line represents a slope of unity.

pellet response should therefore be corrected to the surface dose. A simple MC calculation of the dose gradient through the dimensions of the alanine pellet dosimeter was carried out using a 62 keV monoenergetic photon source. The result of this simple calculation was a correction to surface dose of roughly 2 %. Applying this correction to the EPR response would result in small reduction in F^{F}_{Q,Q_0} and thus a slight increase in k^{F}_{Q}, resulting in an increase the film dosimeter measured dose of approximately 1 %.

For the analysis of microbiological test filters, the dose determined by alanine pellet dosimeters was used. The dose measured by film dosimeters was used to verify that the individual test pieces has been irradiated to the desired doses.

7.3 Microbicidal Effectiveness

After incubation of test filters, the surviving fraction was calculated by the approach described in Section 7.1 using Equation (7.1). The use of DS 8 – DS 3 irradiated at suitable doses allowing countable numbers of colony forming units to grow on the incubated test filters. This approach made it possible for the dose-log survival curve to cover six log cycles of inactivation. The log surviving fraction of *B. puilus* spores irradiated at the 150 kV x-ray beam is shown in Figure 7.6 together with log surviving fraction after irradiations in cobalt-60 gammacells from Figure 7.1.

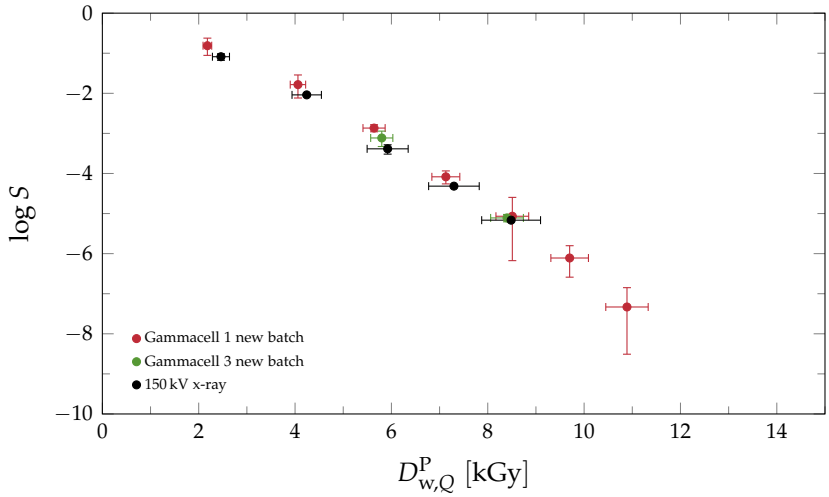

Figure 7.6: Log surviving fraction of *B. pumilus* spores after irradiation in a 150 kV x-ray field, and two cobalt-60 gammacells respectively. The error bars represent uncertainties at $k = 2$.

Excellent agreement is observed for inactivation of *B. pumilus* spores after irradiation at these beam qualities, under similar conditions for the spores. The D_{10}-value, the dose required for inactivation of 90 % of viable spores, was determined as $D_{10} = -1/a$ where a is the slope of a linear regression $\log S = a \cdot D + b$ performed on each individual set of survival data. The calculated D_{10}-values was (1.33 ± 0.12) kGy and (1.44 ± 0.10) kGy for the cobalt-60 gammacell and 150 kV x-ray irradiations, respectively.

Further comparison with data from the previous studies (Tallentire, Miller, and Helt-Hansen 2010; Tallentire and Miller 2015) shown in Figure 7.7, indicates that the inactivation of *B. puilus* spores due to irradiation in a 150 kV x-ray field is identical to the inactivation observed for high energy x-ray and low and high energy electron irradiations.

The slopes of linear regressions performed for all beam qualities shown in Figure 7.7 and the corresponding D_{10}-values are listed in Table 7.2. The values depicted in Table 7.2 differ slightly from the values presented by Tallentire, Miller, and Helt-Hansen (2010) even though the same data is used for the analysis. This is because the linear regression, used to determine the slope listed in Table 7.2, is weighted by the uncertainty in both dose and log surviving fraction.

The common radiation response independent on radiation quality determined in these studies can however only be considered valid on the basis of common irradiation conditions, established by the specially designed test

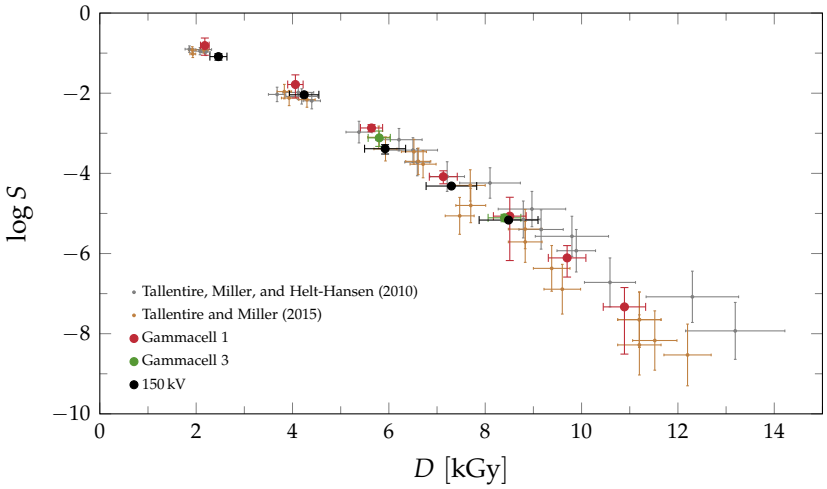

Figure 7.7: Log surviving fraction of spores of *B. pumilus* for beam qualities investigated in the present study, compared with literature data for cobalt-60, low and high energy electron irradiation (Tallentire, Miller, and Helt-Hansen 2010), and high energy x-rays (Tallentire and Miller 2015). The error bars represent uncertainties at $k = 2$.

Table 7.2: D_{10}-values for radiation qualities investigated in the present study and literature data from Tallentire, Miller, and Helt-Hansen (2010) and Tallentire and Miller (2015). Stated uncertainties are at $k = 1$

Beam	Quality	Slope, kGy^{-1}	D_{10}, kGy
Cobalt-60†		-0.65 ± 0.01	1.54 ± 0.04
electron†	80 keV	-0.63 ± 0.02	1.58 ± 0.05
electron†	100 keV	-0.61 ± 0.02	1.65 ± 0.05
electron†	10 MeV	-0.65 ± 0.03	1.54 ± 0.06
x-ray‡	6.6 MV	-0.79 ± 0.05	1.27 ± 0.08
x-ray‡	6.6 MV	-0.78 ± 0.05	1.27 ± 0.08
x-ray‡	7 MV	-0.78 ± 0.04	1.29 ± 0.06
Cobalt-60		-0.75 ± 0.03	1.33 ± 0.06
x-ray	150 kV	-0.69 ± 0.02	1.44 ± 0.05

† Tallentire, Miller, and Helt-Hansen 2010
‡ Tallentire and Miller 2015

piece. Applying the process outlined in Chapter 6 for establishing traceable dose measurements using the alanine pellet dosimetry system in kV x-ray fields, it has been shown that for the beam qualities studied here and in the previous two publications the conclusion stands that the microbicidal effectiveness is the same in the dose range 2 kGy to 11 kGy.

Conclusion and Outlook

The gradual replacement of cesium irradiators by small self-shielded x-ray irradiators has increased the need for improved dosimetry for low and medium energy x-rays.

The present work investigated the energy dependence of the alanine pellet dosimeter for low and medium energy x-rays using both experimental and theoretical methods. Literature data on the energy dependence of the alanine pellet dosimeter was used to determine quality correction factors to be applied to cobalt-60 calibrated dose to water measurements to establish traceable dose to water measurements in low energy x-ray fields.

Relative Detector Efficiency and Response

An energy dependence of the measured electron paramagnetic resonance (EPR)-response for alanine pellet dosimetry has been known for several decades. The decrease in detector response has been determined to originate from two factors. One from a decrease in the relative ratio of dose to alanine and water and the other from a decrease in the intrinsic detector efficiency from x-ray to cobalt.

Experimental Approach

An experimental determination of both the relative response and efficiency of the alanine pellet dosimeter was carried out in two separate sets of irradiations. The first set of irradiations was done using a 40 kV x-ray tube at the Technical University of Denmark (DTU) Risø, while the second set of irradiations was carried out at National Physical Laboratory (NPL) using two different beam qualities with high-voltage (HV) 135 kV and 280 kV, respectively. The investigated beam qualities had effective energies above and below the beam qualities for which values for the relative response, and efficiency, was previously available in the literature. The relative response was determined using ionization

chamber measurements of the dose to water as reference, and the relative efficiency was calculated by comparison of the relative response with a Monte Carlo (MC) calculated value of the relative ratio of doses.

Some issues regarding the experimental approaches are highlighted by these measurements. Both for the measurements carried out here and in the literature, the relative response is determined in reference fields. This includes known fields in well-defined geometries. For applications as a routine dosimetry system, irradiations will typically be performed in less ideal setups. Therefore, the influence on the relative response from the translation from reference conditions to some user beam will need to be addressed.

The Microdosimetric One-Hit Detector Model

The microdosimetric one-hit detector model (OHDM) was in this study proposed as a tool for exploring the dependence of the dosimeter response on primarily the spectral distribution, but also different irradiation conditions such as the position in a phantom or scatter from surrounding material.

Here, the microdosimetric OHDM is used to calculate the relative efficiency of the alanine pellet dosimeter for monoenergetic photons, comparing the results with literature data on the relative efficiency expressed as a function of the effective energy of the x-ray beams. To test whether a single beam qualifier such as half-value layer (HVL) (or effective energy) is sufficient to fully characterize the relative efficiency, two sets of x-ray spectra – for low and medium energies respectively – was produced. The spectra were produced using varying external filtration of the beam, resulting in different HVLs for the same HV. The results showed that the relative response could be reasonably well described as a function of HVL, with residuals well within 1 % of a 3rd order polynomial regression. Combination of calculated values of the relative efficiency with MC calculated values for the ratio of doses for both sets of x-ray spectra indicated that the relative response can be well approximated by a single function of HVL (or effective energy) for the medium energy set, while a more pronounced spread in calculated relative responses is obtained for the low energy set.

Traceability of the Alanine Pellet Dosimetry System

A general approach for establishing traceable dose measurements in kilovoltage (kV) x-ray fields, based on literature data, was proposed. The approach was based on calibration in cobalt-60 and multiplication with a beam quality correction factor k_Q. The outlined approach, and associated uncertainties, was based on alanine pellet dosimetry for use in blood irradiators, since this is the primary application at Risø High Dose Reference Laboratory (HDRL), however the approach is general. For a the case of x-ray blood irradiators with effective energy of approximately 80 keV the k_Q-factor was 1.20 with an uncertainty of roughly 4 % at $k = 1$.

Since it was shown using the microdosimetric OHDM that the variation in relative response for a specific effective energy of the x-ray beam is relatively small, the critical factor in estimating the relative response, and thus k_Q, of the dosimeter in a user beam is the definition of the effective energy of the beam.

Microbicidal Effectiveness

The outlined approach for traceable alanine pellet dosimetry was applied for irradiation of test filters containing spores of *Bacillus pumilus* to investigate the microbicidal effectiveness of low energy x-rays. Previous publications on the microbicidal effectiveness of cobalt-60, high energy x-rays, and low and high energy electron beams had shown identical radiation response, when the spores were irradiated under reference conditions. The survival curve for *B. pumilus* test filters irradiated in a 150 kV x-ray beam was shown to agree well with the previous findings, thus extending the conclusion to include low energy x-rays as well.

The alternative assumption that the radiation response of the *B. pumilus* spores is independent of beam quality, one could view the results of this experiment as a validation of the dosimetry system.

An interesting observation was made regarding the relative response of alanine film dosimeters. The relative response of the film dosimeters was determined to be approximately unity, while being 0.79 for the pellet dosimeter. A difference in relative response is expected due to the difference in physical volume and chemical composition of the dosimeters, however, a 20 % difference seems quite large.

Future Work

In the present study the free parameters of the microdosimetric OHDM was determined using literature data obtained from Waldeland et al. (2010). The x-ray spectra were calculated from the information available in their work and related to their experimentally determined values for the relative efficiency. Originally plans were made for experimental determination of the relative efficiency of the alanine pellet dosimeter, which should be used to fix the free model parameters, however, a global pandemic interrupted these plans. A more detailed comparison between the theoretical and experimental determinations of the relative efficiency will improve the confidence in the model predictions. Furthermore, the model prediction for other beams (protons and heavy charged particles) would also be of interest, for instance to fix the free model parameters, since the higher linear energy transfer (LET) results in a more pronounced decrease in detector efficiency.

In order to apply the microdosimetric OHDM, it is of particular interest to scrutinize the model in more complex geometries, for instance realistic models of different blood irradiator geometries, to investigate how the detector

response is influenced by the deviation from reference conditions. For these complex geometries, where proper experimental measurements of response and efficiency of the dosimeter is difficult to carry out, the model calculations could contribute to validating the use of quality correction factors for traceable dosimetry.

In general, the work towards increased confidence in the determination of quality correction factors to be applied for traceable alanine pellet dosimetry in kV x-ray fields is the primary goal of future work. A first step would be experimental comparison between laboratories, for irradiations in relevant user beams.

Bibliography

Agostinelli S, J Allison, Ka Amako, J Apostolakis, H Araujo, P Arce, M Asai, D Axen, S Banerjee, G2 Barrand, et al. (2003). GEANT4—a simulation toolkit. *Nuclear instruments and methods in physics research section A: Accelerators, Spectrometers, Detectors and Associated Equipment* **506**(3), 250–303.

Andersen C, L Bøtter-Jensen, and A Murray (2003). A mini X-ray generator as an alternative to a 90Sr/90Y beta source in luminescence dating. *Radiation Measurements* **37**(4-5), 557–561.

Andreo P, D Burns, K Hohlfeld, MS Huq, T Kanai, F Laitano, V Smyth, and S Vynckier (2000). IAEA TRS-398–Absorbed dose determination in external beam radiotherapy: an international code of practice for dosimetry based on standards of absorbed dose to water. *International Atomic Energy Agency*.

Andreo P, DT Burns, AE Nahum, J Seuntjens, and FH Attix (2017). *Fundamentals of ionizing radiation dosimetry*. John Wiley & Sons.

Anton M and L Büermann (2015). Relative response of the alanine dosimeter to medium energy x-rays. *Physics in Medicine & Biology* **60**(15), 6113.

Anton M, T Hackel, K Zink, P von Voigts-Rhetz, and H Selbach (2015). Response of the alanine/ESR dosimeter to radiation from an Ir-192 HDR brachytherapy source. *Physics in Medicine & Biology* **60**(1), 175.

Anton M, R Kapsch, A Krauss, P von Voigts-Rhetz, K Zink, and M McEwen (2013). Difference in the relative response of the alanine dosimeter to megavoltage x-ray and electron beams. *Physics in Medicine & Biology* **58**(10), 3259.

Anton M (2005). Development of a secondary standard for the absorbed dose to water based on the alanine EPR dosimetry system. *Applied Radiation and Isotopes* **62**(5), 779–795.

Anton M, RP Kapsch, M Krystek, and F Renner (2008). Response of the alanine/ESR dosimetry system to MV x-rays relative to 60Co radiation. *Physics in Medicine & Biology* **53**(10), 2753.

Arber J and P Sharpe (1993). Fading characteristics of irradiated alanine pellets: the importance of pre-irradiation conditioning. *Applied Radiation and Isotopes* **44**(1-2), 19–22.

Aukett R, J Burns, A Greener, R Harrison, C Moretti, A Nahum, and K Rosser (2005). Addendum to the IPEMB code of practice for the determination of absorbed dose for x-rays below 300 kV generating potential (0.035 mm Al–4 mm Cu HVL). *Physics in Medicine & Biology* **50**(12), 2739.

Aukett R, R Harrison, C Moretti, A Nahum, K Rosser, et al. (1996). The IPEMB code of practice for the determination of absorbed dose for x-rays below 300 kV generating potential (0.035 mm Al-4 mm Cu HVL; 10-300 kV generating potential). *Physics in Medicine & Biology* **41**(12), 2605.

Beatty J, P Biggs, K Gall, P Okunieff, F Pardo, K Harte, M Dalterio, and A Sliski (1996). A new miniature x-ray device for interstitial radiosurgery: Dosimetry. *Medical physics* **23**(1), 53–62.

Berger M (2010). XCOM: photon cross sections database. *http://www. nist. gov-/pml/data/xcom/index. cfm*.

Bergstrand E, H Bjerke, and E Hole (2005). An experimental investigation of the electron energy dependence of the EPR alanine dosimetry system. *Radiation measurements* **39**(1), 21–28.

Bergstrand ES, KR Shortt, CK Ross, and EO Hole (2003). An investigation of the photon energy dependence of the EPR alanine dosimetry system. *Physics in Medicine & Biology* **48**(12), 1753.

Bernal M, M Bordage, J Brown, M Davídková, E Delage, Z El Bitar, S Enger, Z Francis, S Guatelli, V Ivanchenko, et al. (2015). Track structure modeling in liquid water: A review of the Geant4-DNA very low energy extension of the Geant4 Monte Carlo simulation toolkit. *Physica Medica* **31**(8), 861–874.

Bernier J, EJ Hall, and A Giaccia (2004). Radiation oncology: a century of achievements. *Nature Reviews Cancer* **4**(9), 737–747.

Bradshaw W, D Cadena, G Crawford, and H Spetzler (1962). The use of alanine as a solid dosimeter. *Radiation research* **17**(1), 11–21.

Chen F, P Nicolucci, and O Baffa (2008). Enhanced sensitivity of alanine dosimeters to low-energy X-rays: Preliminary results. *Radiation measurements* **43**(2-6), 467–470.

Coninckx F, H Schönbacher, A Bartolotta, S Onori, and A Rosati (1989). Alanine dosimetry as the reference dosimetric system in accelerator radiation envi-

ronments. *International Journal of Radiation Applications and Instrumentation. Part A. Applied Radiation and Isotopes* **40**(10-12), 977–983.

Desrosiers MF, SL Cooper, JM Puhl, AL McBain, and GW Calvert (2004). A study of the alanine dosimeter irradiation temperature coefficient in the- 77° C to+ 50° C range. *Radiation Physics and Chemistry* **71**(1-2), 365–370.

Dodd B and RJ Vetter (2009). Replacement of 137Cs irradiators with x-ray irradiators. *Health physics* **96**(2), S27–S30.

EDQM (2015). *Guide to the preparation, use and quality assurance of blood components*. Guide. Strasbourg, FR: European Directorate for the Quality of Medicines and HealthCare.

Famulari G, P Pater, and SA Enger (2017). Microdosimetry calculations for monoenergetic electrons using Geant4-DNA combined with a weighted track sampling algorithm. *Physics in Medicine & Biology* **62**(13), 5495.

Follett P et al. (2014). Phytosanitary irradiation for fresh horticultural commodities: generic treatments, current issues, and next steps. *Stewart Postharvest Review* **3**(1).

Gall K, M Desrosiers, D Bensen, and C Serago (1996). Alanine EPR dosimeter response in proton therapy beams. *Applied radiation and isotopes* **47**(11-12), 1197–1199.

Greenbaum BH (1991). Transfusion-associated graft-versus-host disease: historical perspectives, incidence, and current use of irradiated blood products. *Journal of clinical oncology* **9**(10), 1889–1902.

Hansen JW (1984). "Experimental investigation of the suitability of the track structure theory in describing the relative effectiveness of high-LET irradiation of physical radiation detectors". PhD thesis. Risoe National Lab.

Hansen J, M Waligorski, and E Byrski (1989). Intercomparison of gamma ray, X ray, and fast neutron dosimetry using alanine detectors. *Radiation protection dosimetry* **27**(2), 85–92.

Hazekamp A (2016). Evaluating the effects of gamma-irradiation for decontamination of medicinal cannabis. *Frontiers in pharmacology* **7**, 108.

Helt-Hansen J and A Miller (2004). RisøScan—a new dosimetry software. *Radiation Physics and Chemistry* **71**(1-2), 361–364.

Hjørringgaard JG, C Ankjærgaard, M Bailey, and A Miller (2020). Alanine pellet dosimeter efficiency in a 40 k V x-ray beam relative to cobalt-60. *Radiation Measurements*, 106374.

Horowitz Y (2006). *Microdosimetric response of physical and biological systems to low-and high-LET radiations: Theory and applications to dosimetry*. Elsevier.

Hubbell JH and SM Seltzer (1995). *Tables of X-ray mass attenuation coefficients and mass energy-absorption coefficients 1 keV to 20 MeV for elements Z= 1 to 92 and 48 additional substances of dosimetric interest*. Tech. rep. National Inst. of Standards and Technology-PL, Gaithersburg, MD (United ...

ICRU Report 36 (1983). *Microdosimetry*. International Commision on Radiation Units and Measurements, Bethesda, MD.

ICRU Report 64 (2001). *Dosimetry of High-Energy Photon Beams based on Standards of Absorbed Dose to Water*. International Commission on Radiation Units and Measurements, Bethesda, MD.

ICRU Report 80 (2008). *Dosimetry Systems for Use in Radiation Processing*. International Commision on Radiation Units and Measurements, Bethesda, MD.

ICRU Report 85 (2011). *Fundamental Quantities and Units for Ionizing Radiation*. International Commission on Radiation Units and Measurements, Bethesda, MD.

ICRU Report 90 (2016). *Key Data for Ionizing-Radiation Dosimetry: Measurement Standards and Applications*. International Commision on Radiation Units and Measurements, Bethesda, MD.

Incerti S et al. (2010a). Comparison of GEANT4 very low energy cross section models with experimental data in water. *Medical physics* **37**(9), 4692–4708.

Incerti S et al. (2010b). The geant4-dna project. *International Journal of Modeling, Simulation, and Scientific Computing* **1**(02), 157–178.

Incerti S, I Kyriakou, M Bernal, M Bordage, Z Francis, S Guatelli, V Ivanchenko, M Karamitros, N Lampe, SB Lee, et al. (2018). Geant4-DNA example applications for track structure simulations in liquid water: A report from the Geant4-DNA Project. *Medical physics* **45**(8), e722–e739.

ISO/ASTM 51939 (2017). *Standard practice for blood irradiation dosimetry*. Standard. Geneva, CH: International Organization for Standardization.

Janatpour K, L Denning, K Nelson, B Betlach, M Mackenzie, and P Holland (2005). Comparison of X-ray vs. gamma irradiation of CPDA-1 red cells. *Vox Sanguinis* **89**(4), 215–219.

Kawrakow I, D Rogers, E Mainegra-Hing, F Tessier, R Townson, and B Walters (2000). *EGSnrc toolkit for Monte Carlo simulation of ionizing radiation transport*. doi:10.4224/40001303 [release v2021].

Kellerer AM et al. (1985). Fundamentals of microdosimetry. *The dosimetry of ionizing radiation* **1**, 77–162.

Kellerer AM and D Chmelevsky (1975). Concepts of microdosimetry. *Radiation and environmental biophysics* **12**(4), 321–335.

Khoury H, E da Silva Jr, K Mehta, V de Barros, V Asfora, P Guzzo, and A Parker (2015). Alanine-EPR as a transfer standard dosimetry system for low energy X radiation. *Radiation Physics and Chemistry* **116**, 147–150.

Ma CM, C Coffey, L DeWerd, C Liu, R Nath, S Seltzer, and J Seuntjens (2001). AAPM protocol for 40–300 kV x-ray beam dosimetry in radiotherapy and radiobiology. *Medical physics* **28**(6), 868–893.

Malinen E, MZ Heydari, E Sagstuen, and EO Hole (2003). Alanine radicals, part 3: Properties of the components contributing to the EPR spectrum of X-irradiated alanine dosimeters. *Radiation research* **159**(1), 23–32.

Mastrangelo T, A Parker, A Jessup, R Pereira, D Orozco-Dávila, A Islam, T Dammalage, and J Walder (2010). A new generation of X ray irradiators for insect sterilization. *Journal of economic entomology* **103**(1), 85–94.

McEwen M, A Miller, I Pazos, and P Sharpe (2020). Determination of a consensus scaling factor to convert a Co-60-based alanine dose reading to yield the dose delivered in a high energy electron beam. *Radiation Physics and Chemistry* **171**, 108673.

McEwen M, P Sharpe, and S Vörös (2015). Evaluation of alanine as a reference dosimeter for therapy level dose comparisons in megavoltage electron beams. *Metrologia* **52**(2), 272.

McEwen M, J Sephton, and P Sharpe (2006). "Alanine as a precision validation tool for reference dosimetry". In: *Proceedings of the PTB Workshop PTB-Dos-51 on Alanine Dosimetry for Clinical Applications (Braunschweig: Physikalisch-Technische Bundesanstalt)*.

Mehta K and A Parker (2011). Characterization and dosimetry of a practical X-ray alternative to self-shielded gamma irradiators. *Radiation Physics and Chemistry* **80**(1), 107–113.

Nagy V, JM Puhl, and MF Desrosiers (2000). Advancements in accuracy of the alanine dosimetry system. Part 2. The influence of the irradiation temperature. *Radiation Physics and Chemistry* **57**(1), 1–9.

Nasreddine A, F Kuntz, and Z El Bitar (2020). Absorbed dose to water determination for kilo-voltage X-rays using alanine/EPR dosimetry systems. *Radiation Physics and Chemistry*, 108938.

Niroomand-Rad A, MT Gillin, F Lopez, and DF Grimm (1987). Performance characteristics of an orthovoltage x-ray therapy machine. *Medical physics* **14**(5), 874–878.

Olko P (2002). The microdosimetric one-hit detector model for calculating the response of solid state detectors. *Radiation measurements* **35**(3), 255–267.

Poludniowski GG (2007). Calculation of x-ray spectra emerging from an x-ray tube. Part II. X-ray production and filtration in x-ray targets. *Medical physics* **34**(6Part1), 2175–2186.

Poludniowski GG and PM Evans (2007). Calculation of x-ray spectra emerging from an x-ray tube. Part I. Electron penetration characteristics in x-ray targets. *Medical physics* **34**(6Part1), 2164–2174.

Powers E, C Ehret, and A Bannon (1957). The membrane filter technique in radiation studies of spores of Bacillus megaterium. *Applied microbiology* **5**(2), 61.

Prescott S (1904). The effect of radium rays on the colon bacillus, the diphtheria bacillus and yeast. *Science* **20**(503), 246–248.

Röntgen WC (1895). Uber eine neue Art von Strahlen. *Sitzungsber Phys Med Ges Wurtzburg* **9**, 132–141.

Rossi HH and M Zaider (1996). *Microdosimetry and its Applications*. Springer.

Sagstuen E, EO Hole, SR Haugedal, and WH Nelson (1997). Alanine radicals: Structure determination by EPR and ENDOR of single crystals X-irradiated at 295 K. *The Journal of Physical Chemistry A* **101**(50), 9763–9772.

Scrimger J and S Connors (1986). Performance characteristics of a widely used orthovoltage x-ray therapy machine. *Medical physics* **13**(2), 267–269.

Sharpe P, A Miller, J Sephton, C Gouldstone, M Bailey, and J Helt-Hansen (2009). The effect of irradiation temperatures between ambient and 80 C on the response of alanine dosimeters. *Radiation Physics and Chemistry* **78**(7-8), 473–475.

Sleptchonok OF, V Nagy, and MF Desrosiers (2000). Advancements in accuracy of the alanine dosimetry system. Part 1. The effects of environmental humidity. *Radiation Physics and Chemistry* **57**(2), 115–133.

Tallentire A and A Khan (1975). "Tests of the validity of a model relating frequency of contaminated items and increasing radiation dose". In: *Radiosterilization of medical products 1974*.

Tallentire A and A Miller (2015). Microbicidal effectiveness of X-rays used for sterilization purposes. *Radiation Physics and Chemistry* **107**, 128–130.

Tallentire A, A Miller, and J Helt-Hansen (2010). A comparison of the microbicidal effectiveness of gamma rays and high and low energy electron radiations. *Radiation Physics and Chemistry* **79**(6), 701–704.

Verhaegen F, A Nahum, S Van De Putte, and Y Namito (1999). Monte Carlo modelling of radiotherapy kV x-ray units. *Physics in Medicine & Biology* **44**(7), 1767.

Vörös S, M Anton, and B Boillat (2012). Relative response of alanine dosemeters for high-energy electrons determined using a Fricke primary standard. *Physics in Medicine & Biology* **57**(5), 1413.

Wagner JK, JA Dillon, EK Blythe, and JR Ford (2009). Dose characterization of the rad sourceTM 2400 X-ray irradiator for oyster pasteurization. *Applied Radiation and Isotopes* **67**(2), 334–339.

Waldeland E, EO Hole, E Sagstuen, and E Malinen (2010). The energy dependence of lithium formate and alanine EPR dosimeters for medium energy x rays. *Medical physics* **37**(7Part1), 3569–3575.

Wieser A and R Girzikowsky (1996). A unique calibration curve for alanine EPR dosimetry systems. *Applied radiation and isotopes* **47**(11-12), 1269–1275.

Zaider M (1990). Microdosimetry and Katz's track structure theory: I. One-hit detectors. *Radiation research* **124**(1s), S16–S22.

Zeng G and J McCaffrey (2005). The response of alanine to a 150 keV X-ray beam. *Radiation physics and chemistry* **72**(5), 537–540.

Zeng G, M McEwen, D Rogers, and N Klassen (2005). An experimental and Monte Carlo investigation of the energy dependence of alanine/EPR dosimetry: II. Clinical electron beams. *Physics in Medicine & Biology* **50**(6), 1119.

Part II

Publications

Paper I

Title:

Alanine Pellet Dosimeter Efficiency in a 40 kV X-ray beam relative to Cobalt-60.

Authors:

Hjørringgaard JG, Ankjærgaard C, Bailey M, and Miller A

Submitted to:

Radiation Measurements,
October 2019.

Status:

Published August 2020.

Digital Object Identifier:

10.1016/j.radmeas.2020.106374

Radiation Measurements 136 (2020) 106374

Contents lists available at ScienceDirect

Radiation Measurements

journal homepage: http://www.elsevier.com/locate/radmeas

Alanine pellet dosimeter efficiency in a 40 kV x-ray beam relative to cobalt-60

Jakob G. Hjørringgaard *, Christina Ankjærgaard, Mark Bailey, Arne Miller

Center for Nuclear Technologies, Technical University of Denmark, Roskilde, Denmark

ARTICLE INFO

Keywords:
Low energy
X-rays
Alanine
EPR
Dosimetry

ABSTRACT

The electron paramagnetic resonance (EPR) response of alanine pellet dosimeters irradiated in a 40 kV x-ray beam with effective energy 9 keV was investigated, which is a factor of three lower than for currently available literature data. The response was compared to the EPR response of alanine pellets irradiated in a reference cobalt-60 field to obtain the relative efficiency of the dosimeter – the ratio of detector response per dose-to-detector in the x-ray beam relative to the reference field. Due to the low filtration of the beam, and subsequent low half-value layer, a correction for the dose gradient within the pellet was necessary to implement for the EPR response of x-ray irradiated pellets. Calculation of the dose gradient in a pellet, together with dose-to-alanine to dose-to-water ratio, was carried out using the EGSnrc Monte Carlo code. The relative efficiency of the alanine pellet dosimeter in this x-ray field compared to a reference cobalt-60 field was found to be $G_{Q,Q_0} = 0.91 \pm 0.04$.

1. Introduction

Kilovoltage (kV) x-rays have extensive applications in radiotherapy, radiation processing, small animal irradiation, blood irradiation, the latter showing a demand for replacement of Cs-137 irradiators with x-ray irradiaters (Dodd and Vetter, 2009). Dosimetry protocols recommend water based dosimetry using ion chambers (Aukett et al., 1996; IAEA, 2001), however for applications like blood irradiation, where blood bags are irradiated from two or more directions in a sealed canister, ion chamber measurements are impractical due to the geometry of the irradiation cavity or the complex x-ray fields. Here both placement of the ion chamber and determination of beam quality through half-value layer (HVL) measurements are difficult. In these cases the use of the alanine/electron paramagnetic resonance (EPR) dosimeter may be more practical.

The alanine/EPR dosimetry system consists of L-α-alanine, in the form of pellets or films, that produce stable free radicals when irradiated. The amount of stable free radicals produced is proportional to dose to the dosimeter for a wide range of beam qualities (Olsen et al., 1990; Sharpe and Duane, 2003; Bergstrand et al., 2003; Zeng et al., 2004, 2005; Anton et al., 2008) and is stable with a signal loss of few percent over years (Sleptchonok et al., 2000). The concentration of stable free radicals is analyzed with an EPR spectrometer.

The ratio of alanine to water mass energy absorption coefficients for monoenergetic x-rays normalized to cobalt-60 is shown in Fig. 1.

For photon energies below approximately 200 keV the mass energy absorption coefficient ratio decreases by up to 30%. Since dose to a material is dependent on the mass energy absorption coefficient, the large energy dependence of this ratio for lower energies implies that a reduction in the stable free radical production per dose to water is expected for these beam qualities. Several studies (Olko, 2002; Zeng and McCaffrey, 2005; Waldeland et al., 2010; Anton and Büermann, 2015; Khoury et al., 2015) suggest that an observed reduction in stable free radical production is not only due to this change in mass energy absorption coefficient ratios but also in part due to an intrinsic decrease in stable free radical production per dose to alanine for lower photon energies. This intrinsic decrease can be described by the relative efficiency G_{Q,Q_0}.

The energy dependence of stable free radical production in alanine is more prominent towards lower photon energies. It is therefore of interest to extend the experimental determination of this dependence to x-ray fields with lower effective energy. Here we aim to determine the efficiency of stable free radical formation for a 40 kV x-ray beam relative to a cobalt-60 reference field.

* Corresponding author.
E-mail address: jakg@dtu.dk (J.G. Hjørringgaard).

https://doi.org/10.1016/j.radmeas.2020.106374
Received 30 October 2019; Received in revised form 24 April 2020; Accepted 5 May 2020
Available online 30 May 2020

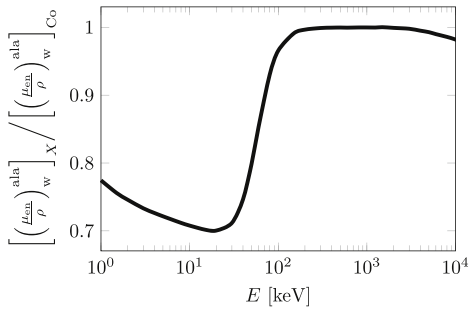

Fig. 1. Ratio of alanine to water mass energy absorption coefficients for monoenergetic x-rays relative to cobalt-60 γ radiation. Data from Hubbell and Seltzer (1995).

2. Method

2.1. General formalism

For the analysis we adopt the formalism proposed by Waldeland et al. (2010). Here the total energy dependence F_{Q,Q_0} of the alanine/EPR dosimeter in an x-ray beam quality Q relative to a reference cobalt-60 quality Q_0 is the response to x-ray radiation quality Q with respect to dose-to-water, relative to a reference cobalt-60 quality Q_0

$$F_{Q,Q_0} = \frac{(r/D_w)_Q}{(r/D_w)_{Q_0}}, \tag{1}$$

where r is the EPR response and D_w is the dose to water. The total energy dependence can be divided into two parts (Olko, 2002)

$$F_{Q,Q_0} = \frac{(r/D_{dos})_Q}{(r/D_{dos})_{Q_0}} \cdot \frac{(D_{dos}/D_w)_Q}{(D_{dos}/D_w)_{Q_0}}, \tag{2}$$

where the first term concerns the EPR response per dose to dosimeter D_{dos} equivalent to the relative efficiency which we aim to determine, and the second term concerns the ratio of dose-to-alanine to dose-to-water relative to the corresponding ratio for the reference radiation quality.

The total energy dependence F_{Q,Q_0} can be obtained experimentally by measurements of the alanine EPR response after irradiation to known levels of dose to water in the respective fields. The ratio of doses

$$H_{Q,Q_0} = \frac{(D_{dos}/D_w)_Q}{(D_{dos}/D_w)_{Q_0}}, \tag{3}$$

can be obtained by Monte Carlo (MC) calculations where the scoring volume is made of detector material and water respectively. Combination of the quantities H_{Q,Q_0} and F_{Q,Q_0} leads to a determination of the relative efficiency of the alanine pellet dosimeter

$$G_{Q,Q_0} = \frac{(r/D_{dos})_Q}{(r/D_{dos})_{Q_0}}. \tag{4}$$

G_{Q,Q_0} is thus a measure for the difference in radiation induced stable free radicals in alanine in beam quality Q relative to reference quality Q_0.

2.2. Irradiation procedure

kV x-ray irradiations of the alanine pellets were carried out at the Center for Nuclear Technologies at the Technical University of Denmark using a Varian VF-50J x-ray tube. This tube has a tungsten target and is capable of producing x-rays at accelerating potentials in the range of 4 kV – 50 kV. The beam is emitted through a 76 μm beryllium window. The tube is mounted on a brass collimator with a 70 μm aluminium end window. Schematic and detailed information on tube and collimator can be found in Andersen et al. (2003). The first HVL was measured to 0.08 mm of aluminium, corresponding to an effective energy E_{eff} = 9 keV.

Ionization chamber measurements were carried out in order to experimentally determine the dose-to-water at the point of interest. For these measurements a PTW 23344 soft x-ray chamber was placed in a designated PTW 2962 soft x-ray PMMA slab phantom (13 cm × 13 cm × 7.5 cm), see Fig. 2 (a). The distance from end window to phantom surface was 12.5 cm and the circular field diameter at this position was 4.0 cm. The phantom was centered in the x-ray field using radiochromic film. The absorbed dose to water was then determined by

$$D_w = M N_w k_Q k_{T,p} k_{field}, \tag{5}$$

where M is the chamber reading, $N_w = 9.383 \times 10^7 \text{Gy C}^{-1}$ is the calibration factor for absorbed dose to water in a circular 3 cm diameter field at distance 30 cm, with radiation quality correction factor k_Q = 1.000, both from the calibration certificate of the manufacturer traceable to PTB, and $k_{T,p}$ is the air density correction. A MC study of the effect of change in irradiation conditions relative to the calibration conditions showed a variation of k_{field} = 1.009 ± 0.9 %, which is included in the calculation of dose. The slot for the ion chamber in the phantom is located such that the entrance window, and effective point of measurement, of the ion chamber is at the surface of the phantom during irradiations, so that the dose to water at the surface can be determined. One of the additional PMMA slabs of the phantom was modified to fit four alanine pellets placed with center in the corners of a 1 cm × 1 cm square in a 2.5 cm diameter circular ABS holder (see Fig. 2 (b)). For the alanine irradiations this slab could be moved to the top of the phantom, such that they are in the same position as the ion chamber. Dose-to-water delivered to the alanine pellet dosimeter range from 30 Gy to 150 Gy. The tube current I, accelerating potential U, and ambient temperature next to the PMMA phantom T was monitored continuously during all irradiations to ensure stabillity. Measurements roughly each second during all irradiations of alanine pellets yield I = (1.000 ±0.004) mA, U = (40.0 ±0.3)kV, and T = (24.8 ±0.2) °C, where the variation stated is the standard deviation.

Cobalt-60 reference irradiations are carried out in a Gammacell – a shielded enclosure, with a number of cylindrical cobalt-60 source pencils arranged around the sample at an approximate radial distance of 10 cm and which have an approximate height of 20 cm. The irradiator is very similar to the Nordion GC-220 in design (Hefne, 2000; Rodrigues et al., 2009). The standard ABS holder containing four alanine pellets is placed inside polyether ether ketone (PEEK, $C_{19}H_{12}O_3$) cylinders inside an aluminium can which is able to have its temperature controlled, which is all placed at the sample position. The dose rate inside this irradiator in this geometry is calibrated using alanine transfer dosimeters supplied and measured by the National Physical Laboratory, UK. In calibration irradiations, a standard temperature of 25°C is used, and this is maintained within approximately 0.5°C.

2.3. Materials

The Alanine pellets used in this experiment are obtained from Har-

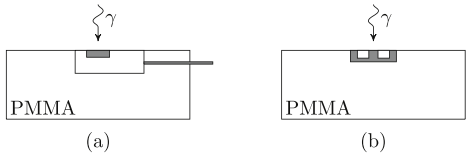

Fig. 2. Sideview of the irradiation geometry, with (a) the ion chamber located in the surface slab of a PMMA phantom (b) four alanine pellets in an ABS holder located in the same position in the surface slab. Not to scale.

well Dosimeters. They are cylindrical with a diameter of 4.8 mm, height of 2.7 mm, and average mass of 60 mg. The binding material used is paraffin wax in a mixture of ~91 % L-α-alanine and ~ 9 % paraffin wax. The temperature correction for the alanine pellet dosimeters is 0.14 %°C^{-1} (Helt-Hansen et al., 2009). The contributions to the uncertainty in measured dose is thus 0.04%($k = 1$) for the temperature variations for both Cobalt-60 and x-ray irradiations.

EPR measurements of the stable free radicals induced in the alanine pellets were carried out on a Bruker EMXmicro spectrometer operating at 9.53 GHz. The alanine pellets where placed in a quartz tube in the resonator for identical positioning. The parameters chosen for the data acquisition were magnetic sweep width 20.0 G, modulation amplitude 10.0 G, and sweep time 21.0 s with conversion time 41.0 ms. A microwave power of 3.375 mW and a center field of 339.8 mT was used. Three sweeps were done for each alanine pellet. The peak-to-peak value of fitted EPR resonance in the first derivative of the absorption spectrum, corrected for individual mass of the pellets, was used as the EPR response r. Four pellets were irradiated at each dose level to ensure reproducibility.

2.4. Monte Carlo calculations

MC calculations were performed using the EGSnrc toolkit for simulation of ionizing radiation transport (Kawrakow et al., 2017). The C++ class library of EGSnrc, egs++, was used for its general purpose geometry package. Material files for non-standard materials used in the MC calculation were constructed based on the information available from the suppliers. Material files used in the MC calculations had ae = 512 kV and ap = 1 keV as lower limit for creation of secondary electrons and photons respectively. The same values were chosen for cutoff energies for particle transport. Particle transport options for Rayleigh scattering and photoelectron angular scattering are applied.

The energy distribution of photons produced by the x-ray tube was calculated. A general geometry consisting of the tube head, brass collimater, and end window was set up in egs++ using all available information on materials and dimensions. The calculated energy distribution of x-rays resulting from 40 keV electrons is shown in Fig. 3.

The calculated x-ray spectrum was validated by HVL measurements in the irradiation geometry. Measurements was carried out by inserting varying thickness of attenuating material (aluminium) in front of the detector. The MC calculated spectra was able to reproduce the measured attenuation profile with a relative standard deviation of 2.7% for the 40 kV x-ray beam, see Fig. 4.

Uncertainties arising from the filtration used in the x-ray spectrum calculation are assessed by a sensitivity analysis described in the following section. The calculated x-ray spectrum is used as the photon source in further MC calculations of dose ratios and dose gradient within the alanine pellets.

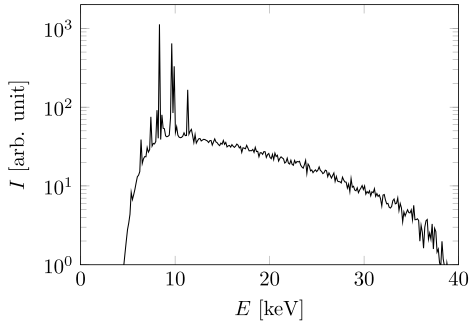

Fig. 3. Calculated x-ray energy distribution for 40 keV electrons imparted on a tungsten target. The L-shell emission lines of tungsten are clearly visible around 10 keV. Calculations were done using egs++ with geometry of the x-ray tube head. The fluence weighted mean energy of the calculated spectrum is $E_{\mathrm{av},\Phi}$ = 14.3 keV.

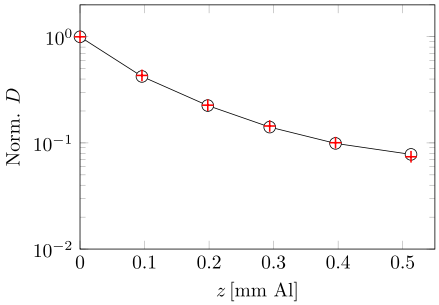

Fig. 4. Attenuation profile of the 40 kV x-ray beam measured (black circles) and MC calculated using the spectral distribution shown in Fig. 3 (red cross). (For interpretation of the references to colour in this figure legend, the reader is referred to the Web version of this article.)

For all calculations the photon cross sections option mcdf-xcom was used. This option uses the renormalized photoelectric cross sections of Sabbatucci and Salvat (2016) with xcom (Berger et al., 1998) for all other cross sections (option recommended for low energy applications in the PIRS509a BEAMnrc user manual).

2.5. Uncertainties

An estimated uncertainty budget is shown in Fig. 1. The uncertainty for the total energy dependence of the dosimeter F_{Q,Q_0} depends on the uncertainties in dose-to-water determination and the curve fit of the EPR response function for x-rays and cobalt-60 respectively. The uncertainty related to dose-to-water determination is primarily due to uncertainty in the calibration factor σ_{cal} (2.5% for the PTW 23344 ionization chamber and 1.4% in the reference position in the cobalt-60 Gammacell). A correction for the change in irradiation conditions between x-ray irradiations at Risø and the calibration of the PTW 23344 ionization chamber is included, with a statistical uncertainty $\sigma_{k_{\mathrm{field}}}$ = 0.9 %. The uncertainty on the slope σ_{fit} is evaluated from the residuals of the linear regression, see Fig. 5. EPR responses are normalized to the mass of individual pellets. The uncertainty contribution due to pellet mass (< 0.05 % at k = 1) is negligible in the analysis. Irradiation temperature in the cobalt-60 Gammacell was kept at a stable 25°C, while it was continuously measured to 24.8°C during x-ray irradiations. The

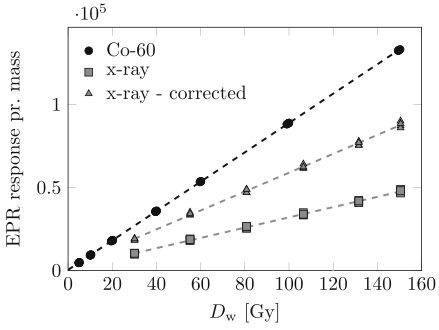

Fig. 5. Measured EPR response per mass of pellet as a function of dose to water for alanine pellets irradiated in a cobalt-60 field (black circles), 40 kV x-ray field (gray squares), and 40 kV x-ray field corrected for dose gradient in the pellet (gray triangles).

influence of irradiation temperature on the generated EPR response (< 0.04 %) is thus negligible. Alanine pellet dosimeters were placed in the ABS holders during all irradiations to minimize effects of surrounding material. Therefore we assume that σ_{cal} and σ_{fit} are the sole contributors to the uncertainty in F_{Q,Q_0}. For the uncertainty in F_{Q,Q_0} the contributions from σ_{cal} and σ_{fit} for x-ray and cobalt-60 irradiations respectively are added in quadrature.

From MC calculations both statistical and geometrical uncertainties arise. Statistical uncertainties $\sigma_{statistical}$ are minimized purely by increasing the number of simulated initial particles. The value of 0.9% shown in Table 1 is the statistical uncertainty for all MC calculations used for determination of H_{Q,Q_0} added in quadrature. Geometrical uncertainties $\sigma_{geometrical}$ refer to unknowns in material specifications and accuracy of dimension specifications. Other components of uncertainty σ_{other} arise from the choices of algorithms and cross-sections used. The geometrical and computational uncertainties given in Table 1 are conservative estimates. The statistical, geometrical and computational contributions to the uncertainty in H_{Q,Q_0} are added in quadrature.

A sensitivity analysis in the spectrum calculation of the effect of varying aluminium filtration was carried out. No information on the uncertainty of filtration thickness was available. A conservative estimate in the order of ±10 % was chosen for the sensitivity analysis. Using x-ray spectra calculated with this 10% variation in aluminium filtration thickness showed no effect on the calculation of H_{Q,Q_0}, while a variation of ±1.6 % was observed for the k_{thick} calculation described in Section 3.1. This variation is adopted as an estimate of the uncertainty for k_{thick}.

The uncertainty contributions from F_{Q,Q_0}, H_{Q,Q_0}, and k_{thick} are added in quadrature to obtain the final uncertainty on the relative efficiency G_{Q,Q_0}.

All uncertainties stated are at $k = 1$.

3. Results

The determination of the energy dependence of the alanine pellet dosimeter in an x-ray beam relative to a reference cobalt-60 beam is based on the ratio of the slopes of EPR response to dose to water (see Fig. 5). From the raw measurement of EPR response, the obtained response function for cobalt-60 is

$$r_{Co}(D_w) = 884.05\text{Gy}^{-1} \cdot D_w + 430.89, \quad (6)$$

and for the 40 kV x-ray beam

$$r_X(D_w) = 309.19\text{Gy}^{-1} \cdot D_w + 1094.51. \quad (7)$$

Using the ratio of the slopes and a combined uncertainty of 3.4% (see Table 1), we obtain a preliminary result for the total energy dependence of this alanine pellet dosimeter of

$$F_{Q,Q_0} = 0.350 \pm 0.012, \quad (8)$$

a roughly 65 % decrease in EPR response per dose to water. However, this value has to be corrected for the dose gradient inside the detector as descried in the following section.

Table 1
Uncertainty components, given as relative standard uncertainty.

Contributor	Type A	Type B	Combined
X-ray			
σ_{cal}		2.5%	
$\sigma_{k_{field}}$		0.9%	
σ_{fit}	1.3%		
Cobalt-60			
σ_{cal}		1.4%	
σ_{fit}	0.8%		
F_{Q,Q_0}			3.4%
Monte Carlo			
$\sigma_{geometrical}$		1.0%	
$\sigma_{statistical}$	0.9%		
σ_{other}		2.0%	
H_{Q,Q_0}			2.4%
k_{thick}		1.6%	
G_{Q,Q_0}			4.5%

3.1. Thickness correction

The low filtration of the beam (see Section 2.2) gives rise to a steep dose gradient within the thickness of an alanine pellet. MC calculation of the depth dose curve inside the geometry of the alanine pellet show a reduction in dose to alanine of approximately 70 % from the surface to the back (see Fig. 6).

For the irradiations in the cobalt-60 Gammacell the alanine pellets are placed in a geometry that ensures secondary electron equilibrium, so the dose deposition inside the pellets is completely homogeneous. A large part of the reduction in total energy dependence F_{Q,Q_0} can therefore be attributed to the difference in dose deposition. In order to give a comparable value, the EPR signal of the x-irradiated pellets must be corrected for the dose gradient in the pellet – a thickness correction.

The thickness correction is calculated by the ratio of homogenous dose deposition to decreasing dose gradient as

$$k_{thick} = \frac{z_p \cdot D_0}{\int_0^{z_p} D(z)\mathrm{d}z}, \quad (9)$$

where D_0 is the surface dose and z_p is the thickness of the pellet. From the MC calculated depth dose curve in Fig. 6, a thickness correction of $k_{thick} = 1.84 \pm 0.03$ is obtained.

3.2. Corrected response

Applying the correction factor to the EPR response from x-irradiated pellets reduces the difference in detector response relative to cobalt-60 irradiated pellets (see Fig. 5). The corrected value of the total energy dependence of the alanine pellet dosimeter can then be obtained in a similar way as for the uncorrected signal, by ratio of slopes, or simply taking the product of the uncorrected value of the total energy dependence and the thickness correction factor. The corrected total energy dependence is

$$F_{Q,Q_0}^{corr} = F_{Q,Q_0} \cdot k_{thick} = 0.64 \pm 0.02. \quad (10)$$

A 35 % reduction in the EPR response per dose to water is thus observed for x-irradiated pellets corrected for dose gradient relative to the reference cobalt-60 irradiated pellets.

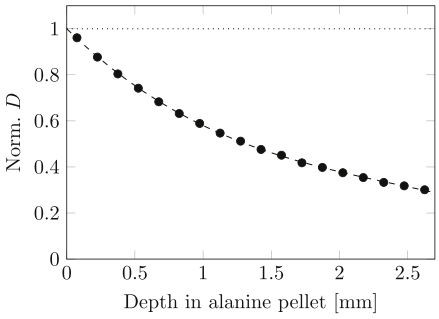

Fig. 6. Dose gradient whithin the alanine pellet geometry normalized to the surface dose to alanine. Calculation carried out using egs++ with geometry setup as in Fig. 2 (b).

The correction of the EPR response for dose gradient is part of the process in isolating the effect of reduction in chemical yield – formation of stable free radicals – for alanine from other physical aspects influencing the EPR response. Another factor that influences the total energy dependence of the dosimeter is the difference in dose-to-alanine to dose-to-water ratio for low energy x-rays relative to the cobalt-60 reference (see Fig. 1). MC calculations of the dose to an alanine pellet in the irradiation geometry can be carried out, as well as the same calculation where the alanine pellet has been replaced with a water pellet of equal dimensions. The dose gradient through a pellet (of both alanine and water) in the x-ray beam was calculated, and an extrapolation to surface dose is used as the dose-ratio for calculation of H_{Q,Q_0}. The calculations were carried out using the cavity-usercode in egs++ for the 40 kV x-ray beam, and the g-usercode for the cobalt-60 reference beam. The dose-to-alanine to dose-to-water ratio for the 40 kV x-ray beam relative to the cobolt-60 reference is

$$H_{Q,Q_0} = 0.71 \pm 0.02. \tag{11}$$

The relative efficiency of the alanine pellet dosimeter in this x-ray field can then be calculated according to Equation (2) as

$$G_{Q,Q_0} = \frac{F^{\text{corr}}_{Q,Q_0}}{H_{Q,Q_0}} = 0.91 \pm 0.04. \tag{12}$$

4. Discussion

In the present work the relative efficiency of an alanine pellet dosimeter following irradiation in a 40 kV x-ray beam has been studied. The result is a (8.9 ± 4.1) % decrease in the relative efficiency for this beam quality relative to the reference Co-60 quality.

Previous studies of the radiation yield of alanine radicals have shown a decrease in relative efficiency towards lower effective x-ray energies at tube voltages in the range 30 kV – 280 kV (Zeng and McCaffrey, 2005; Waldeland et al., 2010; Anton and Büermann, 2015; Khoury et al., 2015). Some issues arise concerning comparison of results; Zeng and McCaffrey (2005) use an air kerma based dosimetry protocol contrary to the water based dosimetry. Khoury et al. (2015) does not specify either HVL or effective energy of the studied x-ray beam, and only list the tube potential used (125 kV) and the average energy of a 150 kV spectrum in material of fruit fly pupae. Anton and Büermann (2015) do not list values for G_{Q,Q_0} (denoted η in their work), but instead correct the MC calculated dose ratios by the relative efficiency obtained with the microdosimetric one-hit detector model. A compilation of the respective results in regards to relative efficiency is shown in Fig. 7; no results of (Anton and Büermann, 2015) are included due to their different focus.

The compilation of literature data indicates a continuous decrease in the relative efficiency for x-ray qualities with an effective energy decreasing from 100 keV. The trend observed in the literature data is extended to below 10 keV in effective energy with the result presented here.

Anton and Büermann (2015) carried out an extensive study of the relative response of the alanine dosimeter extending the range of x-ray qualities from 280 kV down to 30 kV. The focus of their work is on experimental determination of the relative response. Low dosimetric uncertainties was obtained using a water calorimeter as primary standard. Here the relative efficiency was calculated using the microdosimetric one-hit detector model (Olko, 1999; Olko and PR Waligórski, 2002; Olko, 2002) and used to correct the MC calculated dose ratio to obtain good agreement with measurements of EPR response per unit dose to water. Comparison of our experimentally obtained value of relative response F_{Q,Q_0} presented in Equation (10) is in good agreement with the results of Anton and Büermann (2015), however the MC calculated ratio of doses H_{Q,Q_0} indicates a slight deviation which probably arises due to the use of different cross section data.

For use as a transfer dosimeter in the low energy range of photons a cobalt-60 calibration of the EPR signal per unit dose to water combined with a correction for the relative efficiency should be used. The result presented here is an extension of the literature data for the energy dependence of the alanine pellet dosimeter. How the relative efficiency is dependent on different beam characteristics (HVL, mean/effective energy, dose-rate, temperature, etc.) is still unclear, implying data from the literature may not be directly comparable. Further work on characterizing this intrinsic property, for example by isolating the dependence on specific beam qualifiers, is required.

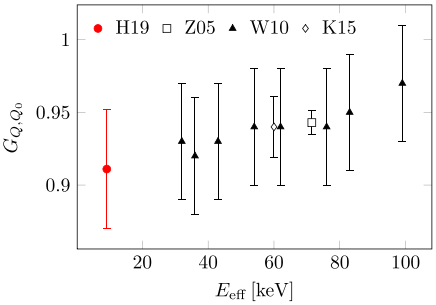

Fig. 7. Comparison of literature values for G_{Q,Q_0}. Legend entries refer to data from H19: the present study, Z05: Zeng and McCaffrey (2005) (using air kerma based dosimetry rather than water based), W10: Waldeland et al. (2010), and K15: Khoury et al. (2015) (using average energy instead of effective energy).

5. Conclusion

In this study we have investigated the relative efficiency of the alanine/EPR dosimeter subject to a 40 kV x-ray beam, with effective energy $E_{\text{eff}} = 9$ keV, relative to cobalt-60 γ-rays. The relative efficiency of this x-ray beam was measured to $G_{Q,Q_0} = 0.91 \pm 0.04$. The effective energy of the beam is about a factor three lower than the beam qualities investigated in the literature, and serves as an continuation of the trend observed mainly by Waldeland et al. (2010).

For comparison of EPR-response of x-irradiated and cobalt-60 irradiated alanine pellets, a geometrical correction based on MC calculated depth-dose curve in alanine was shown to be necessary. Correcting for this difference in dose gradient allows us to isolate the relative effectivness from the dose-to-alanine to dose-to-water ratio dependence.

The result presented in the present paper contributes to the overall characterization of the energy dependence of the alanine dosimeter. The validity of using effective energy (or tube potential, average energy, homogeneity factor, etc.) as beam qualifier is not clear, and should be investigated in greater detail for proper use of a correction for relative efficiency in alanine pellet dosimetry.

References

Andersen, C., Bøtter-Jensen, L., Murray, A., 2003. A mini x-ray generator as an alternative to a 90sr/90y beta source in luminescence dating. Radiat. Meas. 37, 557–561.
Anton, M., Büermann, L., 2015. Relative response of the alanine dosimeter to medium energy x-rays. Phys. Med. Biol. 60, 6113.
Anton, M., Kapsch, R.P., Krystek, M., Renner, F., 2008. Response of the alanine/esr dosimetry system to mv x-rays relative to 60co radiation. Phys. Med. Biol. 53, 2753.
Aukett, R., Harrison, R., Moretti, C., Nahum, A., Rosser, K., et al., 1996. The ipemb code of practice for the determination of absorbed dose for x-rays below 300 kv generating potential (0.035 mm al-4 mm cu hvl; 10-300 kv generating potential). Phys. Med. Biol. 41, 2605.
Berger, M., Hubbell, J., Seltzer, S., Chang, J., Coursey, J., Sukumar, R., Zucker, D., Olson, K., 1998. Xcom: Photon Cross Sections Database (Nbsir 87-3597). National Institute of Standards and Technology, Washington DC.
Bergstrand, E.S., Shortt, K.R., Ross, C.K., Hole, E.O., 2003. An investigation of the photon energy dependence of the epr alanine dosimetry system. Phys. Med. Biol. 48, 1753.
Dodd, B., Vetter, R.J., 2009. Replacement of 137cs irradiators with x-ray irradiators. Health Phys. 96, S27–S30.

Hefne, J., 2000. The dose distribution inside the irradiation chamber of the gamma cell 220 at kacst using mcnp4b. J. Nucl. Sci. Technol. 37, 402–405.
Helt-Hansen, J., Rosendal, F., Kofoed, I.M., Andersen, C.E., 2009. Medical reference dosimetry using epr measurements of alanine: development of an improved method for clinical dose levels. Acta Oncol. 48, 216–222.
Hubbell, J.H., Seltzer, S.M., 1995. Tables of X-Ray Mass Attenuation Coefficients and Mass Energy-Absorption Coefficients 1 keV to 20 MeV for Elements Z= 1 to 92 and 48 Additional Substances of Dosimetric Interest. Technical Report. National Inst. of Standards and Technology-PL, Gaithersburg, MD (United.
IAEA, 2001. Absorbed Dose Determination in External Beam Radiotherapy. Number 398 in Technical Reports Series. IAEA, Vienna.
Kawrakow, I., Mainegra-Hing, E., Rogers, D.W.O., Tessier, F., Walters, B.R.B., 2017. The EGSnrc Code System: Monte Carlo Simulation of Electron and Photon Transport. Technical Report PIRS-701. National Research Council Canada. URL. http://nrc-cnrc.github.io/EGSnrc/doc/pirs701-egsnrc.pdf.
Khoury, H., da Silva Jr., E., Mehta, K., de Barros, V., Asfora, V., Guzzo, P., Parker, A., 2015. Alanine-epr as a transfer standard dosimetry system for low energy x radiation. Radiat. Phys. Chem. 116, 147–150.
Olko, P., 1999. Calculation of the relative effectiveness of alanine detectors to x rays and heavy charged particles using microdosimetric one-hit detector model. Radiat. Protect. Dosim. 84, 63–66.
Olko, P., 2002. The microdosimetric one-hit detector model for calculating the response of solid state detectors. Radiat. Meas. 35, 255–267.
Olko, P., PR Waligórski, M., 2002. Microdosimetric one hit detector model for calculation of dose and energy response of some solid state detectors. Radiat. Protect. Dosim. 99, 381–382.
Olsen, K., Hansen, J., Wille, M., 1990. Response of the alanine radiation dosemeter to high-energy photon and electron beams. Phys. Med. Biol. 35, 43.
Rodrigues, R.R., Ribeiro, M.A., Grynberg, S.E., Ferreira, A.V., Meira-Belo, L.C., Sousa, R. V., Sebastiao, R.d.C., 2009. Gamma Irradiator Dose Mapping: a Monte Carlo Simulation and Experimental Measurements.
Sabbatucci, L., Salvat, F., 2016. Theory and calculation of the atomic photoeffect. Radiat. Phys. Chem. 121, 122–140.
Sharpe, P., Duane, S., 2003. Progress Report on Radiation Dosimetry at Npl. Report CCRI (I)/99-20.
Sleptchonok, O.F., Nagy, V., Desrosiers, M.F., 2000. Advancements in accuracy of the alanine dosimetry system. part 1. the effects of environmental humidity. Radiat. Phys. Chem. 57, 115–133.
Waldeland, E., Hole, E.O., Sagstuen, E., Malinen, E., 2010. The energy dependence of lithium formate and alanine epr dosimeters for medium energy x rays. Med. Phys. 37, 3569–3575.
Zeng, G., McCaffrey, J., 2005. The response of alanine to a 150 kev x-ray beam. Radiat. Phys. Chem. 72, 537–540.
Zeng, G., McEwen, M., Rogers, D., Klassen, N., 2004. An experimental and Monte Carlo investigation of the energy dependence of alanine/epr dosimetry: I. clinical x-ray beams. Phys. Med. Biol. 49, 257.
Zeng, G., McEwen, M., Rogers, D., Klassen, N., 2005. An experimental and Monte Carlo investigation of the energy dependence of alanine/epr dosimetry: ii. clinical electron beams. Phys. Med. Biol. 50, 1119.

Paper II

Title:

Comparison of the microbicidal effectiveness of 150 kV x-rays and cobalt-60 gamma rays.

Authors:

Hjørringgaard JG, Miller A, Andersen CE, Cloetta D, Wandfluh W, and Tallentire A

Submitted to:

Radiation Physics and Chemistry,
May 2021.

Status:

Under review.

Comparison of the microbicidal effectiveness of 150 kV x-rays and cobalt-60 gamma rays

Jakob G. Hjørringgaard*[1], Arne Miller[1], Claus E. Andersen[1], Dominique Cloetta†[2], Willi Wandfluh†[2], and Alan Tallentire[3]

[1]Department of Health Technology, Technical University of Denmark, Roskilde, Denmark
[2]ebeam Technologies, COMET AG, CH-3175, Flamatt, Switzerland
[3]Apt. 3 Osborne House, 73 Alderly Road, Wilmslow, Cheshire SK9 1 PA, UK

May 3, 2021

Abstract

The radiation response, quantified by the dose-log survival curve, of spores of *Bacillus pumilus* subjected to irradiation in a 150 kV x-ray beam was examined and compared with the response obtained by irradiation in a reference cobalt-60 field. The spores were irradiated at doses ranging from 2 kGy to 11 kGy. The responses were the same for both beam qualities within measurement uncertainties. Further comparison with literature data showed that the 150 kV response of *B. pumilus* spores is the same as the response at high energy x-rays, low and high energy electron beams, and cobalt-60 gamma beams.

1 Introduction

In two previous papers it has been shown that the dose response of *Bacillus pumilus* spores irradiated under specified standardized conditions, namely fully water-hydrated spores in the presence of air, is independent of beam quality for cobalt-60 gamma rays, high energy x-rays, and low and high energy electrons (Tallentire et al., 2010; Tallentire and Miller, 2015).

Low energy x-irradiators are attracting interest as replacement for gamma irradiators for several applications involving cell inactivation and potentially sterilization. A recent example is decontamination of medicinal cannabis which is currently carried out using cobalt-60 gamma irradiators (Hazekamp, 2016), but x-ray alternatives are being examined. Similarly for applications in irradiation of fruit as a quarantine treatment. For applications such as blood irradiation and the sterile insect technique commercially available self-shielded x-ray units are available, typically using peak voltage in the order of 150 kV (Khoury et al., 2015). With these developments it is of interest to assess the microbicidal effectiveness of x-rays in this energy region, expanding on the work presented in Tallentire et al. (2010) and Tallentire and Miller (2015).

Here we investigate the dose-log survival response, in the dose range 2 kGy to 11 kGy, of *B. pumilus* spores present in the above 'standardized' conditions and irradiated with a 150 kV x-ray beam. Also, as the supplier of the stock *B. pumilus* spore suspension used to prepare the batch of test filters employed in the present study was different from the supplier used previously, it was deemed necessary to verify the suitability of the new batch for assessing comparable microbicidal

*E-mail: jakg@dtu.dk
†present address: Tetra Pak eBeam Systems AG, Herrengasse 10, 3175 Flamatt, Switzerland

effectiveness. This was achieved by generating the dose-log survival response for cobalt-60 gamma rays and comparing it with previous findings.

Throughout this paper the term dose is used to mean absorbed dose to water.

2 Materials and methods

2.1 Microbiological test filters

The production of microbiological test filters is based broadly on the methods described by Powers et al. (1957) with the exact procedure being equivalent to that used for our previous work (Tallentire et al., 2010; Tallentire and Miller, 2015). A test piece consists of a test filter possessing a known number of hydrated spores of *B. pumilus*, ranging from around 4×10^1 to 4×10^7, located on the surface of a GS grade cellulose acetate membrane filter placed in a 9 cm Petri dish. X-irradiation was carried out with predetermined, well-defined doses to give numbers of survivors that were countable as colonies following incubation of the irradiated test piece placed on nutrient medium.

A new batch of test filters was made for the present low energy x-ray experiments using a suspension of spores of *B. pumilus* (cell line 27142 LOT PU140) containing 2.5×10^9 spores/cm^3 obtained from Crosstex[1]. This batch of test filters was produced in July 2018.

2.2 Gamma irradiation

Cobalt-60 irradiation of test pieces was carried out in two separate Gammacells located at Risø HDRL, DTU Health Tech. Gammacell 3 is a Nordion GC-220 (geometry described in e.g. Hefne (2000); Rodrigues et al. (2009)) with dose rate of approximately 85 Gy min^{-1} in the reference position, and Gammacell 1 is very similar in design with dose rate of approximately 3.4 Gy min^{-1}. Irradiation of test pieces in Gammacell 1 was done immediately (over the course of a few weeks) after production of test filters to examine the suitability of the batch. Irradiation of test pieces in Gammacell 3 was done prior to irradiation in the low energy x-ray field to reconfirm the validity of the batch since 18 months had elapsed since the time of its production.

The procedure for dose measurement in the Gammacells followed the description by Tallentire et al. (2010).

2.3 X-ray irradiation

The low energy x-irradiation was carried out at ebeam Technologies, Comet, Flamatt, Switzerland. An XBA-200/270H x-ray tube was used. This is an x-ray emitter with a large tantalum transmission target, window height 270 mm and width 40 mm, allowing for irradiation of several test pieces simultaneously. The tube parameters used was an accelerating potential of 150 kV and filament current of 20 mA. The test pieces were placed on a turntable at 10 cm distance from the turntable

[1] https://www.crosstex.com/

central axis to the exit window of the x-ray emitter. The turntable ensured homogeneous dose distribution in the irradiated Petri dishes.

2.3.1 Dose measurement

The delivered dose was monitored during irradiation of test pieces by measurements using both alanine film and pellet dosimeters. The alanine dosimeters are calibrated for dose to water in a reference cobalt-60 field, a Nordion GC-220 (Risø HDRL Gammacell 3), the dose rate of which is determined with traceability to the national standards at the National Physical Laboratory, UK.

The alanine pellets used are obtained from Harwell Dosimeters, and they consist of $\sim 91\,\%$ L-α-alanine and $\sim 9\,\%$ paraffin wax. They are cylindrical with a diameter of 4.8 mm, height 2.7 mm, and average mass 60 mg.

The alanine film dosimeters are obtained from Kodak (BioMax, lot B0312). They consist of a mixture (by weight) of 50 % L-α-alanine and 50 % binder material $(C_2H_2F_2)_n(C_2F_4)_p$ coated (45 mm $\times$ 4 mm) on a polyester stick. The thickness of the coating is 135 µm and the polyester stick thickness is 175 µm.

The electron paramagnetic resonance (EPR) response, defined as the peak-to-peak height of the first derivative of the EPR spectrum normalized to individual pellet mass, of the alanine pellets was measured using a Bruker e-scan and EMXmicro for high and low doses respectively. For the alanine films the EPR measurement is done entirely on the EMXmicro.

The EPR response of alanine is however energy dependent for low energy x-rays (Zeng and McCaffrey, 2005; Waldeland et al., 2010; Khoury et al., 2015; Anton and Büermann, 2015; Hjørringgaard et al., 2020), and as such the response per dose to water of the two types of alanine dosimeters in the x-ray field relative to the reference cobalt-60 field must be determined. The relative response F_{Q,Q_0} of the alanine dosimeters in the x-ray field Q compared to a reference cobalt-60 gamma field Q_0 can be written as

$$F_{Q,Q_0} = \frac{(r/D_{\text{ala}})_Q}{(r/D_{\text{ala}})_{Q_0}} \cdot \frac{(D_{\text{ala}}/D_{\text{w}})_Q}{(D_{\text{ala}}/D_{\text{w}})_{Q_0}} \tag{1}$$

$$= \frac{(r/D_{\text{w}})_Q}{(r/D_{\text{w}})_{Q_0}}, \tag{2}$$

where r is the EPR response, D_{ala} is the dose to the alanine dosimeter, and D_{w} is the corresponding dose to a water at the effective point of measurement of the alanine dosimeter. On the right hand side of Equation (1) the first term takes care of the change in signal production between radiation quality Q and Q_0, while the second term address the change in dose ratios. A combination of these two effects result in the relative response described as the change in signal production per dose to water. The relative response of the alanine pellet dosimeter as a function of the effective energy in low and medium energy x-ray fields has been experimentally determined for alanine pellet dosimeters in several publications (Waldeland et al., 2010; Anton and Büermann, 2015).

To maintain traceability to national standards the dose to water in a low energy x-ray field $D_{\text{w},Q}$ can then be calculated from the dose to water determined from a cobalt-60 calibration D_{w,Q_0} by

applying a quality correction factor $k_Q = F^{-1}_{Q,Q_0}$ as

$$D_{w,Q} = k_Q D_{w,Q_0}. \quad (3)$$

For the alanine pellet dosimeters the relative response was determined by interpolation of literature data from Waldeland et al. (2010) and Anton and Büermann (2015), based on the effective energy of the x-ray beam. The dose to water calculated in this manner for measurements using either alanine pellet or film dosimeters, is assumed to be representative for the dose to the test filter.

For the alanine film dosimeters no literature data on the relative response is available. To assess the relative response of the alanine film dosimeters, film and pellet dosimeters were irradiated under identical conditions in the 150 kV x-ray field and the relative EPR responses were compared to those obtained by dosimeters irradiated in a cobalt-60 reference field.

The choice of using alanine dosimeters for dose measurements in the present experiment, rather than using more well-established methods like ionization chambers, was made on the basis that code of practices for low and medium energy x-rays ionization chamber dosimetry (Aukett et al., 1996; Ma et al., 2001) are primarily assuming point-like sources (circular field at detector position). The different components required for ionization chamber dosimetry, e.g. backscatter factor, is highly dependent on field size. It is not clear how to apply these corrections to the ionization chamber readings for the kind of x-ray field (270 mm window height and 40 mm window width) used in the present study.

2.4 Irradiation of test pieces

For each dose two test pieces were irradiated and scored separately. An overview of the different test filters and the nominal dose required to obtain statistically relevant and countable number of colony forming units is given in Table 1. The selected exposure times were estimated by measurements of the air kerma rate at the central position of the stack of Petri dishes.

Table 1: Overview of test filters used for x-ray irradiations at Comet, showing test filter name and suspension of *B. pumilus* spores, and the nominal dose D used for dose planning. The selected exposure time in the x-ray field, to deliver the nominal dose, is also listed.

Test filter	Spores on filter	D [kGy]	t_{exp} [h]
DS8	4×10^1	0.0	
DS7	4×10^2	2.5	4.19
DS6	4×10^3	4.3	7.20
DS5	4×10^4	5.8	9.72
DS4	4×10^5	7.2	12.06
DS3	4×10^6	8.4	14.07

Irradiation of test pieces was done in intervals. For each irradiation interval a stack of 14 Petri dishes was placed on a turntable in front of the x-ray emitter. The stack of Petri dishes consists of:

- Three empty Petri dishes in both bottom and top of the stack to ensure full and equal scatter conditions for all irradiated test pieces.

- Next in the stack from both bottom and top is one Petri dish containing four alanine pellets located on a dry filter pad to mimic irradiation conditions of test pieces.

- In the center are six test pieces with alanine film dosimeters attached on the bottom.

Furthermore three alanine film dosimeters were placed on the outside bottom of each Petri dish containing test pieces. See Figure 1 for a picture of the irradiation geometry. The stack of Petri dishes is placed with the center at a 10 cm distance to the x-ray exit window.

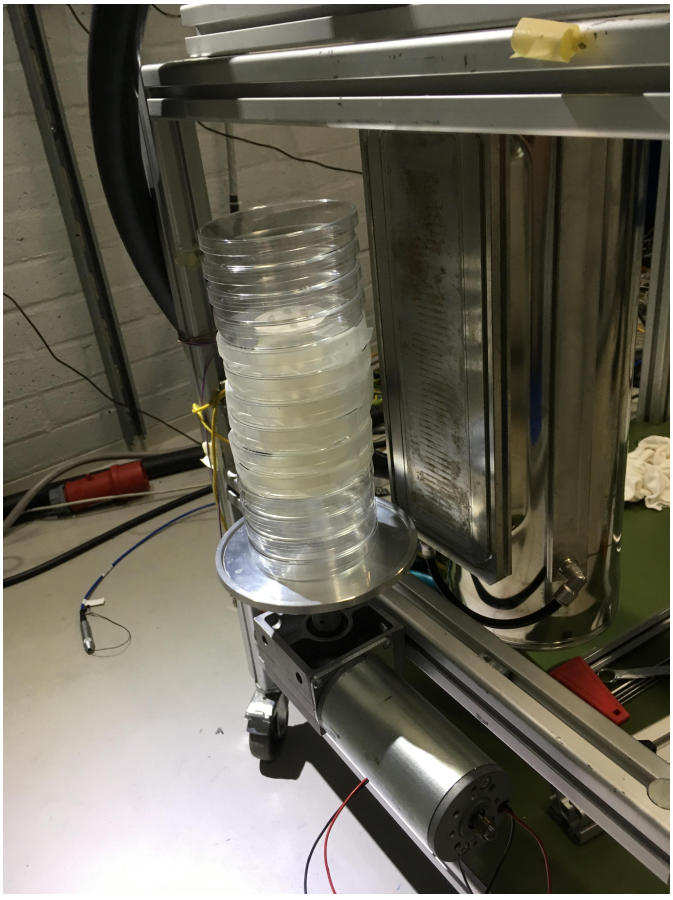

Figure 1: Example of x-ray irradiation geometry consisting of a stack of Petri dishes, containing either nothing (top and bottom three), alanine pellet dosimeters (number four from top and bottom), or test pieces and alanine film dosimeters (middle six). The stack is located on a turntable with central axis at 10 cm distance to the exit window.

3 Results and discussion

3.1 Beam characterization

To verify uniform dose across the test filters, the dose distribution across the bottom of each Petri dish in a 14 piece stack was measured using Gafchromic HD-V2 (GAF) film. These measurements were relative and only used to assess the homogeneity of the dose delivery. The film dosimeters were analyzed using the RisøScan software (Helt-Hansen and Miller, 2004), showing an average variation in dosimeter response across individual films of 1.5 % with no significant gradient in response across the GAF films. Comparisons between GAF films irradiated at different positions in the stack of Petri dishes show that the response drops off for the top and bottom ones, however for the central Petri dishes, at positions in the stack where dosimeters and test pieces are placed, the response is uniform.

The half-value layer (HVL) of the x-ray beam was measured using a PTW 23344 soft x-ray ionization chamber. The ionization chamber was placed at the surface of a PTW 2962 polymethyl methacrylate (PMMA) slab phantom with the effective point of measurement at 10 cm distance from the x-ray tube exit window. An increasing number of attenuating aluminum plates was placed between the ionization chamber and the source to estimate the HVL. The HVL data are shown in Figure 2, indicating a HVL of roughly 17 mm of aluminum for this particular geometry. Since the HVL measurements are carried out in a irradiation geometry significantly different from recommended HVL measurement conditions (Ma et al., 2001), the effective energy of the x-ray tube can not be directly calculated from mass attenuation coefficients.

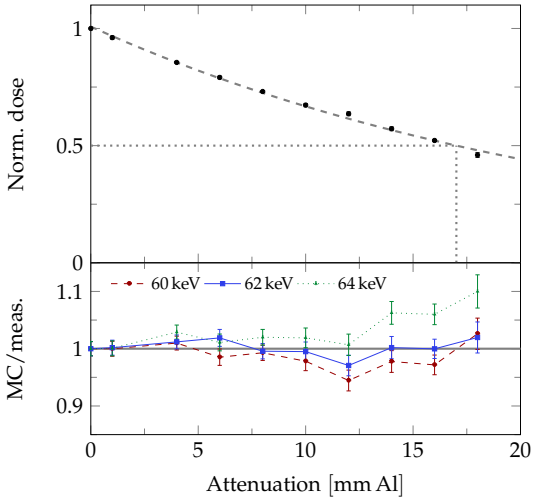

Figure 2: *Top:* Ionization chamber measurements of the attenuation of the x-ray beam by insertion of aluminum plates between the detector and source. *Bottom:* Ratio of MC calculated to measured attenuation for monoenergetic photon beams.

To estimate the effective energy of the x-ray tube Monte Carlo (MC) calculations of the attenuation of monoenergetic photon beams in the applied geometry were carried out, using the `flurznrc`

usercode of the EGSnrc MC software (Kawrakow et al., 2017). The irradiation geometry was approximated in EGSnrc by a cylindrical PMMA phantom of diameter equal to the side length of the actual phantom. The photon fluence was scored in an air volume located at the position of the ionization chamber volume in the phantom, for increasing aluminum attenuation thickness. The ratio of MC calculated fluence to ionization chamber measurement, both normalized to the zero attenuation value, for three monoenergetic photon beams is shown in Figure 2. The best agreement is obtained for monoenergetic photon energy 62 keV where the mean ratio of calculated to measured attenuation is 1.002 with standard deviation 1.4 %. This energy is adopted as the effective energy of the x-ray tube $E_{\text{eff}} = 62\,\text{keV}$.

By interpolation of literature data on the relative response of the alanine pellet dosimeter, a value of[2] $F^{\text{P}}_{\text{Q},\text{Q}_0} = 0.79$ is obtained for $E_{\text{eff}} = 62\,\text{keV}$.

3.2 Relative response of alanine films

To assess the response of the alanine film dosimeters in the 150 kV x-ray field relative to a cobalt-60 reference field a comparison of the EPR response, measured from alanine film and pellet dosimeters after equal exposure, were carried out. The alanine film and pellet dosimeters were separately placed at the surface of the PTW 2962 PMMA phantom, with surface at 10 cm distance to the x-ray source. The relationship between the EPR response of the two dosimeters after irradiation in the 150 kV x-ray field and a reference cobalt-60 field is shown in Figure 3.

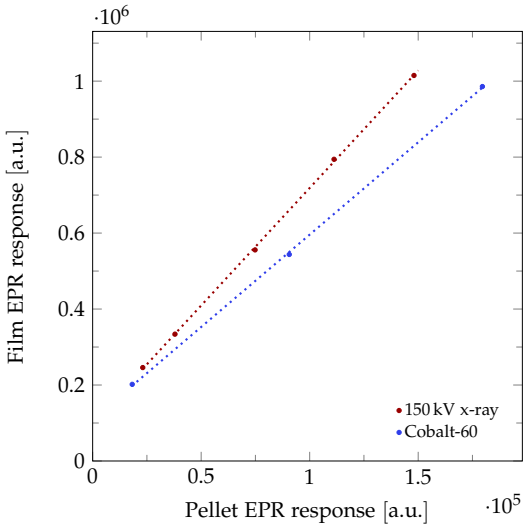

Figure 3: The EPR response of alanine film dosimeters versus alanine pellet dosimeters for equal exposures in the 150 kV x-ray field under investigation in the present study, and in a cobalt-60 reference field.

[2]The superscript P is used here to denote the relative efficiency for the pellet dosimeter. A superscript F will be used to denote film dosimeters.

The relative response of the alanine film dosimeter F^{F}_{Q,Q_0} was then determined by correcting the relative response of the alanine pellet dosimeter by the ratio of the slopes obtained by linear regression to data shown in Figure 3. The slopes were determined to be 6.19 and 4.86 for the 150 kV x-ray and the cobalt-60 gamma respectively. Using $F^{P}_{Q,Q_0} = 0.79$ for the alanine pellet dosimeter a relative response of $F^{F}_{Q,Q_0} = 1.01$ is obtained for the film dosimeter.

3.3 Dose measurements

Comparison of dose measurements The dose to test filters measured during irradiation of the test pieces using alanine film and pellet dosimeters, $D^{F}_{w,Q}$ and $D^{P}_{w,Q}$ respectively, are compared in Figure 4. The doses determined by the two individual dosimeters agree well within the estimated

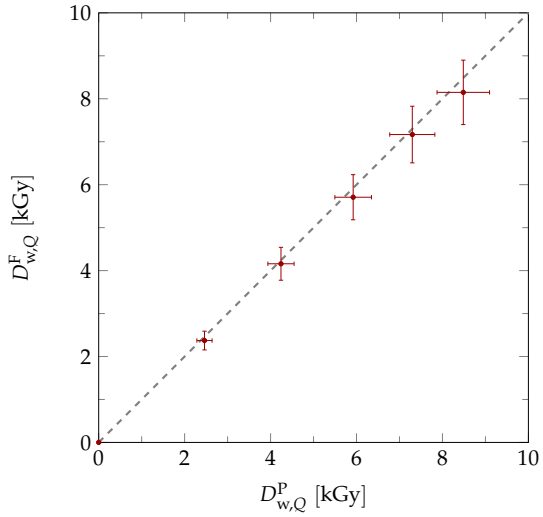

Figure 4: Comparison of doses measured by alanine film $D^{F}_{w,Q}$ and pellet $D^{P}_{w,Q}$ dosimeters. The error bars represent uncertainties at $k = 2$. The dashed gray line represent a slope of unity.

uncertainties, however dose determined by alanine film dosimeters is on average 3.0 % lower than the dose determined with the alanine pellet dosimeter. Since the measured EPR response is an average over the dosimeter, this variation may be due to the difference in dosimeter volume.

Uncertainties The uncertainties on the measured doses shown in Figure 4 are obtained by summation in quadrature of all independent uncertainty components. An overview of the considered uncertainty components is given in Table 2. The total uncertainty obtained for $D^{P}_{w,Q}$ and $D^{F}_{w,Q}$ include all components of uncertainty considered for establishing traceability of the dosimetry system. All uncertainties are stated at $k = 1$.

The uncertainty on the dose to water determined by alanine dosimeters consist of contributions from the dose to water calibration in the cobalt-60 Gammacell and the determination of the relative response. The uncertainty of the relative response of the alanine pellet dosimeter is estimated from

Table 2: Uncertainty budget for the dose measurements with alanine pellet and film dosimeters in the x-ray beam. All uncertainties are stated at $k = 1$.

Parameter	Comment	Type	σ ($k = 1$)
D_w measured by alanine pellet dosimeters in x-ray field Q:			
D_{w,Q_0}	D_w calibration of alanine pellet dosimeter in cobalt-60	B	1.7 %
F^P_{Q,Q_0}	Estimated from fit to literature data	B	3.3 %
$D^P_{w,Q}$	Combined uncertainty of D_{w,Q_0} and F^P_{Q,Q_0}	Combined	3.6 %
Relative response of alanine film dosimeter:			
EPR fit	Linear regression for x-ray EPR response	A	1.4 %
	Linear regression for cobalt-60 EPR response	A	2.5 %
F^F_{Q,Q_0}	Combination of uncertainties in EPR response and F^P_{Q,Q_0}	Combined	3.9 %
D_w measured by alanine film dosimeters in x-ray field Q:			
$D^F_{w,Q}$	Combined uncertainty of D_{w,Q_0} and F^F_{Q,Q_0}	Combined	4.6 %

the experimental uncertainties stated in Waldeland et al. (2010) and Anton and Büermann (2015) in combination with a conservative estimate of the uncertainty on the effective energy of the x-ray beam (5 % at $k = 1$). The relative response of alanine film dosimeters consist of contributions from EPR response of film and pellet dosimeters in the respective radiation fields as well as the stated uncertainty of the relative response of the alanine pellet dosimeter. The uncertainty of the measured EPR response is evaluated from the residuals of the linear regression of EPR response of pellet versus film dosimeters.

3.4 Microbiological responses

A wide range of viable spores present on the unirradiated test filters (see Table 1), combined with suitable choices of dose yielding number of survivors in the range of 15 to 50 colony forming units, allow for a linear dose-log survival curve to cover six log-cycles of inactivation of *B. pumilus* spores in the x-ray field and eight log-cycles in the cobalt-60 Gammacell irradiations. The choice to not extend the dose range in the x-ray field was made due to time considerations. Data for the survival fraction of spores irradiated in Gammacell 1, Gammacell 3, and the low energy x-ray field is shown in Figure 5. The dose used for the 150 kV x-ray quality shown in Figure 5 is the dose measured using alanine pellet dosimeters. It is evident that a common response function can describe the survivability of *B. pumilus* spores irradiated with cobalt-60 gamma rays and the 150 kV x-ray beam.

D_{10}-values were calculated from the slope of a linear regression to the log surviving fraction $\log S = a \cdot D + b$ for each individual radiation quality by $D_{10} = -1/a$. The calculated D_{10}-values are (1.33 ± 0.12) kGy and (1.44 ± 0.10) kGy, at $k = 2$, for the cobalt-60 and 150 kV x-ray irradiations respectively.

Uncertainties The uncertainty on the spore count on the test filters was estimated by the relative difference between the individual spore counts on test filters irradiated at same dose in each beam

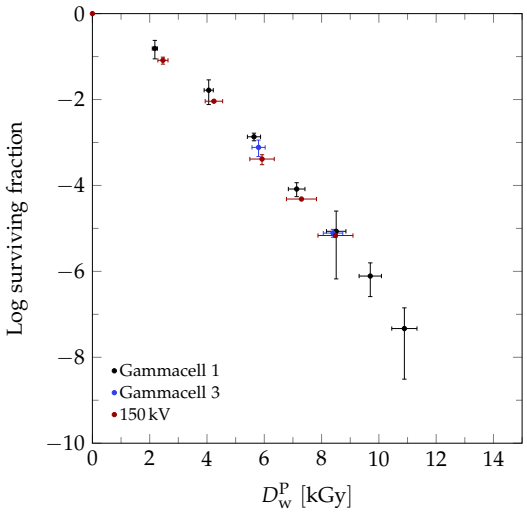

Figure 5: Surviving fraction of water hydrated *B. pumilus* spores irradiated at cobalt-60 gamma and at 150 kV x-ray. The error bars represent uncertainties at $k = 2$.

quality, divided by $\sqrt{3}$ in the same manner as in Tallentire et al. (2010). The error bars shown in Figure 5 represent the survival fraction obtained at these limiting cases, at $k = 2$.

Uncertainties for slope and D_{10}-values are estimated by the standard error of the least squares used to fit the data.

4 Conclusion

The radiation response of water-hydrated *B. pumilus* spores irradiated in air to a 150 kV x-ray beam was found to be the same as the response in a reference cobalt-60 field within experimental uncertainties. The results obtained in the present study serve as an expansion on previously published results on the radiation response of *B. pumilus* spores for low and high energy electron beams, high energy x-ray beams, and cobalt-60 gamma beams. The conclusion stands that the microbicidal effectiveness of these beam qualities are equal in the dose range 2 kGy to 11 kGy.

References

Anton, M. and L. Büermann (2015). Relative response of the alanine dosimeter to medium energy x-rays. *Physics in Medicine & Biology 60*(15), 6113.

Aukett, R., R. Harrison, C. Moretti, A. Nahum, K. Rosser, et al. (1996). The ipemb code of practice for the determination of absorbed dose for x-rays below 300 kv generating potential (0.035 mm al-4 mm cu hvl; 10-300 kv generating potential). *Physics in Medicine & Biology 41*(12), 2605.

Hazekamp, A. (2016). Evaluating the effects of gamma-irradiation for decontamination of medicinal cannabis. *Frontiers in pharmacology 7*, 108.

Hefne, J. (2000). The dose distribution inside the irradiation chamber of the gamma cell 220 at kacst using mcnp4b. *Journal of Nuclear Science and Technology 37*(sup1), 402–405.

Helt-Hansen, J. and A. Miller (2004). Risøscan—a new dosimetry software. *Radiation Physics and Chemistry 71*(1-2), 361–364.

Hjørringgaard, J. G., C. Ankjærgaard, M. Bailey, and A. Miller (2020). Alanine pellet dosimeter efficiency in a 40 k v x-ray beam relative to cobalt-60. *Radiation Measurements*, 106374.

Kawrakow, I., E. Mainegra-Hing, D. W. O. Rogers, F. Tessier, and B. R. B. Walters (2017). The EGSnrc code system: Monte Carlo simulation of electron and photon transport. Technical Report PIRS-701, National Research Council Canada.

Khoury, H., E. da Silva Jr, K. Mehta, V. de Barros, V. Asfora, P. Guzzo, and A. Parker (2015). Alanine-epr as a transfer standard dosimetry system for low energy x radiation. *Radiation Physics and Chemistry 116*, 147–150.

Ma, C.-M., C. Coffey, L. DeWerd, C. Liu, R. Nath, S. Seltzer, and J. Seuntjens (2001). Aapm protocol for 40–300 kv x-ray beam dosimetry in radiotherapy and radiobiology. *Medical physics 28*(6), 868–893.

Powers, E., C. Ehret, and A. Bannon (1957). The membrane filter technique in radiation studies of spores of bacillus megaterium. *Applied microbiology 5*(2), 61.

Rodrigues, R. R., M. A. Ribeiro, S. E. Grynberg, A. V. Ferreira, L. C. Meira-Belo, R. V. Sousa, and R. d. C. Sebastiao (2009). Gamma irradiator dose mapping: a monte carlo simulation and experimental measurements.

Tallentire, A. and A. Miller (2015). Microbicidal effectiveness of x-rays used for sterilization purposes. *Radiation Physics and Chemistry 107*, 128–130.

Tallentire, A., A. Miller, and J. Helt-Hansen (2010). A comparison of the microbicidal effectiveness of gamma rays and high and low energy electron radiations. *Radiation Physics and Chemistry 79*(6), 701–704.

Waldeland, E., E. O. Hole, E. Sagstuen, and E. Malinen (2010). The energy dependence of lithium formate and alanine epr dosimeters for medium energy x rays. *Medical physics 37*(7Part1), 3569–3575.

Zeng, G. and J. McCaffrey (2005). The response of alanine to a 150 kev x-ray beam. *Radiation physics and chemistry 72*(5), 537–540.

Paper III

Title:

Comparison of detector efficiency for different alanine pellet dosimetry systems in kilovoltage x-ray fields.

Authors:

Hjørringgaard JG and Nasreddine A

Status:

To be submitted to Radiation Physics and Chemistry

Comparison of detector efficiency for different alanine pellet dosimetry systems in kilovoltage X-ray fields

Jakob G. Hjørringgaard*[1] and Abbas Nasreddine†[2]

[1]Department of Health Technology, Technical University of Denmark, Roskilde, Denmark
[2]Aerial, 250 Rue Laurent Fries, 67400, Illkirch, Graffenstaden, France

May 2, 2021

Abstract

During the last two decades several experimental studies have been published, characterizing the energy dependence of different alanine pellet dosimeters in low and medium energy X-ray fields. Here we present a comparison of the energy dependence of two different alanine pellet dosimetry systems.

Alanine pellets, differing in size and chemical composition, were irradiated under identical conditions at the National Physical Laboratory (Teddington, UK), for X-ray beams at accelerating potential 135 kV and 280 kV. Analysis of the induced detector signal was carried out independently for the two sets of alanine pellets.

The relative response of the alanine pellet dosimeters was in agreement with a relative difference of 1.5 % and 2.2 % while the relative difference for the relative efficiency was 0.4 % and 1.0 % for the the respective X-ray beam qualities.

1 Introduction

Due to both safety concerns and increasing difficulty in acquiring and transporting radioactive sources, industrial applications of ionizing radiation, such as blood (Saglam et al., 2011) and food irradiation (Barkai-Golan and Follett, 2017), are increasingly looking for low to medium energy X-ray alternatives.

However, issues regarding the energy dependence of the alanine pellet dosimeters for routine dosimetry at low to medium X-ray energies have been highlighted in a range of studies (Zeng and McCaffrey, 2005; Waldeland et al., 2010; Khoury et al., 2015; Anton and Büermann, 2015; Hjørringgaard et al., 2020; Nasreddine et al., 2020). Results suggest that the detector response per dose to water in low energy X-ray fields relative to reference fields (typically cobalt-60) decrease with decreasing effective energy. Furthermore, Monte Carlo calculations of the dose ratios of detector material to water show that a change in radiation absorption properties for lower energies can not fully explain the decrease in detector response, implying a decrease in the stable free radical production for lower X-ray energies. Several geometries, X-ray fields, and dosimeters are used across the published data, making direct comparison questionable.

*E-mail: jakg@dtu.dk
†E-mail: a.nasreddine@aerial-crt.com

Here we investigate the relative efficiency of two different alanine pellet dosimetry systems. The dosimetry systems consist of alanine pellets obtained from Aerial (Illkirch, FRANCE) and Harwell Dosimeters (Oxforshire, UK) respectively, using different Electron Paramagnetic Resonance (EPR) spectrometers and reference radiation fields. In this study, the alanine pellets were irradiated in the same X-ray fields using identical irradiation conditions in order to make a direct comparison possible.

2 Materials and Methods

2.1 Relative efficiency

The energy dependence of a dosimeter subject to radiation at beam quality Q relative to a reference beam quality Q_0 can be quantified by the relative response F_{Q,Q_0} as:

$$F_{Q,Q_0} = \frac{(R/D_{\mathrm{w}})_Q}{(R/D_{\mathrm{w}})_{Q_0}}, \tag{1}$$

where R is the dosimeter EPR response and D_{w} is the absorbed dose to water at the effective point of measurement. For a linear relationship between dosimeter response and dose to water the relative response can be experimentally determined as the ratio of the slopes of response functions. This is true at absorbed doses that are smaller than $\sim 10\,\mathrm{kGy}$ where the alanine pellet dosimeter shows linear response with respect to absorbed dose to water (Goodman et al., 2017).

The right hand side of Equation (1) can be expanded to include the dose to dosimeter material D_{dos} as

$$F_{Q,Q_0} = \frac{(D_{\mathrm{dos}}/D_{\mathrm{w}})_Q}{(D_{\mathrm{dos}}/D_{\mathrm{w}})_{Q_0}} \cdot \frac{(R/D_{\mathrm{dos}})_Q}{(R/D_{\mathrm{dos}})_{Q_0}}, \tag{2}$$

where the first term is the dosimeter to water ratio of doses in the investigated beam quality relative to the reference beam quality. This ratio is later on referred as:

$$H_{Q,Q_0} = \frac{(D_{\mathrm{dos}}/D_{\mathrm{w}})_Q}{(D_{\mathrm{dos}}/D_{\mathrm{w}})_{Q_0}}. \tag{3}$$

The second term is the relative efficiency of the dosimeter, and is expressed as:

$$G_{Q,Q_0} = \frac{(R/D_{\mathrm{dos}})_Q}{(R/D_{\mathrm{dos}})_{Q_0}}. \tag{4}$$

The relative efficiency of a dosimeter refer to the efficiency of signal production after receiving a dose of ionizing radiation at a specific beam quality Q relative to a reference beam quality Q_0.

The relative dosimeter to water ratio of doses H_{Q,Q_0} can be obtained through Monte Carlo (MC) calculations, while the relative efficiency G_{Q,Q_0} can be determined as the discrepancy between the experimentally measured relative response and the relative ratio of doses, when all known influencing factors are accounted for.

2.2 Alanine dosimetry systems

Two different alanine pellet dosimetry systems was investigated. The first system uses the commercial alanine dosimeters from Aerial (LOT 09/11) (Nasreddine, 2020). The pellets are cylindrical with diameter 4 mm and height 2.35 mm with an average mass of 36.05 ± 0.05mg. The composition of the dosimeter is 91.63 % pure L-alanine, 6.37 % EUDRAGIT NE 30D and 2 % MYVATEX (Marchioni et al., 2002). The EPR readout was performed using a Megnettech MS5000 spectrometer (Freiberg Instruments, GERMANY) operating at 9.253 GHz. The parameters used for the EPR readout is a 20 mT field width, 15 s sweep time, modulation amplitude and frequency of 1 mT and 100 kHz respectively. The microwave power was 2 mW. Each alanine pellet is placed separately in a quartz tube which is then inserted in the EPR cavity. A reference ruby is permanently positioned in the resonant cavity. This reference is used to correct the measured alanine EPR response by comparing the EPR response of the ruby reference at the measurement and its value when the calibration curve was established.

A second alanine pellet dosimetry system consisted of dosimeters obtained from Harwell Dosimeters. They consist of 91 % L-α-alanine and 9 % paraffin wax. They are cylindrical with a diameter of 4.8 mm, height 2.7 mm, and average mass 60 mg. The EPR readout was performed using a Bruker EMXmicro sepctrometer operating at 9.53 GHz. The alanine pellets are placed in a quartz tube in the resonator for all measurements to assure identical positioning. The data acquisition parameters were a sweep width of 2 mT, sweep time 21 s, modulation amplitude 1 mT, and microwave power 3.375 mW.

2.3 Experimental procedure

2.3.1 Kilovoltage x-ray irradiation prodcedure

The X-ray irradiations were carried out at the National Physical Laboratory (NPL), UK. Two of the NPL reference beam qualities were used for irradiation of alanine pellet dosimeters. Specifications of beam qualities is given in Table 1.

Table 1: NPL reference beam qualities used for irradiations of alanine pellet dosimeters. The relevant parameters for converting ionization chamber measurement to dose to water is also listed.

Half Value Layer		Nominal potential	Filtration			k_{ch}	$\left[\left(\frac{\overline{\mu}_{en}}{\rho}\right)_{w/air}\right]_{z=2,\phi}$
mm Al	mm Cu	kV	mm Sn	mm Cu	mm Al		
8.8	0.50	135	-	0.27	1.2	1.023	1.046
20.0	4.0	280	1.50	0.26	1.0	1.023	1.101

The irradiation geometry consisted of a Solid Water® phantom (WT1, Phoenix Dosimetry Ltd.) with an inlet for a farmer type ionization chamber, where the effective point of measurement is positioned in the central region of the phantom at 2 cm water equivalent depth. An ionization chamber dummy made of Solid Water® material, with room for three alanine pellets in the same position as the effective point of measurement of the ionization chamber (see Figure 1), was used

for the alanine pellet irradiations. The Solid Water® phantom was placed at a source to surface distance (SSD) of 75 cm. Full backscatter conditions were obtained by adding 26 cm of Solid Water® slabs behind the dosimeters.

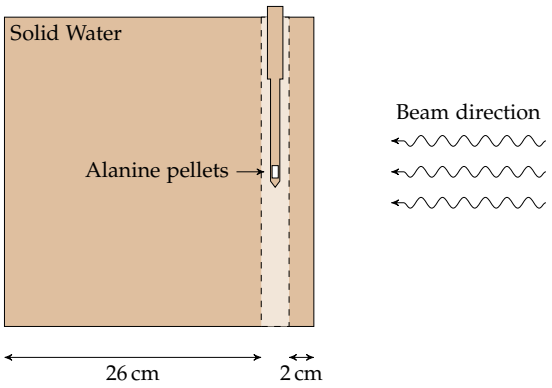

Figure 1: Side view of Solid Water® geometry with ionization chamber dummy containing alanine pellets at the effective point of measurement of the actual ionization chamber.

Ionization chamber dosimetry in terms of absorbed dose to water was performed according to the IPEMB code of practice (Aukett et al., 1996) using a PTW 30012 Farmer type ionization chamber. According to the protocol the dose to water can be calculated, for in-phantom measurements, by

$$D_{w,z=2} = MN_K k_{ch} \left[\left(\frac{\overline{\mu}_{en}}{\rho} \right)_{w/air} \right]_{z=2,\phi}, \tag{5}$$

where $D_{w,z=2}$ is the absorbed dose to water at 2 cm depth in water (chamber position), M is the chamber response (electrometer reading) corrected to air temperature 20 °C and ambient air pressure 1013.25 mbar, N_K is the chamber calibration factor, k_{ch} is a correction factor accounting for the change in response of the chamber between calibration and measurement in a phantom, and $[(\overline{\mu}_{en}/\rho)_{w/air}]_{z=2,\phi}$ is the mass energy absorption coefficient ratio of water to air averaged over the photon spectrum at 2 cm depth in water equivalent material and field diameter ϕ. Values for corrections used are listed in Table 1. Ionization chamber measurements were used to determine the dose rate at 2 cm depth in water for the different beam qualities for relevant filament currents.

Three Harwell alanine pellets could be placed in the solid water ionization chamber dummy at a time, while the smaller volume of the Aerial alanine pellets allowed for four pellets to be irradiated simultaneously. The smaller volume of the Aerial alanine pellets does however introduce an air gap between the alanine pellets and the solid water holder. The effect of the air gap on the energy deposition in the dosimeter is evaluated by MC calculations.

2.3.2 Cobalt-60 reference irradiations

Aerial's alanine EPR dosimetry system is calibrated using alanine pellets that were irradiated with cobalt-60 reference beam quality. These dosimeter were purchased from NPL. All dosimeters were

irradiated at an ambient temperature of 25 ± 2 °C.

For the Harwell dosimeters the cobalt-60 reference irradiations was carried out in the Risø HDRL Gammacell 1[1]. The Gammacell is very similar in design to the Nordion GC-220. The dose rate at position of the alanine pellets inside the shielded radiation enclosure is calibrated using alanine transfer dosimeters from NPL. The temperature inside the enclosure can be controlled in order to obtain a temperature of 25.0 ± 0.5°C as for the calibration irradiations.

2.4 Monte Carlo calculations

For MC calculation of the dosimeter to water ratio of absorbed doses, the experimental geometry for the X-ray irradiations described in Section 2.3 was implemented in the `EGSnrc` software with simulation parameters described in Table 2, in the case of Harwell dosimeters. The same irradiation conditions were modelled using the `MCNPX version 2.7` (Pelowitz, 2011) MC simulation code, in the case of Aerial alanine dosimeters. The same simulation parameters, that are listed in Table 2 were used in `MCNPX` simulations.

Table 2: Summary of the Monte Carlo simulation parameters based on the guidelines by the AAPM TG-268 (Sechopoulos et al., 2018).

Item name	Description	References
Code, version	`EGSnrc` code system, `cavity` user code.	Kawrakow et al. (2017)
Validation	Half Value Layer comparison.	
Source description	Tabulated spectrum files. Library `egs_angular_spread_source` was used with $\sigma = 1$.	

Transport parameters	`Global Ecut = 0.512`
	`Global Pcut = 0.001`
	`Rayleigh scattering = ON`
	`Electron Impact Ionization = ON`
	`Photon cross sections = mcdf-xcom`
		Sabbatucci and Salvat (2016)

Variance reduction technique (VRT)	No VRT was applied.	
Scored quantities	Dose per fluence in alanine pellet and water substitute (total volume or in smaller slabs).	
No. histories	Typically 1×10^9.	
Statistical methods	Batch method.	
Post-processing	See text.	

The use of the MC model is threefold:

i) To calculate the ratio of absorbed doses in the X-ray fields. Combined with a calculation of the ratio of mass energy absorption coefficients for the reference cobalt-60 field, the relative ratio

[1] `https://www.nutech.dtu.dk/english/products-and-services/industrial-dosimetry/hdrl/hdrl_gamma_cells`

of doses can be calculated according to Equation (3), assuming

$$\left(\frac{D_{\mathrm{dos}}}{D_{\mathrm{w}}}\right)_{Q_0} = \left(\frac{\left[\frac{\mu_{\mathrm{en}}}{\rho}\right]_{\mathrm{dos}}}{\left[\frac{\mu_{\mathrm{en}}}{\rho}\right]_{\mathrm{w}}}\right)_{Q_0} . \tag{6}$$

ii) A difference in homogeneity of dose distribution within the dosimeter dimensions is expected between the kilovoltage (kV X-rays) and reference cobalt-60 irradiations. The dose gradient within the dosimeter dimensions is therefore calculated for evaluation of this difference.

iii) A sensitivity analysis of the effect of the air gap in the alanine cavity of the Solid Water® ionization chamber dummy. The effect on both dosimeter to water dose ratios and the dose gradient correction is investigated. This investigation is particularly relevant for the Aerial alanine pellets since they have a smaller diameter than the Harwell alanine pellets while the same cavity is used for placement of the pellets.

3 Results

3.1 Relative response

The EPR response of the alanine pellet dosimeters per dose to water is shown in Figure 2.

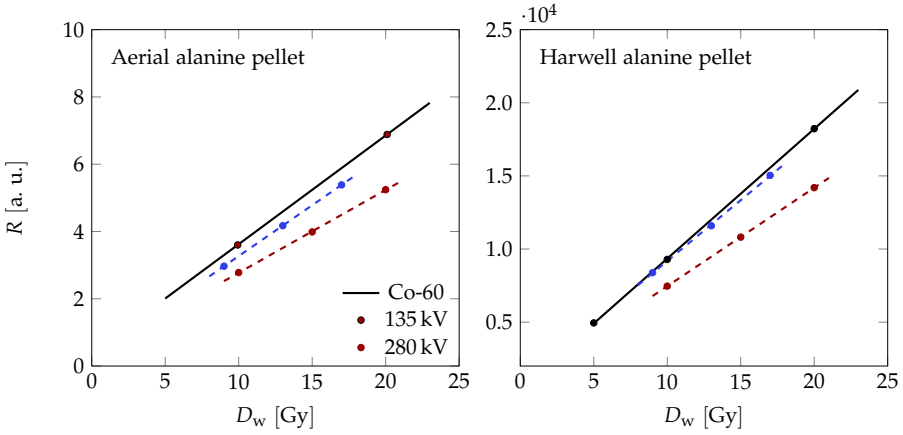

Figure 2: EPR response of alanine pellet dosimeters per dose to water irradiated in cobalt-60 reference beam quality (black) and the 135 kV (red) and 280 kV (blue) X-ray fields.

Since the response of the alanine pellet dosimeters in the respective X-ray fields relative to the cobalt-60 reference field is defined as in Equation (1), the relative response of the alanine pellet dosimeter can be calculated as the ratio of the slopes of the calibration curves presented in Figure 2. The calculated values for the relative response F_{Q,Q_0} are listed in Table 3. The relative difference between the relative response obtained by the respective dosimetry systems is 1.5 % and 2.2 % for the 135 kV and 280 kV X-ray beams respectively.

Homogeneity of dose distribution in alanine pellet To determine the relative efficiency of the respective dosimeters, all other factors impacting the dosimeter response must be considered. For instance the difference in radiation absorption properties is handled by the MC calculated ratio of doses in Equation (3). Another factor impacting the induced response is the relative homogeneity of the dose distribution in the dosimeter volume in the x-ray beam relative to the reference field.

During exposure the cylindrical alanine pellets are irradiated perpendicular to the axis of symmetry making a direct MC assessment of the dose gradient in the detector volume impractical. The situation is therefore approximated by a box of alanine with side lengths 4.0 mm and 4.8 mm, for the Aerial and Harwell dosimeters respectively, representing the dosimeter diameters. The dose per fluence was then scored in individual slabs in the alanine box, see Figure 3.

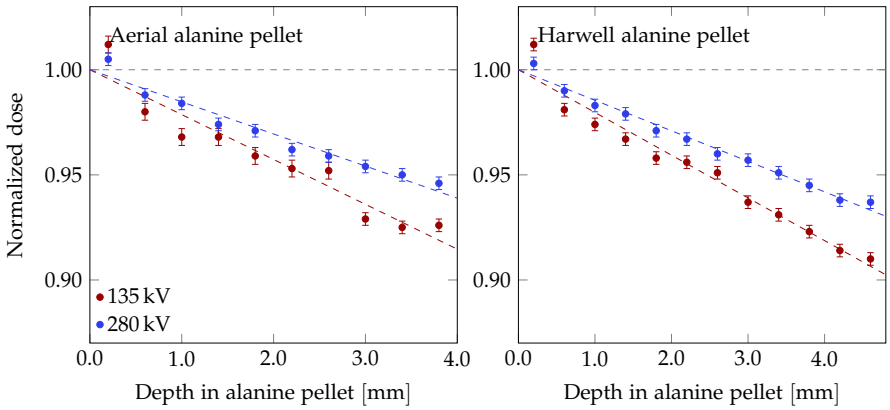

Figure 3: Dose gradient in alanine pellets normalized to surface dose.

Since the ionization chamber dose measurement point is located at the central axis, and the dose gradient within the detector volume is constant for all combinations of alanine pellets and beam qualities, the EPR response of the irradiated pellets correspond to the dose at the central point of the pellets. In this case the volume correction is unity ($k_{\text{vol}} = 1$).

3.2 Relative ratio of doses

The ratio of absorbed dose to dosimeter to dose to water in the X-ray fields, relative to the cobalt-60 reference field was obtained by MC calculations using the `cavity`-usercode of the `EGSnrc` MC toolkit (see Table 2). For calculation of dose to dosimeter in the X-ray fields, material files for the true alanine dosimeter compositions was produced. The WT1 Solid Water® phantom material was produced using publicly available information on elemental composition and physical density[2]. The alanine pellet was placed with central position at 2 cm depth in the Solid Water® phantom, with a 75 cm source to surface distance. For the dose to water calculation an identical geometry was used, with the pellet material changed to water.

[2] `https://phoenix-dosimetry.co.uk/solid-water-and-bolus-material/`

For calculation of the ratio of doses in the cobalt-60 reference field the `EGSnrc` g-usercode was used for calculation of the mass energy absorption coefficients μ_{en}/ρ in alanine and water. The mass energy absorption coefficients are related to the collision kerma in the detector K_{col} by

$$K_{col} = \Psi \left(\frac{\mu_{en}}{\rho} \right), \tag{7}$$

where Ψ is the energy fluence in the detector. Assuming the secondary electrons deposit their energy locally, the dose can be approximated by

$$D = K_{col}. \tag{8}$$

Assuming that the energy fluence in the detector is independent on the choice of detector material between alanine and water ($\Psi_{dos} = \Psi_w$), the ratio of doses can then be obtained by

$$\left(\frac{D_{dos}}{D_w} \right)_{Q_0} = \left(\frac{\Psi_{dos} \left[\frac{\mu_{en}}{\rho} \right]_{dos}}{\Psi_w \left[\frac{\mu_{en}}{\rho} \right]_w} \right)_{Q_0} = \left(\frac{\left[\frac{\mu_{en}}{\rho} \right]_{dos}}{\left[\frac{\mu_{en}}{\rho} \right]_w} \right)_{Q_0}. \tag{9}$$

The dose ratios calculated for the X-ray fields and the cobalt-60 reference are combined according to Equation (3) to calculate the relative ratio of doses H_{Q,Q_0}. The obtained values are listed in Table 3.

For Aerial's alanine pellets, the same irradiation geometry was modelled using the `MCNPX` MC simulation code. True alanine composition was used as well as the same chemical composition of the Solid Water® phantom that was used in the `EGSnrc` code. For cobalt-60 dosimeter to water dose ration calculation, the same geometry was used.

3.3 Relative detector efficiency

The relative detector efficiency is calculated by:

$$G_{Q,Q_0} = k_{vol} \cdot H^{-1}_{Q,Q_0} \cdot F_{Q,Q_0}. \tag{10}$$

The obtained values of G_{Q,Q_0} is listed in Table 3, together with the corresponding values of F_{Q,Q_0} and H_{Q,Q_0}.

Table 3: Overview of response, dose ratio, and efficiency of the two alanine pellet dosimeters in the examined X-ray fields relative to cobalt-60 reference fields.

Dosimeter	F_{Q,Q_0}		H_{Q,Q_0}		G_{Q,Q_0}	
	135 kV	280 kV	135 kV	280 kV	135 kV	280 kV
Aerial	0.751	0.921	0.842	0.978	0.892	0.941
Harwell	0.762	0.941	0.863	0.990	0.883	0.951
Difference	0.011	0.020	0.021	0.012	-0.009	0.010
Rel. Difference	1.5 %	2.2 %	2.5 %	1.2 %	1 %	1.1 %

The relative difference of the relative efficiency determined for the two alanine pellet dosimeters is 1 % and 1.1 % for the 135 kV and 280 kV X-ray beam qualities respectively.

3.4 Uncertainty budget

The uncertainties listed for the obtained values of F_{Q,Q_0}, H_{Q,Q_0}, and G_{Q,Q_0} are obtained in the following manner (see Table 4 and Table 4 for the combined uncertainty budget):

Relative response The uncertainty on the experimentally determined value for the relative response F_{Q,Q_0} is obtained by summation in quadrature of uncertainty components from the calibration of the ionization chamber, the dose rate in the cobalt-60 Gammacell, and the linear regressions of the EPR response in the respective fields. The uncertainty on the linear regression of EPR response is evaluated from the residuals of the linear regression shown in Figure 2.

Relative dose ratios For the relative dose ratio H_{Q,Q_0} the combined uncertainty consist of contributions from statistical, geometrical, and model considerations. The statistical uncertainty is evaluated for individual calculations using `EGSnrc` by the batch method, and is minimized by increasing the number of initial particles included in the calculation. The geometrical component refer to unknowns in material specifications and the accuracy of specified dimensions, while the model component account for choices of algorithms and cross-sections. The values of the geometrical and model uncertainty components listed in Table 4 and Table 5 are conservative estimates. An additional component of uncertainty concerning the effect of an air gap in the alanine pellet cavity of the ionization chamber dummy is estimated by a sensitivity analysis in the MC calculation. The calculation of H_{Q,Q_0} was repeated for varying air gap sizes, and the uncertainty component for relevant air-gap sizes was estimated.

Volume correction The dose distribution in the pellets have been calculated for varying air gap sizes in the detector cavity to ensure that the constant dose gradient in the detector volume was independent of the air gap. Constant dose gradients was found for all air gap sizes (0.0 mm to 0.6 mm).

Relative efficiency The combined uncertainty on the relative efficiency of the alanine pellet dosimeters is obtained by adding the individual constituents of Equation (10) in quadrature.

Table 4: Estimated uncertainty budget for the Harwell alanine dosimeter. All uncertainties are stated at $k = 1$.

Parameter	Description	Type	σ ($k = 1$)
F_{Q,Q_0}	Ionization chamber calibration in X-ray field	B	2.2 %
	Linear regression of EPR response in X-ray field	A	0.6 %
	Calibration of dose rate in ^{60}Co Gammacell (Risø)	B	1.4 %
	Linear regression of EPR response in ^{60}Co Gammacell (Risø)	A	0.6 %
	Combined		2.7 %
H_{Q,Q_0}	Statistical uncertainty	A	0.2 %
	Geometrical uncertainty	B	1.0 %
	Model uncertainty	B	2.0 %
	Air gap calculation	A	0.6 %
	Combined		2.3 %
G_{Q,Q_0}	Summation in quadrature of uncertainty on F_{Q,Q_0} and H_{Q,Q_0}		3.6 %

Table 5: Estimated uncertainty budget for the Aerial alanine dosimeter. All uncertainties are stated at $k = 1$.

Parameter	Description	Type	σ ($k = 1$)
F_{Q,Q_0}	Ionization chamber calibration in X-ray field	B	2.2 %
	Linear regression of EPR response in X-ray field	A	0.6 %
	Calibration curve for the EPR system with ^{60}Co reference quality	B	1.6 %
	Combined		2.9 %
H_{Q,Q_0}	Statistical uncertainty	A	0.2 %
	Model and geometry uncertainty	B	2.0 %
	Air gap for Aerial dosimeters	A	0.5 %
	Combined		2.1 %
G_{Q,Q_0}	Summation in quadrature of uncertainty on F_{Q,Q_0} and H_{Q,Q_0}		3.6 %

4 Discussion

The present study explores the comparability of the energy dependence of two different alanine pellet dosimetry systems. Two sets of alanine pellets obtained from different manufacturers (Aerial and Harwell Dosimeters) have been irradiated under identical conditions. The induced signal was read out using different EPR-spectroscopy systems, simulating the variations between different dosimetry systems used in the literature. The two sets of alanine pellets differ in both geometry and chemical composition (from the use of different type and amount of binder material). The experimentally determined relative response at the investigated X-ray beam qualities agreed with a relative difference of 1.5 % and 2.2 % between the two dosimetry systems, well within the experimental uncertainties.

Several studies have previously been published describing the decline in detector response with decreasing effective energy of X-ray beams ((Hansen et al., 1989; Coninckx et al., 1989; Zeng and McCaffrey, 2005; Chen et al., 2008; Waldeland et al., 2010; Khoury et al., 2015; Anton and Büermann,

2015; Hjørringgaard et al., 2020; Nasreddine et al., 2020)). A compilation of published data, consisting of X-ray beam qualities in the effective energy range from roughly 10 keV to 170 keV, is shown in Figure 4 including the data obtained in this study. An overall trend in the relative response data is evident, however a significant spread in the observed values are present where multiple sources overlap. For the data obtained in the present study, the relative response at $E_{\text{eff}} = 58.9$ keV is on the lower end of the general trend (assumed to follow the wide range of data points by Anton and Büermann (2015) with quite small uncertainties), although within the standard uncertainty.

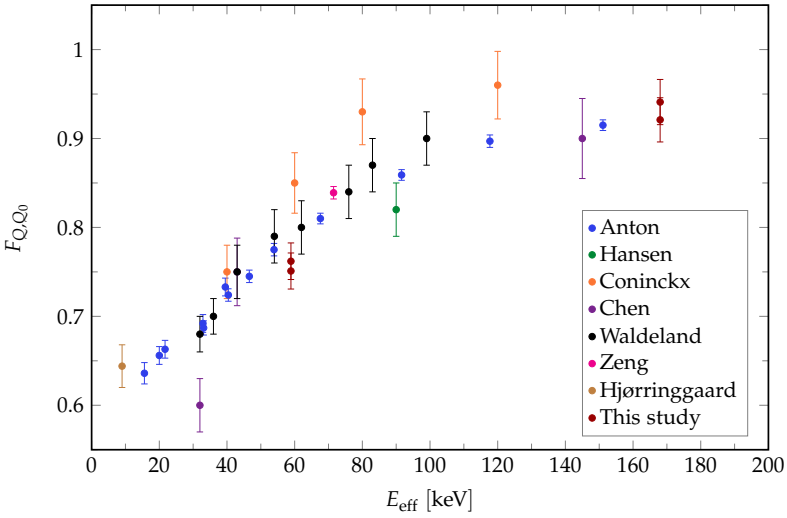

Figure 4: Literature data for the relative response F_{Q,Q_0} of alanine pellet dosimeters in low and medium energy X-ray fields. Error bars represent the standard uncertainty ($k = 1$).

For the calculation of the relative efficiency G_{Q,Q_0}, an agreement between the two dosimetry systems was obtained with relative difference of 1.0 % and 1.1 % for the 135 kV and 280 kV beams respectively, again well within measurement uncertainty.

A few of the published studies on the energy dependence also calculate the alanine to water ratio of doses in the relevant X-ray fields relative to the reference field and determine the relative efficiency of the dosimeter. Literature values for the relative efficiency, together with the obtained values from the present study, are shown in Figure 5. Anton and Büermann (2015) does not directly calculate the relative efficiency, rather they correct the Monte Carlo calculated ratio of doses by an intrinsic efficiency factor determined by use of a microdosimetric one-hit detector model carried out by P. Olko. The relative efficiency values published by Anton and Büermann (2015) and shown in Figure 5 are however obtained by simply taking the ratio of relative response with respect to alanine to water dose ratios listed in Table 6 and 7 of Anton and Büermann (2015). An interesting feature of the published data for relative efficiency of the alanine pellet dosimeter is the small increase in efficiency around effective energy 20 keV to 30 keV which is also predicted for monoenergetic photons by the microdosimetric one-hit detector model (Olko, 2002). As with the relative response,

the relative efficiency determined in the present study is a bit lower than other published data.

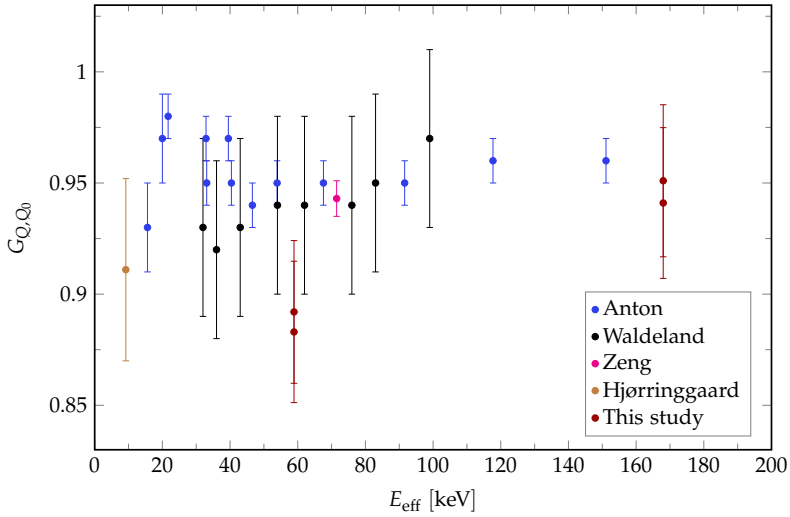

Figure 5: Literature data for the relative efficiency G_{Q,Q_0} of alanine pellet dosimeters in low and medium energy x-ray fields. Error bars represent the standard uncertainty ($k = 1$).

The largest component of uncertainty for determining the relative response and efficiency of the alanine pellet dosimeter is the dose to water calibration (see Table 4 and Table 5).

5 Conclusion

The relative response and efficiency of two sets of alanine pellet dosimeters was investigated. The two sets were irradiated under identical conditions, with two different X-ray beam qualities at NPL. EPR readout was carried out independently and with different reference fields in order to assess the variability between different alanine pellet dosimetry systems in low to medium energy X-ray fields. A comparison of the relative response and relative efficiency of the two alanine pellet dosimetry systems showed good agreement, however both the relative response and efficiency were lower than other published data for comparable effective energies of the X-ray beams.

References

Anton, M. and L. Büermann (2015). Relative response of the alanine dosimeter to medium energy x-rays. *Physics in Medicine & Biology 60*(15), 6113.

Aukett, R., R. Harrison, C. Moretti, A. Nahum, K. Rosser, et al. (1996). The ipemb code of practice for the determination of absorbed dose for x-rays below 300 kv generating potential (0.035 mm al-4 mm cu hvl; 10-300 kv generating potential). *Physics in Medicine & Biology 41*(12), 2605.

Barkai-Golan, R. and P. Follett (2017). *Irradiation for Quality Improvement, Microbial Safety and Phytosanitation of Fresh Produce*. Academic Press.

Chen, F., P. Nicolucci, and O. Baffa (2008). Enhanced sensitivity of alanine dosimeters to low-energy x-rays: Preliminary results. *Radiation measurements 43*(2-6), 467–470.

Coninckx, F., H. Schönbacher, A. Bartolotta, S. Onori, and A. Rosati (1989). Alanine dosimetry as the reference dosimetric system in accelerator radiation environments. *International Journal of Radiation Applications and Instrumentation. Part A. Applied Radiation and Isotopes 40*(10-12), 977–983.

Goodman, B. A., N. Worasith, S. Ninlaphruk, H. Mungpayaban, and W. Deng (2017). Radiation dosimetry using alanine and electron paramagnetic resonance (epr) spectroscopy: A new look at an old topic. *Applied Magnetic Resonance 48*(2), 155–173.

Hansen, J., M. Waligorski, and E. Byrski (1989). Intercomparison of gamma ray, x ray, and fast neutron dosimetry using alanine detectors. *Radiation protection dosimetry 27*(2), 85–92.

Hjørringgaard, J. G., C. Ankjærgaard, M. Bailey, and A. Miller (2020). Alanine pellet dosimeter efficiency in a 40 k v x-ray beam relative to cobalt-60. *Radiation Measurements*, 106374.

Kawrakow, I., E. Mainegra-Hing, D. W. O. Rogers, F. Tessier, and B. R. B. Walters (2017). The EGSnrc code system: Monte Carlo simulation of electron and photon transport. Technical Report PIRS-701, National Research Council Canada.

Khoury, H., E. da Silva Jr, K. Mehta, V. de Barros, V. Asfora, P. Guzzo, and A. Parker (2015). Alanine-epr as a transfer standard dosimetry system for low energy x radiation. *Radiation Physics and Chemistry 116*, 147–150.

Marchioni, E., J.-Y. Pabst, and F. Kuntz (2002). Characterization and application of two kinds of esr dosimeters.

Nasreddine, A. (2020, September). *Alanine/EPR dosimetry for low to medium energy X-ray radiation processing control*. Phd thesis, Université de Strasbourg.

Nasreddine, A., F. Kuntz, and Z. El Bitar (2020). Absorbed dose to water determination for kilovoltage x-rays using alanine/epr dosimetry systems. *Radiation Physics and Chemistry*, 108938.

Olko, P. (2002). The microdosimetric one-hit detector model for calculating the response of solid state detectors. *Radiation measurements 35*(3), 255–267.

Pelowitz, E. D. B. (2011). *MCNPX Users Manual Version 2.7.0.* Los Alamos National Laboratory.

Sabbatucci, L. and F. Salvat (2016). Theory and calculation of the atomic photoeffect. *Radiation Physics and Chemistry 121*, 122–140.

Saglam, S., A. Cakir, and S. Kuter (2011). *Blood irradiation, from the book: Modern Approaches To Quality Control*. InTech.

Sechopoulos, I., D. W. O. Rogers, M. Bazalova-Carter, W. E. Bolch, E. C. Heath, M. F. McNitt-Gray, J. Sempau, and J. F. Williamson (2018). Records: improved reporting of monte carlo radiation transport studies: Report of the aapm research committee task group 268. *Medical Physics 45*(1), e1–e5.

Waldeland, E., E. O. Hole, E. Sagstuen, and E. Malinen (2010). The energy dependence of lithium formate and alanine epr dosimeters for medium energy x rays. *Medical physics 37*(7Part1), 3569–3575.

Zeng, G. and J. McCaffrey (2005). The response of alanine to a 150 kev x-ray beam. *Radiation physics and chemistry 72*(5), 537–540.

Paper IV

Title:

The microdosimetric one-hit detector model for calculating the relative efficiency of the alanine pellet dosimeter in low energy x-ray beams.

Authors:

Hjørringgaard JG, Ankjærgaard C, and Andersen CE.

Submitted to:

Radiation Measurements,
May 2021.

Status:

Under review.

The microdosimetric one-hit detector model for calculating the relative efficiency of the alanine pellet dosimeter in low energy x-ray beams

Jakob G. Hjørringgaard*[1], Christina Ankjærgaard[1], and Claus E. Andersen[1]

[1]Department of Health Technology, Technical University of Denmark, Roskilde, Denmark

May 3, 2021

Abstract

Background: The alanine pellet dosimeter is used extensively as a routine and reference dosimeter for a range of radiation modalities. For dose measurements in low energy x-ray beams the dosimeter show a decline in relative efficiency. The dependence of this decline on various beam characteristics is investigated here.

Method: We have applied the microdosimetric one-hit detector model to characterize the relative efficiency of an alanine pellet dosimeter in low energy x-ray beams. The free parameters of the model was determined by fitting to literature data on the relative efficiency of alanine pellets in known x-ray fields.

Result: Microdosimetric distributions for monoenergetic electrons were calculated using track structure calculations carried out with the `Geant4-DNA` Monte Carlo software. Microdosimetric distributions for primary x-ray beams were calculated by folding the distributions from monoenergetic electrons with the energy distributions of initial secondary electrons produced in the detector by the primary x-ray beam. In this manner, the relative efficiency of the alanine pellet dosimeter was calculated for a wide range of x-ray beams.

Conclusion: For a set of generated low energy x-ray spectra with tube potential 40 kV to 170 kV with varying external filtration the reduction in detector efficiency was found to be on average 6.3 % with a variation of -1.0 % to 1.5 %. For a set of medium energy x-ray spectra with tube potential 100 kV to 300 kV and varying external filtration the reduction in detector efficiency depends strongly on the half-value layer of the primary x-ray beam – varying between 2.0 % and 7.0 %.

1 Introduction

Kilo-voltage (kV) x-rays have extensive applications in for example radiotherapy, radiation processing, small animal irradiation, and blood irradiation, the latter showing a demand for replacement of Cs-137 irradiators with x-ray emitters (Dodd and Vetter, 2009). Dosimetry protocols recommend water based dosimetry using ion chambers (Aukett et al., 1996; IAEA, 2001), however for applications like blood irradiation, where blood bags are typically irradiated from two or more directions in a closed canister, ion chamber measurements are impractical due to the geometry of the irradiation cavity or the complex x-ray fields. Here both placement of the ion chamber and determination of beam quality through half-value layer (HVL) measurements are difficult. In these cases the use of the alanine/electron paramagnetic resonance (EPR) dosimeter may prove more practical.

*E-mail: jakg@dtu.dk

The alanine/EPR dosimetry system consists of L-α-alanine, in the form of pellets or films, which produce stable free radicals when irradiated. The concentration of stable free radicals produced is proportional to dose to the dosimeter for a wide range of beam qualities (Olsen et al., 1990; Sharpe and Duane, 2003; Bergstrand et al., 2003; Zeng et al., 2004; Zeng and McCaffrey, 2005; Anton et al., 2008) and is stable with a signal loss of few percent over years (Sleptchonok et al., 2000). The signal from the concentration of stable free radicals is measured with an EPR spectrometer.

An important characteristic for ionizing radiation detectors is the photon energy response. The relative response F_{Q,Q_0} after a dose of photons of quality Q, normalized to the response for reference quality Q_0 (typically cobalt-60 or cesium-137 gamma-rays) is defined as

$$F_{Q,Q_0} = \frac{(R/D_\mathrm{w})_Q}{(R/D_\mathrm{w})_{Q_0}} = G_{Q,Q_0} \cdot H_{Q,Q_0}, \tag{1}$$

where R is the detector response and D_w is the dose to water. H_{Q,Q_0} is the ratio of dose to detector material D_dos to D_w in the photon quality Q relative to the reference quality Q_0

$$H_{Q,Q_0} = \frac{(D_\mathrm{dos}/D_\mathrm{w})_Q}{(D_\mathrm{dos}/D_\mathrm{w})_{Q_0}}, \tag{2}$$

and G_{Q,Q_0} is the relative detector efficiency

$$G_{Q,Q_0} = \frac{(R/D_\mathrm{dos})_Q}{(R/D_\mathrm{dos})_{Q_0}}. \tag{3}$$

The EPR response of the alanine pellet dosimeter irradiated at low energy x-ray qualities relative to cobalt-60 is energy dependent. Recently efforts has been made in characterizing this intrinsic energy dependence from experiments (Zeng and McCaffrey, 2005; Waldeland et al., 2010; Anton and Büermann, 2015; Khoury et al., 2015; Hjørringgaard et al., 2020). All experimental characterizations of the relative efficiency are carried out in well defined x-ray fields. It is not obvious how the transfer from reference conditions to non-reference conditions, such as blood irradiators, affects the relative efficiency of the alanine pellet dosimeter. Direct measurements of the relative efficiency in these kind of geometries are difficult at best, and other approaches for determining the relative efficiency are desired.

Olko (2002) investigated the energy dependence with a microdosimetric one-hit detector model. The focus was on different thermoluminescence detector materials, but alanine was included in the analysis. The one-hit detector model refer to types of detectors showing a linear response at low doses and saturating exponentially for higher doses as

$$R\,(D) = R_0 \left[1 - \exp\left(-\frac{D}{D_0}\right)\right], \tag{4}$$

where $R\,(D)$ is the response at dose D, R_0 is the saturation response, and D_0 is the dose at which 63 % of saturation response is obtained. This characteristic is observed in alanine dosimeters with a characteristic dose D_0 in the order of 100 kGy (see Figure 1 and Hansen et al. (1987)).

Here we apply the microdosimetric one-hit detector model to calculate the efficiency of an alanine pellet dosimeter in low energy x-ray beams relative to a cobalt-60 beam. Literature values for the

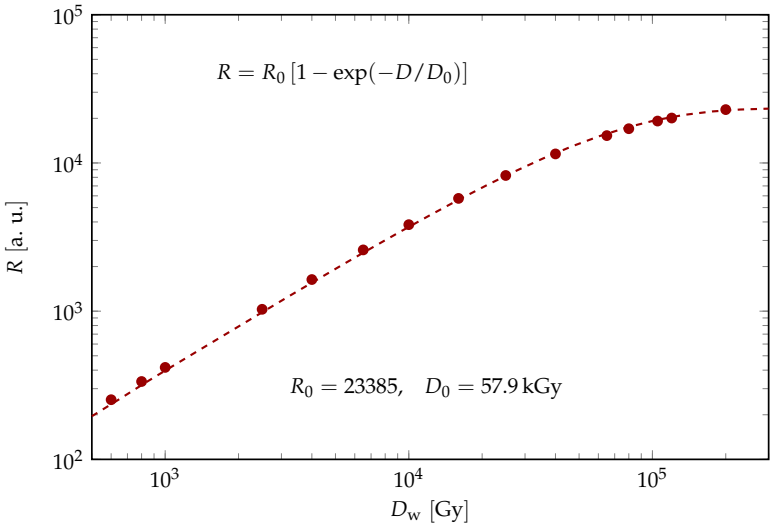

Figure 1: EPR response of alanine pellet dosimeters irradiated in a cobalt-60 Gammacell for doses ranging from 1 kGy to 200 kGy. Multiple pellets are irradiated at each dose and individual responses are shown here (circles). A function of the form of Equation (4) is fitted to the data (dashed line) with parameters R_0 and D_0 shown in the figure.

relative efficiency in known beam qualities are adopted from Waldeland et al. (2010) in order to fix the free parameters of the model. Validation of the calculated values of the relative efficiency of the alanine pellet dosimeter is carried out by comparison with literature data. A successful and validated model for calculation of the relative efficiency of the alanine pellet dosimeter can be used to explore the behavior of the dosimeter in more complex fields, as well as to investigate the dependence on different beam characteristics.

2 Background

Detection of ionizing radiation is based on our ability to produce and assess an induced signal, ionizations or radiation damage, in the detector volume (Waligórski, 1988). For the alanine dosimeter the induced signal is due to an increase in the concentration of stable free radicals which can be measured in an EPR spectrometer as an average over the detector volume. On a microscopic scale the production of free radicals by ionizations can not be considered as uniformly distributed, as it occurs as discrete events (Olko, 2006).

2.1 Microdosimetry

Charged particle tracks containing information on spatial positions – and sizes – of energy depositions in a medium can be obtained by Monte Carlo calculations. Several MC codes for track structure calculations are available for a selection of beam parameters and materials (`Geant4-DNA`,

PHITS etc.). In microdosimetry a target volume in the material is considered. An ionizing particle passing through the target volume, producing at least one ionization in the target volume, is called a single event. Single events leading to a production of detector signal (stable free radical formation in alanine) is called a hit. Since the transfer of energy occurs as discrete events (ionizations and excitations) the energy deposited in the target volumes is not uniform but constitutes a characteristic microdosimetric distribution.

The energy ε deposited in a target volume for a single event is related to the number of ionizations j within the target volume by $\varepsilon = j \cdot W$, where W is the mean energy required to produce an ion pair in the material. The energy deposited normalized to the mass m of the the target volume is the specific energy $z = \varepsilon/m$ in the target volume – the microdosimetric analogue of dose. The stochastic nature of ionizations and the related specific energy motivates the consideration of the frequency distributions $f_1(z)$. For a frequency distribution normalized to one event ($\int_0^\infty f_1(z)\,\mathrm{d}z = 1$) the first moment (mean specific energy) is

$$\overline{z_F} = \int_0^\infty z f_1(z)\ \mathrm{d}z. \tag{5}$$

The subscript 1 refers to a single event. Distributions of the various microdosimetric quantities are defined in an analogous way. Single event distributions are independent of the dose, but do depend on track and target volume characteristics, such as size and shape.

2.2 The microdosimetric one-hit detector model

The microdosimetric one-hit detector model is based on the multi-hit model which can describe inactivation of microorganisms. In multi-hit theory it is assumed that the detector contains a type of target. The target can tolerate a certain amount of hits, however after n hits the target is affected (e.g. cell death, radical formation, trapping of electron in TLD, etc.). It is assumed that the hits occur independently of each other and thus can be described by Poisson statistics. The probability of survival (no effect) S as a function of dose D is then (Kellerer, 1987)

$$S(D) = \sum_{\nu=0}^{n-1} \frac{\mathrm{e}^{-\alpha D}(\alpha D)^\nu}{\nu!}. \tag{6}$$

This is the probability that n hits does not lead to an effect in the target.

One-hit detectors are a special case of Equation (6) where the survival curve is purely exponential ($n = 1$, see Figure 1) so that

$$S(D) = \mathrm{e}^{-\alpha D}, \tag{7}$$

where α is a saturation parameter. The probability of survival in the one-hit model can be expressed in terms of microdosimetric quantities as (Zaider, 1990; Olko, 2002, 2006)

$$S(D) = \exp\left[-\frac{D}{\overline{z_F}}\int_0^\infty \left(1 - \mathrm{e}^{-\alpha z}\right) f_1(z)\,\mathrm{d}z\right]. \tag{8}$$

Here $\overline{z_F}$ is the average dose deposited in the target volume by single events, the ratio $D/\overline{z_F}$ is thus the average number of events occurring in the target volume after irradiation with dose D. The

function $r(z) = 1 - \exp(-\alpha z)$ represents the probability of an effect occurring after irradiation of specific energy z, and is called the response function for a one-hit detector. The integral is then the average probability that the effect takes place in the target volume given a frequency distribution of specific energy $f_1(z)$.

The normalized detector response R after irradiation with dose D is the complement probability of the survival probability

$$R(D) = 1 - S(D) \tag{9}$$

$$= 1 - \exp\left[-\frac{D}{\overline{z_F}} \int_0^\infty \left(1 - \mathrm{e}^{-\alpha z}\right) f_1(z)\,\mathrm{d}z\right]. \tag{10}$$

By setting the characteristic dose D_0 equal to

$$D_0 = \frac{\overline{z_F}}{\int_0^\infty \left(1 - \mathrm{e}^{-\alpha z}\right) f_1(z)\,\mathrm{d}z}, \tag{11}$$

the detector response of Equation (10) can be simplified as

$$R(D) = 1 - \exp\left(-\frac{D}{D_0}\right), \tag{12}$$

which is the characteristic response function for one-hit detectors (see Figure 1).

For low doses $D \ll \overline{z_F}$ Equation (10) reduces to

$$R(D) = \frac{D}{\overline{z_F}} \int_0^\infty \left(1 - \mathrm{e}^{-\alpha z}\right) f_1(z)\,\mathrm{d}z, \tag{13}$$

and since the relative efficiency (see Equation (1)) is

$$G_{Q,Q_0} = \frac{(R/D)_Q}{(R/D)_{Q_0}}, \tag{14}$$

the relative efficiency can be calculated with the microdosimetric one-hit detector model as

$$G_{Q,Q_0} = \frac{\frac{1}{\overline{z_F^Q}} \int_0^\infty \left(1 - \mathrm{e}^{-\alpha z}\right) f_1^Q(z)\,\mathrm{d}z}{\frac{1}{\overline{z_F^{Q_0}}} \int_0^\infty \left(1 - \mathrm{e}^{-\alpha z}\right) f_1^{Q_0}(z)\,\mathrm{d}z}. \tag{15}$$

The microdosimetric one-hit detector model depends on two free parameters, the saturation parameter α and the target diameter d (assuming spherical volume target). The latter does not appear directly in Equation (15), but the frequency distribution of specific energy is dependent on this parameter.

3 Materials and Methods

The general procedure for implementing the microdosimetric one-hit detector model is outlined below

1. A set of monoenergetic electron tracks in water with energy E ranging from 1 keV to 1400 keV is produced. Positions of ionization produced by both the primary electrons and the produced secondaries are scored.

2. Microdosimetric frequency distributions of ionizations for the individual electron energies $f_1(j, E)$ are calculated according to the method described by Kellerer and Chmelevsky (1975), Kellerer et al. (1985), and Rossi and Zaider (1996).

3. Energy distribution of initial Compton- and photoelectrons produced in, or entering, the detector region for a specific primary photon spectrum is scored. Only the electrons produced directly by the primary photon beam, or entering the detector from a different region, is scored in order to avoid double counting in regard to Step 1.

4. Microdosimetric frequency distribution for the primary photon spectra is calculated by folding the monoenergetic electron frequency distributions with the energy distribution of initial secondary electrons[1].

5. The relative detector efficiency for the primary photon spectra at the irradiation conditions used to obtain the secondary electron spectra is calculated according to Equation (15).

Steps 1 and 3 are performed using MC calculation, while steps 2, 4, and 5 are obtained from post-processing of the MC calculated results. An overview of the MC calculations is given in Table 1.

This general procedure will be applied in different contexts. First, to fix the free parameters of the model, α and d, based on literature values of the relative detector efficiency obtained from Waldeland et al. (2010). The determined model parameters will then be validated by comparison of model predictions with experimental determination of the relative detector efficiency presented in the present study. Finally, the model is applied to a variety of constructed x-ray fields to investigate the general dependence of the detector efficiency to different beam characteristics.

3.1 Alanine pellet dosimeters

Since different alanine pellet dosimeters are commercially available, pellets of different size and composition are used throughout the literature. Three different versions of the alanine pellet dosimeter are used for calculations in the present work, and a brief description is given here.

For calculations where data from Waldeland et al. (2010) is used, the alanine pellets investigated in their work are considered. These pellets consist of 96 % alanine and 4 % unspecified binder, with a height of 3 mm and diameter 4.8 mm. For the calculations the binder was assumed to be paraffin wax and a bulk density of $1.2\,\mathrm{g\,cm^{-3}}$ was used.

For calculations concerning irradiations in a cobalt-60 Gammacell, alanine pellets obtained from Harwell Dosimeters were considered. These pellets have height 2.7 mm and diameter 4.8 mm, with a composition of 91 % alanine and 9 % paraffin wax. Calculations for these dosimeters were performed using a dosimeter material composition with bulk density $1.23\,\mathrm{g\,cm^{-3}}$.

[1] The initial energy distribution of secondary electrons will henceforth be referred to as the secondary electron spectrum.

Table 1: Summary of the Monte Carlo simulation parameters based on the guidelines by the AAPM TG-268 (Sechopoulos et al., 2018). *MD* refer to MC calculations of microdosimetric distributions and *SES* refer to MC calculations of secondary electron spectra.

Item name	Description	References
Code, version	`Geant4` v.10.5	Agostinelli et al. (2003)
Validation	Comparison of model calculated relative efficiency with literature data.	
Source description	*MD*: Monoenergetic electrons (1 keV - 1400 keV) initialized in the center of a water box.	
	SES: Source based on individual experimental geometries.	Waldeland et al. (2010)
Transport parameters	*MD*: `Geant4-DNA` physics processes. Specifically `G4DNABornIonisationModel` for ionizations.	Incerti et al. (2010a)
	SES: `G4EmPenelopePhysics` low-energy electromagnetic models.	
Variance reduction technique (VRT)	No VRT was applied.	
Scored quantities	*MD*: (x, y, z)-coordinates of ionizations in water.	
	SES: Energy distribution of Compton- and photoelectrons produced in or entering alanine pellet.	
No. histories	*MD*: Varying significantly to obtain desired number of ionizations.	
	SES: Typically 5×10^7 primary photons.	
Statistical methods	*MD*: Electron tracks are calculated until $\sim 2 \times 10^5$ ionization positions are scored.	
	SES: The batch method was used to evaluate statistical uncertainty on energy distribution.	
Post-processing	Microdosimetric frequency distributions for primary photon spectra are calculated by weighting of the monoenergetic frequency distributions of the secondary electron spectra (see Equation (18)).	

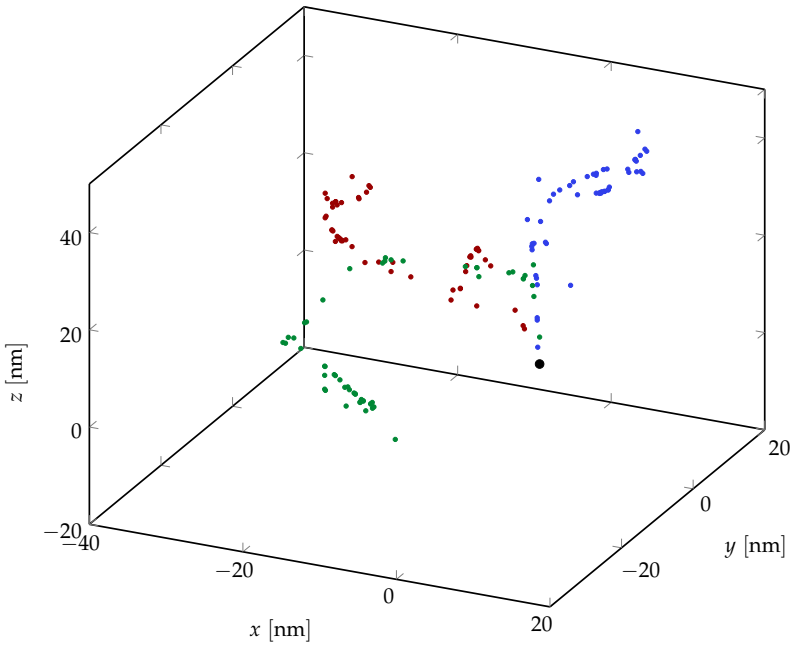

Figure 2: (x, y, z)-coordinates for ionizations produced by three 1 keV electrons in water, starting from the origin (black dot), calculated using the `Geant4-DNA` Monte Carlo code. Each color represent a single electron track.

Finally, for more general considerations of the relative efficiency of monoenergetic photons, where no experimental data is directly involved in the calculations, material data for crystalline alanine, with no binder, and density 1.42 g cm^{-3} is applied.

3.2 Microdosimetric distributions for monoenergetic electrons

A set of monoenergetic electron tracks in water was calculated using the `Geant4-DNA` MC code (Incerti et al., 2010b,a; Bernal et al., 2015; Incerti et al., 2018). The energies range from 1 keV to 1400 keV in steps of 1 keV. The electron tracks consist of (x, y, z)-coordinates for all ionizations produced by the primary electron and the subsequent secondaries. An example of three individual 1 keV electron tracks in water is shown in Figure 2. Water (or water vapor scaled to unity density) is typically used for track structure calculations because of the lack of appropriate cross section data, for other materials, at very low energies. The number of electron tracks at each energy was chosen such that the total number of ionizations produced was of the order 2×10^5, however each individual track was analyzed independently.

The frequency distribution of ionizations for the individual electron energies $f_1(j, E)$ for target diameters ranging from 5 nm to 30 nm was calculated using the weighted sampling procedure described in Kellerer and Chmelevsky (1975), Kellerer et al. (1985), and Rossi and Zaider (1996). By this method the *dose distribution* of ionizations $d_1(j)$ is obtained, and the frequency distribution is

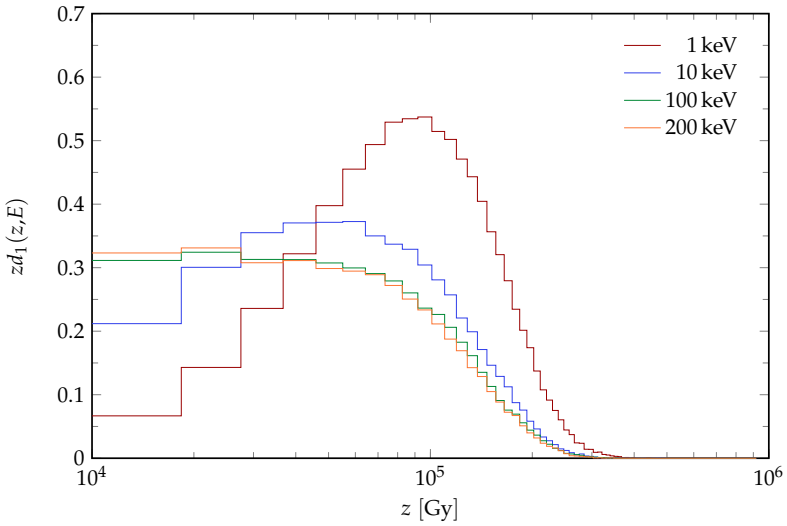

Figure 3: Microdosimetric single-event dose distribution of specific energy for 1 keV, 10 keV, 100 keV and 200 keV electrons in water, using target diameter $d = 10$ nm.

calculated according to

$$f_1(j) = \frac{z^{-1} d_1(j)}{\int_0^\infty z^{-1} d_1(j)\,\mathrm{d}j}. \tag{16}$$

The frequency distribution of specific energy $f_1(z, E)$ was obtained by multiplying the number of ionizations j by a chosen W value of 30 eV per ion pair, identical to what was used by Olko (2002), to obtain the deposited energy ε, and normalizing this to the mass of the target volume. In total the specific energy is calculated by

$$z = \frac{6Wj}{\rho_{\text{target}} \pi d^3}, \tag{17}$$

where ρ_{target} is the density of the target material, which for the calculation in water is $1.0\,\mathrm{g\,cm^{-3}}$. Examples of the obtained frequency distribution of specific energy for monoenergetic electrons in water is shown in Figure 3. Here the distribution is shown for four individual electron energies, 1 keV, 10 keV, 100 keV, and 200 keV, with target diameter $d = 10$ nm. All distributions are normalized. It is evident that increasing the initial electron energy results in a lower mean number of ionizations in the target volumes, as well as a convergence towards a specific distribution. For low electron energies the produced ionizations are more localized resulting in a larger mean number of ionizations (and thus mean specific energy) in the target volumes. The microdosimetric distributions for a complex photon field is therefore very sensitive to the fraction of low to high energy secondary electrons produced in the detector.

3.3 Microdosimetric distributions for photon spectra

To illustrate the process of calculating the microdosimetric distributions from primary photon spectra the following section will be based on a cobalt-60 reference beam. The microdosimetric distributions for the reference beam is required (according to Equation (15)) for calculation of the relative efficiency. The reference beam quality is a Nordion GC220 Gammacell located at Risø High Dose Reference Laboratory (HDRL). The spectral distribution of photons at central position in the Gammacell has previously been calculated using the `FLURZnrc` usercode of the `EGSnrc` MC software, and validated by doserate calculations in the central region of the Gammacell. .

To obtain the microdosimetric distributions, first the initial energy distribution of secondary electrons produced in the detector material by primary photons must be calculated. The secondary electron spectra were calculated using the `Geant4` MC toolkit (Agostinelli et al., 2003). Electrons produced by Compton and photoelectric interactions in alanine by the primary photons were included in the secondary electron spectrum, as well as secondary electrons produced in the surrounding material that enter the alanine pellet. Both the normalized primary gamma spectrum at the central region of the HDRL cobalt-60 Gammacell and the normalized secondary electron spectrum produced in an alanine pellet placed in the central region obtained by calculation are shown in Figure 4. For the calculated secondary electron spectra in the alanine pellet dosimeter approximately 14 % are generated with energy $\leq$ 10 keV. The discontinuity of the secondary electron spectrum at $\approx$ 0.96 MeV and 1.12 MeV correspond to the maximum energy of generated Compton electrons (which is the dominant photon interaction process at the 1 MeV region) for the two cobalt-60 peaks.

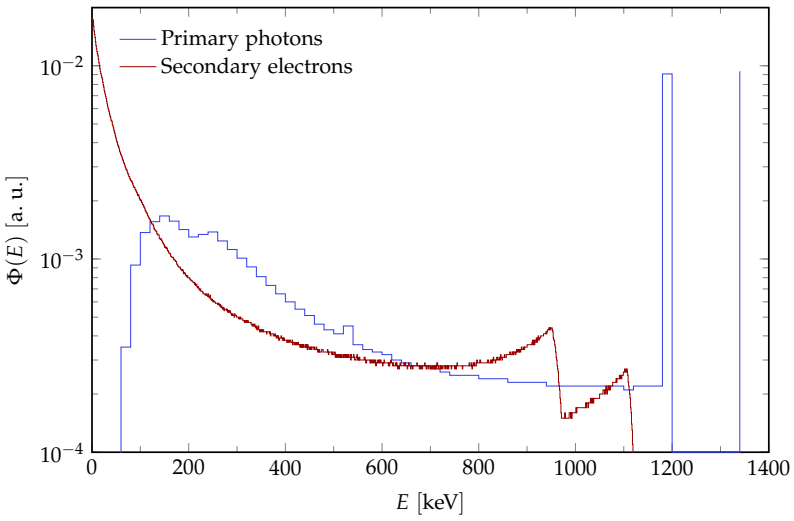

Figure 4: Primary gamma spectrum at central region of the HDRL cobalt-60 Gammacell (blue) and secondary electron spectrum produced in an alanine pellet irradiated in the central position (red) calculated using the `Geant4` MC toolkit. Both spectra are normalized to unit area under the curve.

The microdosimetric dose distribution of specific energy for the photon spectra were then calculated by folding the monoenergetic electron frequency distributions (see Figure 3) over the secondary electron spectra $\Phi(E)$ by

$$d_1^{Q_0}(z) = \frac{\int d_1(z,E)\Phi^{Q_0}(E)E\,\mathrm{d}E}{\int \Phi^{Q_0}(E)E\,\mathrm{d}E}. \tag{18}$$

Here the superscript Q_0 imply that the equation is valid for the reference cobalt-60 quality, however the same equation is applicable for an arbitrary photon beam quality Q. The resulting dose distribution of specific energy is shown in Figure 5 for different target volumes. The red graph in

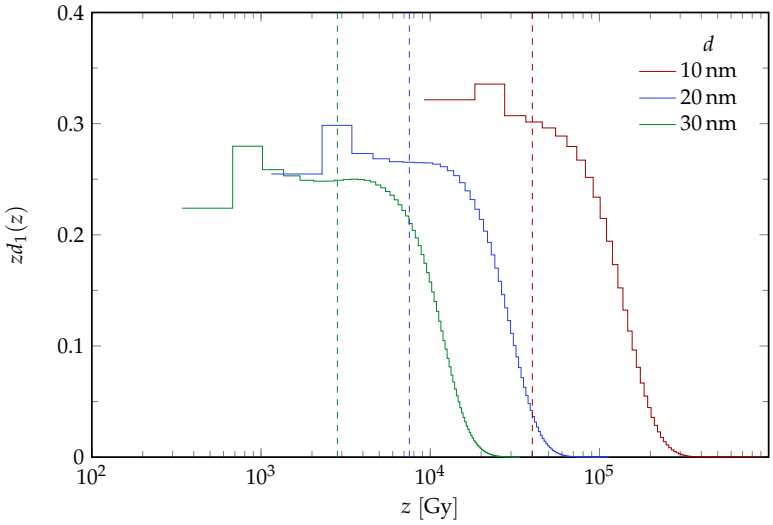

Figure 5: Microdosimetric single-event dose distribution of specific energy for alanine pellet in the HDRL cobalt-60 Gammacell. Different distributions are shown, illustrating the dependence of the microdosimetric distributions on target volume. The vertical dashed lines represent the mean specific energy of each distribution.

Figure 5 corresponding to a target volume of $d = 10\,\mathrm{nm}$ is directly comparable to the microdismetric distributions for electrons shown in Figure 3. The shape of the microdosimetric distributions is governed by the ionization density as well as the size of the target volume. For an increase in target size more ionizations may occur within the target volume, however since the target volume increase the specific energy will typically be shifted towards lower mean values.

The same process for calculating the microdosimetric distribution of specific energy described in this section for the cobalt-60 reference beam is applied for all x-ray and gamma spectra analyzed in the present study.

4 Results

4.1 Fixing free parameters of the microdosimetric one-hit detector model

Literature values of the relative efficiency of the alanine pellet dosimeter are used to determine the value of the two free parameters of the microdosimetric one-hit detector model α and d. The data used for the analysis is obtained from Waldeland et al. (2010). In their work they used spectra of the x-ray beam qualities calculated using `SpekCalc` (Poludniowski and Evans, 2007; Poludniowski, 2007). These spectra are reproduced here using the detailed information about their input for `SpekCalc`. A list of the beam modalities from Waldeland et al. (2010) is shown in Table 2. For the calculation of x-ray spectra the input voltage was adjusted to make the calculated HVL match the measured HVL as done in Waldeland et al. (2010).

Table 2: List of beam modalities produced based on the work of Waldeland et al. (2010).

Potential [kV] Nominal	E_{eff} [keV]	Filtration [mm] Al	Cu	HVL [mm] Al	Cu	G_{Q,Q_0}
50	32	4.2	-	2.6	-	0.93 ± 0.04
70	36	4.0	-	3.4	-	0.92 ± 0.04
100	43	4.4	-	5.0	-	0.93 ± 0.04
120	54	7.0	-	-	0.39	0.94 ± 0.04
135	62	10.5	-	-	0.58	0.94 ± 0.04
150	76	4.0	0.53	-	0.94	0.94 ± 0.04
180	83	6.0	0.53	-	1.16	0.95 ± 0.04
200	99	6.0	0.99	-	1.73	0.97 ± 0.04

Other literature values of the relative efficiency of the alanine pellet dosimeter in this energy range exist, however available information about the beam qualities are insufficient for reproduction using `SpekCalc`.

4.1.1 Secondary electron spectra

The secondary electron spectrum was calculated for all beam modalities listed in Table 2 based on the source, material, and geometrical information available in Waldeland et al. (2010). The irradiation geometry was implemented in `Geant4` with simulation parameters given in Table 1. The alanine pellet dosimeter was placed at 2 cm depth in a water phantom at 50 cm source to surface distance. The calculated energy distribution of Compton- and photoelectrons produced in, or entering, the alanine dosimeter volume is shown in Figure 6 for the 50 kV and 200 kV beam modalities in Table 2. It is evident that the secondary electron spectra for the 50 kV beam is heavily dominated by low energy electrons (e.g. electron energies below 10 keV) compared to the 200 kV spectrum. The fraction of initial secondary electrons with energies below 10 keV to the total number of electrons produced decreases from 74 % for the 50 kV beam to 49 % for the 200 kV beam. The plateau of zero initial secondary electrons observed between 10 keV and 20 keV for the 50 kV beam is an effect of the energy distributions of Compton and photoelectrons generated – photoelectrons have roughly the

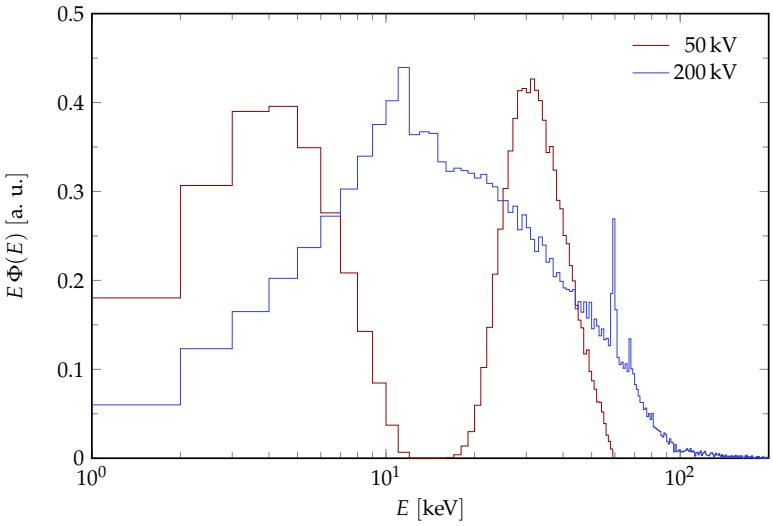

Figure 6: Secondary electron spectra calculated for the 50 kV (red) and 200 kV (blue) beam modalities specified in Table 2.

same energy as the ionizing photon which produces it, while Compton electrons generated by low energy photons have significantly lower energy. This leaves an energy region where none of the competing interactions produce secondary electrons. For greater energies the gap is erased by the greater range of photon energies.

4.1.2 Microdosimetric frequency distribution

The microdosimetric frequency distribution of specific energy is calculated for target diameters in the range 5 nm to 30 nm according to Equation (18). Figure 7 show the single-event dose distribution of specific energy for the 50 kV and 200 kV spectra from Waldeland et al. (2010), using target diameter 10 nm. The single-event dose distribution of specific energy for the cobalt-60 reference shown in Figure 5 is included in Figure 7 for reference. The distinction between the frequency distribution of specific energy for the 50 kV and 200 kV beams are subtle. Greater secondary electron energies result in less localized ionizations in the individual electron tracks and thus a frequency distribution shifted towards lower specific energies – or less localized dose deposition.

4.1.3 Model-fit to litterature data

The free parameters of the model α and d are determined by comparison of calculated and literature values for the relative dosimeter efficiency G_{Q,Q_0}. The microdosimetric frequency distributions calculated in Section 4.1.2 is used to calculate the relative efficiency for a wide range of saturation parameters according to Equation (15). The relative efficiency obtained by use of different combinations of model parameters is then compared to the literature values related to the x-ray spectra

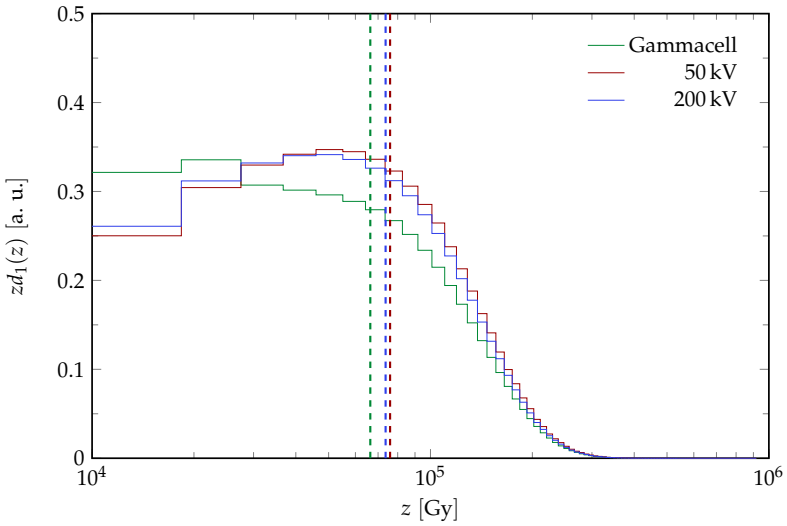

Figure 7: Microdosimetric single-event dose distribution of specific energy for 50 kV (red) and 200 kV (blue) beam modalities specified in Table 2 as well as the cobalt-60 reference (green), also shown in Figure 5, using target diameter in water $d = 10$ nm. Vertical lines show the corresponding mean specific energy $\overline{z_F}$.

used for calculation of the microdosimetric frequency distributions (see Table 2). The optimal set of model parameters is determined by minimizing the relative least squares of the calculated and experimental values

$$M = \sum_{Q=1}^{N} \left(\frac{G_{Q,Q_0}^{\text{exp}} - G_{Q,Q_0}^{\text{calc}}}{G_{Q,Q_0}^{\text{exp}}} \right)^2 , \tag{19}$$

where the sum is over all beam qualities in the set. In addition to the set of literature data obtained from Waldeland et al. (2010) a monoenergetic photon beam with energy 662 keV is used as a cesium-137 beam quality, for which the efficiency of the alanine pellet dosimeter is equal to the cobalt-60 quality. This is included to constrain the model parameters outside of the kV-range.

The obtained values of the parameter M as a function of the saturation parameter α is shown in Figure 8. The optimal saturation parameter, for each target diameter, is then obtained by locating the minimum of M with respect to α. From Figure 8 it appears that target diameters in the range 10 nm to 30 nm are all able to reproduce the literature values of relative efficiency reasonably well with the right choice of saturation parameter. Since no clear correlation between target diameter and the level of agreement is apparent, an additional constraint on the choice of model parameters is introduced.

4.1.4 Linearity index of cobalt-60 reference

As an additional constraint on the choice of free parameters, the predictive ability of the model is evaluated by comparison of experimental and model values for response per dose in the reference cobalt-60 field Q_0 (see Figure 1). The response of alanine in the reference cobalt-60 field Q_0 is

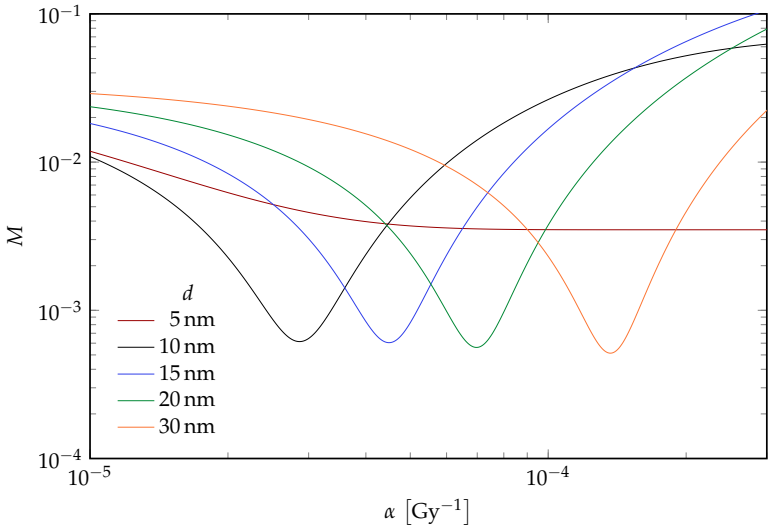

Figure 8: Parameter M, see Equation (19), as a function of the saturation parameter α for different target diameters d in water (shown in legend).

calculated according to Equation (10) as

$$R(D) = 1 - \exp\left[-\frac{D}{\frac{Q_0}{z_F}} \int_0^\infty \left(1 - \mathrm{e}^{-\alpha z}\right) f_1^{Q_0}(z)\, \mathrm{d}z\right]. \tag{20}$$

The linearity index $f(D)$, the response per dose at each dose point normalized to a specific dose point, is calculated by

$$f(D) = \frac{(R/D)_{\text{dose}}}{(R/D)_{\text{ref. dose}}}. \tag{21}$$

Here the reference dose point is chosen to be $D_{\text{w}} = 1\,\text{kGy}$, corresponding to $D_{\text{ala}} = 0.97\,\text{kGy}$. Figure 9 show the calculated response and linearity curves for the free parameter sets obtained in Figure 8 as well as the response curve for pellets irradiated in a cobalt-60 Gammacell also shown in Figure 1, normalized to the saturation response. The relative difference between model and experimental values calculated by

$$\text{Rel. diff.} = \frac{X_{\text{mod}} - X_{\text{exp}}}{X_{\text{exp}}}, \tag{22}$$

where X is the physical quantity investigated. The comparison of model and experimental data in Figure 9 clearly suggest a parameter set of $d = 10\,\text{nm}$ in water, which has a corresponding saturation parameter $\alpha = 2.86 \times 10^{-5}\,\text{Gy}^{-1}$, for calculating the dosimeter properties in the reference cobalt-60 field. Since this set of model parameters display best agreement for a wider range of beam qualities it is adopted for further use in the model.

This comparison of experimental response curves normalized to saturation response with response curves calculated using the microdosimetric one-hit detector model represents an assumption that the saturation of response is only due to a saturation in stable free radical production at

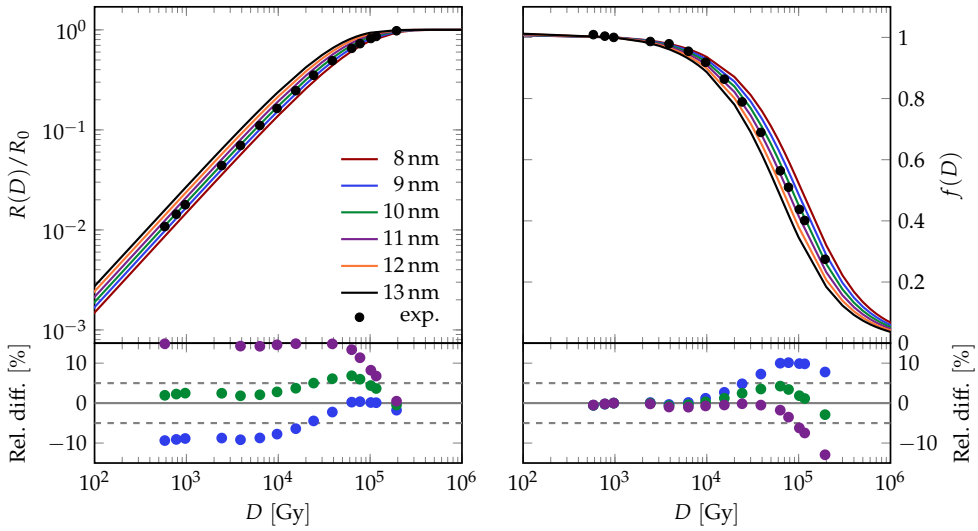

Figure 9: Comparisson of model and experimental values for dosimeter response (left) and linearity index (right) curves. The relative differences of model and experimental values are shown below with the dashed line representing a 5 % difference.

high doses. This assumption implies that the EPR-readout, in this case the peak-to-peak height in the first derivative of the EPR-spectrum, is proportional to the concentration of stable free radicals, which is however not the case. The measured response curves also includes a saturation intrinsic to the spectrometer. For instance different values of the characteristic dose can be measured for different values of the microwave power used in the EPR-spectrometer (Wieser and Girzikowsky, 1996; Malinen et al., 2003). Here the comparison is used to pick out a set of model parameters, from a list of parameter sets which all, according to Figure 8, reproduce literature values at kV x-ray energies reasonably well. The target diameter obtained in this manner match the target diameter obtained by Olko (2002) for alanine pellet dosimeters.

4.2 Uncertainty considerations

In the following section the considerations and handling of uncertainties for the model is described.

4.2.1 Monte Carlo calculations

For MC calculations of radiation transport uncertainties typically include components from translation from laboratory conditions to MC geometry and materials, cross-section data, input physics, and statistical effects. In the present study the relative detector efficiency is calculated according to Equation (15), where $\overline{z_F}$ and $f_1(z)$ are obtained through MC calculations. Since Equation (15) is expressed as a ratio with these parameters appearing in both the numerator and denominator, and these parameters are obtained using the same MC code and input physics, it is assumed that the

contribution to the final uncertainty of the relative efficiency is negligible compared the contribution from the applied experimental data.

4.2.2 Literature values

A significant contribution to the overall uncertainty comes from the use of literature data based on measurements to fix the free parameters of the model. The literature values and associated uncertainties are shown in Table 2. The uncertainties listed on the literature values are included by doing a sensitivity analysis on the obtained model parameters, and thus the model calculated values for the relative efficiency.

To evaluate the model uncertainty the distribution of saturation parameter for target diameter $d = 10\,\text{nm}$ is investigated. This target diameter is both the optimal value chosen for the standard case as well as the mode of the distribution of optimal parameter sets for linearity considerations. The distribution of α for this target diameter is shown in Figure 10, where also a Gaussian fit to the distribution is shown. From the Gaussian distribution a standard deviation of the saturation

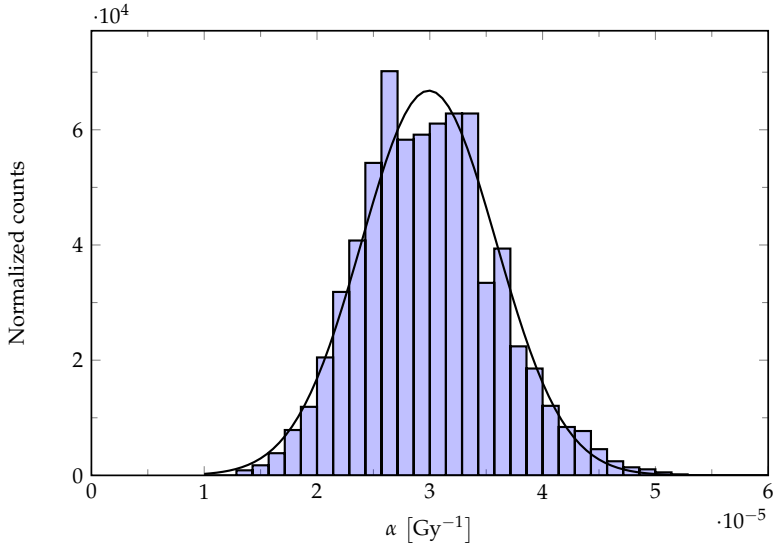

Figure 10: Distribution of saturation parameter α for target diameter $d = 10\,\text{nm}$ for a random sample of relative efficiency for evaluation of optimal parameter sets. The black line represents a Gaussian fit to the distribution.

parameter $\sigma_\alpha = 5.97 \times 10^{-6}\,\text{Gy}^{-1}$ for target diameter $d = 10\,\text{nm}$ is obtained. A $2\sigma_\alpha$ difference in saturation parameter is adopted for calculating upper and lower bounds on the model calculation of the relative efficiency.

4.3 Characterization of the alanine pellet dosimeter

The parameter values obtained in Section 4.1 can now be applied for relevant primary x-ray spectra in order to calculate the relative efficiency of the alanine dosimeter in that particular beam quality. In the following section this has been done in different ways to explore the alanine dosimeter efficiency dependence on several parameters.

The calculation of secondary electron spectra is done using a very simplified geometry representing the alanine pellet dosimeter. Here a box of crystalline alanine with density $\rho_{\text{alanine}} = 1.42\,\text{g}\,\text{cm}^{-3}$ is subject to the primary photon beam. The energies of Compton- and photoelectrons produced by primary photons is scored for the secondary electron spectra.

4.3.1 Monoenergetic photons

The secondary electron spectrum was calculated with the `Geant4` MC toolkit for a range of monoenergetic primary photons. Using Equation (15) together with the free parameter values $d = 10\,\text{nm}$ and $\alpha = 2.86 \times 10^{-5}\,\text{Gy}^{-1}$ and the calculated secondary electron spectra for monoenergetic photons in alanine, relative efficiency is obtained. The top part of Figure 11 show the calculated relative efficiency for monoenergetic primary photons, as well as the result of changing the set of model parameters by $\pm 2\sigma_\alpha$.

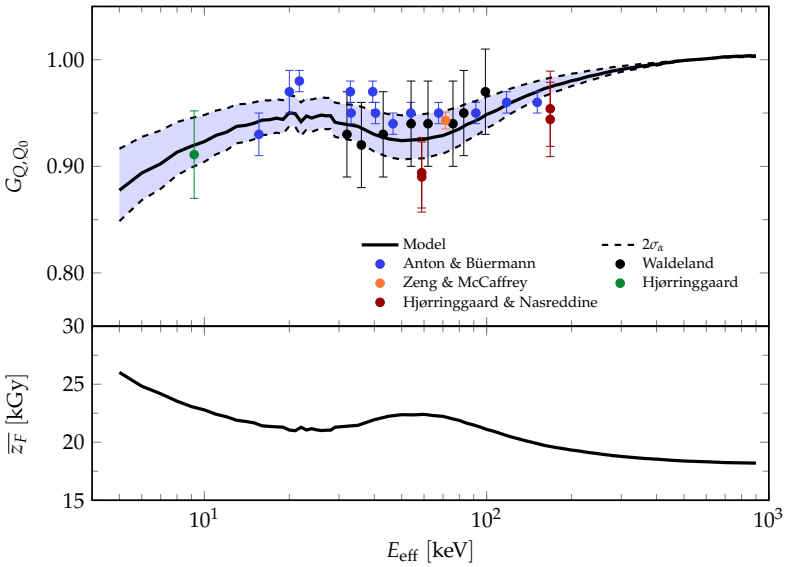

Figure 11: *Top:* Relative efficiency G_{Q,Q_0} calculated with the microdosimetric one-hit detector model for monoenergetic primary photons. Calculations done using model parameters $d = 10\,\text{nm}$ and $\alpha = 2.86 \times 10^{-5}\,\text{Gy}^{-1}$. The upper and lower bound (dashed lines) is determined by the method described in Section 4.2. *Bottom:* The mean specific energy for target diameter $d = 10\,\text{nm}$.

The bottom part of Figure 11 show the corresponding mean specific energy calculated according to Equation (5) using target diameter $d = 10\,\text{nm}$. The mean specific energy is a measure for how

localized the dose deposition is. It is worth noting that the local minimum and maximum apparent in the energy dependence of the relative efficiency – at 20 keV and 50 keV respectively – directly corresponds to the opposite extrema in the mean specific energy. The bump in the curve for mean specific energy occurs as the fraction of secondary electrons produced by Compton scattering increases, since the low energy electrons produced through Compton scattering have greater linear energy transfer.

Literature comparison

The capabilities of the model for calculating the relative efficiency of the alanine pellet dosimeter in low energy x-ray fields is tested by comparison with literature data. In Figure 11 the relative efficiency measured in Zeng and McCaffrey (2005), Waldeland et al. (2010), Anton and Büermann (2015), and Hjørringgaard et al. (2020) is presented as a function of the effective energy of the respective x-ray beams. Also presented is data from Hjørringgaard and Nasreddine for which a publication is in preparation. The data on relative efficiency from Anton and Büermann (2015) is obtained by taking the ratio of relative response to MC calculated dose ratios listed in Table 6 and Table 7 of their paper.

In general good agreement is observed between model calculated relative efficiency for monoenergetic x-rays and experimental data characterized by the effective energy of the x-ray beam. The overall trend with local maximum and minimum around 20 keV and 50 keV appear to be present in the experimental data as well. This agreement between model calculations and literature data is interpreted as a validation of the model, and the applied parameter set.

It is of course not obvious that effective energy as a beam qualifier is sufficient classification of beams to determine the relative efficiency. As such a direct comparison of relative efficiency for monoenergetic photons to effective energy of composite x-ray fields may not be optimal. Lack of knowledge about the spectral distribution for the literature data does however make this comparison the most reasonable. How the relative efficiency depends on other beam characteristics than just the effective energy can now be investigated using the microdosimetric one-hit detector model.

4.3.2 X-ray beam characteristics

Differences in x-ray tube geometry – filtration material and thickness, target material and angle, etc. – entails a wide range in HVL values for the same tube potential. From a survey on the status of clinical x-ray dosimetry in North American clinics the variation in HVL for x-ray tubes with tube potential 10 kV to 300 kV is obtained (see Figure 2 of Ma et al., 2001). This variation gives an indication of the x-ray beam quality range for which the dosimeter properties should be characterized.

Based on the model parameters determined in this study, the general dependence of the relative efficiency of the alanine pellet dosimeter on different x-ray beam qualifiers is investigated. A set of primary x-ray spectra was generated using the `SpekCalc` software. The x-ray spectra was of varying high voltage (HV), 40 kV to 300 kV, and HVL, the latter obtained by varying the external filtration.

Options used for all calculated spectra include filtration of 1.0 mm beryllium and 1000 mm of air, and anode angle 30°. The variation in HVL is obtained by changing the external aluminum or copper filtration. The range in input parameters for the calculation of x-ray spectra was chosen such that the generated spectra cover the range of beam qualities listed in Ma et al. (2001). The same geometry, and alanine pellet size and composition, as was used for fixing the model parameters in Section 4.1, based on the information from Waldeland et al. (2010), was used for calculation of secondary electron spectra in the alanine pellet.

The relative detector efficiency for each beam quality was calculated in the same manner as described in previous sections. Figure 12 show the calculated relative efficiency calculated for the set of x-ray spectra with tube potential 40 kV to 170 kV and HVL $\approx$ 0.2 mm Al to 14 mm Al.

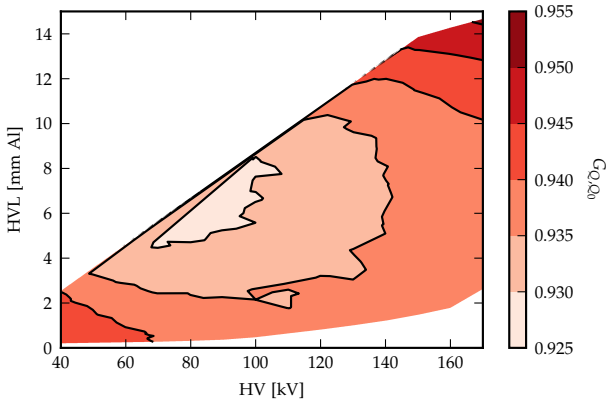

Figure 12: Relative efficiency of the alanine dosimeter (color bar) calculated using the microdosimetric one-hit detector model with parameters $d = 10\,\text{nm}$ and $\alpha = 2.86 \times 10^{-5}\,\text{Gy}^{-1}$. Primary photon spectra was obtained using `SpekCalc` (see text for details).

The general dependence of the relative efficiency on HV and HVL shown in Figure 12 appear to follow the approximation in Figure 11. The range of HVLs displayed correspond to effective energies in the approximate range 15 keV to 90 keV corresponding to the minimum valley in Figure 11. The decrease in detector efficiency for x-ray qualities in this range was found to vary between roughly 5.0 % to 7.0 %.

Figure 13 shows the calculated relative efficiency calculated for the set of x-ray spectra with tube potential 100 kV to 300 kV and HVL $\approx$ 0.2 mm Cu to 5 mm Cu. Note that the range of the colorbar in Figure 13 is different to Figure 12. The HVL in the set of spectra corresponds to effective energies in the range 45 keV to 200 keV. The general tendency is a increase in the relative detector efficiency with increasing HVL in this beam quality region, in accordance with Figure 11. For this set of primary x-ray beam qualities the variation in relative efficiency for a specified tube potential reaches several percent, compared to the low energy set in Figure 12 where the total variation over the entire set of primary x-ray beam qualities is well below 2 % of a mean value.

Figure 14 show the relative detector efficiency as a function of the HVL for the two sets of

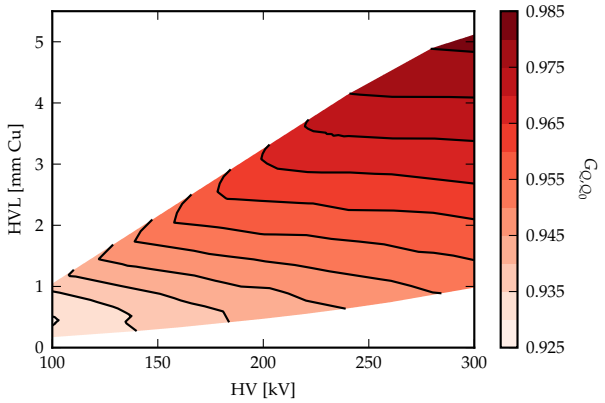

Figure 13: Relative efficiency of the alanine dosimeter (color bar) calculated using the microdosimetric one-hit detector model with parameters $d = 10\,\text{nm}$ and $\alpha = 2.86 \times 10^{-5}\,\text{Gy}^{-1}$. Primary photon spectra was obtained using `SpekCalc` (see text for details).

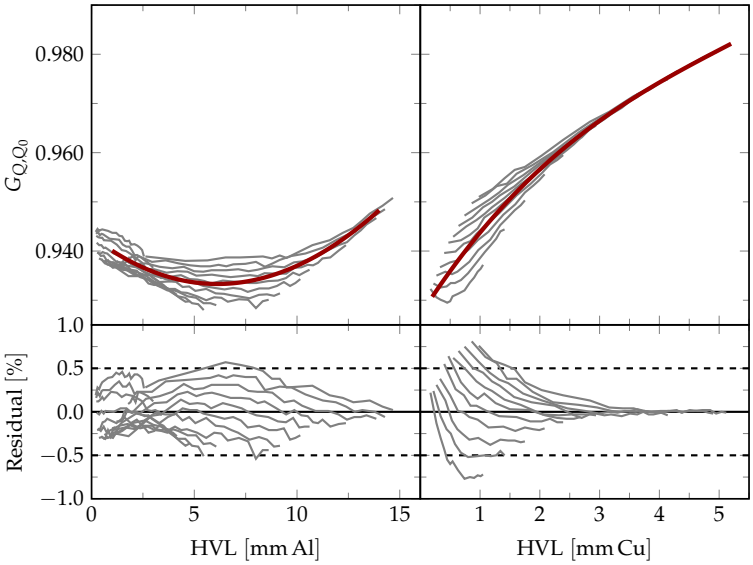

Figure 14: The relative detector efficiency as a function of HVL (top) for the low (left) and high (right) energy sets of primary x-ray beam qualities (gray lines). A polynomial regression to each set is also shown (red lines) with coefficients of regression stated in Table 3. The residuals, $G^{\text{calc}}_{Q,Q_0} - G^{\text{fit}}_{Q,Q_0}$, is also shown (bottom) for both sets of primary x-ray beam qualities.

Table 3: Fit to the relative response as a function of HVL for the two sets of primary x-ray beam qualities. The fit is of the form $G_{Q,Q_0} = \sum_{i=0}^{n} a_i \cdot \mathrm{HVL}^i$.

Energy range	Beam qualifier	a_0	a_1	a_2	a_3
Low, 40 kV to 170 kV	HVL, mm Al	0.943	-3.21×10^{-3}	2.73×10^{-4}	-1.19×10^{-6}
Medium, 100 kV to 300 kV	HVL, mm Cu	0.927	1.90×10^{-2}	-2.40×10^{-3}	1.51×10^{-4}

primary x-ray beam qualities respectively. Each line in the figure corresponds to a specific x-ray tube potential. For the low energy set (left panel) the variation in relative efficiency over the entire set is quite low. A fit of constant value to the set yields a mean relative efficiency over the entire set of 0.937 with maximum and minium values varying by $-1.0\,\%$ and $1.5\,\%$ from this mean value. For the medium energy x-ray beam qualities (right panel) relative detector efficiency appear to be independent of x-ray tube potential for beam qualities with HVL > 3 mm Cu.

An approximate relation between relative detector efficiency and the HVL for both the low and medium energy x-rays is obtained by fitting a third order polynomial. The fitting coefficients for both the low and medium energy sets of x-ray beam qualities are listed in Table 3. The regression analysis displayed in Table 3 can be used to estimate a value of the relative detector efficiency for x-ray beam qualities contained in either of the two sets investigated in the present study. Since the set of primary x-ray beam qualities is chosen to represent the span of x-ray beam qualities used in clinics, typical x-ray beam qualities from 40 kV to 300 kV should be covered by this analysis.

5 Discussion

In the present study the microdosimetric one-hit detector model was applied to the alanine pellet dosimeter to calculate the relative efficiency in low energy x-ray beams with respect to a cobalt-60 reference field. Literature values obtained from Waldeland et al. (2010) were used to fix the free parameters of the model, the target diameter d and the saturation parameter α. Using only the minimization of relative least squares shown in Figure 8 was not sufficient to conclusively determine an optimal parameter set, therefore an additional constraint concerning the prediction of response curves for pellets irradiated in a Cobalt-60 Gammacell was included. The optimal set of model parameters determined in this manner was obtained to be $d = 10$ nm in water and $\alpha = 2.86 \times 10^{-5}\,\mathrm{Gy}^{-1}$. Olko (2002) arrived at a target diameter of $d_{\mathrm{ala}} = 6$ nm corresponding to 8–9 nm in water by converting by density ratio.

The comparison between calculated response, and linearity, curves with measured response curves for alanine pellet dosimeters irradiated in a cobalt-60 Gammacell include an underlying assumption that the measured EPR response (peak-to-peak height of the first derivative of the EPR spectrum) is directly proportional to the concentration of stable free radicals. This assumption implies that the observed saturation in the EPR response is only due to saturation in the production of stable free radicals. Effects of the readout procedure, such as choice of microwave power and modulation amplitude, may influence the relative spectrometer sensitivity for low and high radical

concentrations, and thus affect the dose level at which saturation occurs. This effect would need to be characterized for consistency. In the present study the comparison is applied to pick a set of model parameters from a list of model parameter sets which all reproduce the kV x-ray literature data for relative detector response reasonably well.

As discussed by Olko (2002) this order of target diameter is much larger than the size of an alanine molecule implying the saturation effect at high doses are not due to a lack of unionized alanine molecules. Olko (2002) argue that other effects of ionizing radiation – cross linking, coiling of chains – can trap the free radicals, preventing recombination at normal dose ranges. At high doses, or high Linear Energy Transfer (LET), these structures are destroyed, leading to recombination and a reduced detector efficiency. In this case the target size is interpreted as the effective range of recombination of the free radicals.

The model was validated by calculating the relative efficiency of the alanine pellet dosimeter for monoenergetic photons in the energy range 5 keV to 1000 keV, and comparing with experimentally determined values of the relative efficiency (as a function of the effective energy of the primary x-ray beam) available in the literature. In general good agreement was observed, where deviations can be explained by the experimental uncertainties. The use of effective energy as the single beam qualifier may however be an oversimplification as shown in Section 4.3.2.

Applying the microdosimetric one-hit detector model for a set of monoenergetic primary photon beams showed a similar anomalous dependency of the relative detector efficiency on photon energy. The energy dependence showed a local extremum at 25 keV and 50 keV. The characteristic anomalous shape occurs as with increasing photon energy the fraction of secondary electrons produced by Compton effect increases. The same anomalous shape is obtained by Olko (1999, 2002), however they report local maximum and minimum at 40 keV and 80 keV respectively. This difference may be due to the difference in applied model parameters as well as the choice of alanine detector material. Olko (2002) use a mixture of 90 % alanine and 10 % paraffin wax in an unspecified geometry for calculating the secondary electron spectra, whereas a detector consisting of pure crystalline alanine is used in the present study.

The microdosimetric one-hit detector model has further been applied to two sets of generated x-ray spectra covering a wide range of x-ray beam qualities used in clinics. The low energy set was generated with HV in the range 40 kV to 170 kV and HVL from 0.2 mm Al to 14 mm Al, and the medium energy set consist of HVs from 100 kV to 300 kV with HVL from 0.2 mm Cu to 5 mm Cu. This study was performed to explore the usefulness of different beam qualifiers for characterization of the relative detector efficiency. The relative detector efficiency in the low energy set was shown to vary within -1.0 % and 1.5 % of the average value for the investigated beam quality range. This indicates that the tube potential may be sufficient for practical use in choosing a literature value of the relative detector efficiency to apply to measurements. However further investigation of the influence of e.g. phantom material, alanine pellet position in phantom, etc. should be explored in detail. For the medium energy set of generated x-ray spectra a significant dependence of the relative detector efficiency on the HVL was observed. For HVL > 3 mm Cu the relative detector efficiency

appear to be independent on the x-ray tube potential. The reason for this is probably that the fraction of low energy electrons generated in the detector by these hard filtered beams is quite low for all the investigated tube potentials making variations between spectra insignificant.

For both sets of primary x-ray beam qualities generic values of the relative detector efficiency for practical use is proposed. For the low energy set the variation in relative detector response is sufficiently low that a constant value of $G_{Q,Q_0} = 0.937$ can be used. However a third order polynomial regression was applied to both sets of x-ray spectra to obtain an easily calculated value for the relative detector efficiency. The residuals for the fits show that the variation of the relative efficiency for the low energy set is within $\pm 0.5\,\%$ of the fitted value, while this variation increases to $\pm 1.0\,\%$ for the medium energy set.

Several aspects of the model calculations which may impact the final model prediction of the relative efficiency have not been considered in the present study. MC calculation at very low energies should be interpreted with reservations regarding interaction cross-sections. Different ionization cross-section models for very low energies are available in the `Geant4-DNA` MC toolkit (Bernal et al., 2015). The effect on the model predicted relative efficiency of the alanine pellet dosimeter from using different low energy ionization cross-section models has not been explored in the present study.

The recombination of free radicals has been shown to be dependent on the beam quality (Hansen and Olsen, 1989). For heavy charged particles high LET beams show significantly greater fading compared to lower LET beams. The same effect could be present for x-rays, where low energy x-rays have greater LET (by secondaries) relative to high energy x-rays. This effect may be of importance when assessing the detector response, but have not been investigated here.

6 Conclusion

The microdosimetric one-hit detector model was applied to calculate the relative efficiency of the alanine pellet dosimeter. The free parameters of the model was determined by minimizing the relative least squares of the calculated efficiency for a set of literature values as well as relating response and linearity curves for the HDRL cobalt-60 gammacell calculated using each of the obtained parameter sets with experimentally determined response and linearity curves. The model parameters $d = 10\,\text{nm}$ (in water) and $\alpha = 2.86 \times 10^{-5}\,\text{Gy}^{-1}$ showed the best agreement for the response and linearity curves, and were adopted as the free parameter values of the model.

The model was then applied to a constructed set of primary x-ray beams, monoenergetic and spectral distributions, in order to determine the relative detector efficiency dependence on different beam qualifiers as well as highlight the underlying physical interpretation of the decrease in detector efficiency for low energy x-rays. For the set of monoenergetic primary photons the energy dependence of the relative detector efficiency showed a characteristic shape with a local maximum and minimum at 25 keV and 50 keV respectively. This bump on the curve serves as an indicator that it is the very low energy secondary electron, with high ionization density, for which the detector show a significant decrease in efficiency.

For the set of generated low energy x-ray spectra the decrease in detector efficiency was between 5.0 % and 7.0 % with an average decrease in detector efficiency of 6.3 % for the entire set. For the medium energy set of generated x-ray spectra the decrease in detector efficiency varied from 2.0 % to 7.0 % with a significant correlation with HVL. For practical use in routine dosimetry for dose to water measurements in kV x-ray fields, generic values for the for the relative efficiency of the alanine pellet dosimeter can be obtained by applying the obtained regression coefficients in Table 3 to the regression function described in the same table.

References

Agostinelli, S., J. Allison, K. a. Amako, J. Apostolakis, H. Araujo, P. Arce, M. Asai, D. Axen, S. Banerjee, G. . Barrand, et al. (2003). Geant4—a simulation toolkit. *Nuclear instruments and methods in physics research section A: Accelerators, Spectrometers, Detectors and Associated Equipment 506*(3), 250–303.

Anton, M. and L. Büermann (2015). Relative response of the alanine dosimeter to medium energy x-rays. *Physics in Medicine & Biology 60*(15), 6113.

Anton, M., R.-P. Kapsch, M. Krystek, and F. Renner (2008). Response of the alanine/esr dosimetry system to mv x-rays relative to 60co radiation. *Physics in Medicine & Biology 53*(10), 2753.

Aukett, R., R. Harrison, C. Moretti, A. Nahum, K. Rosser, et al. (1996). The ipemb code of practice for the determination of absorbed dose for x-rays below 300 kv generating potential (0.035 mm al-4 mm cu hvl; 10-300 kv generating potential). *Physics in Medicine & Biology 41*(12), 2605.

Bergstrand, E. S., K. R. Shortt, C. K. Ross, and E. O. Hole (2003). An investigation of the photon energy dependence of the epr alanine dosimetry system. *Physics in Medicine & Biology 48*(12), 1753.

Bernal, M., M. Bordage, J. Brown, M. Davídková, E. Delage, Z. El Bitar, S. Enger, Z. Francis, S. Guatelli, V. Ivanchenko, et al. (2015). Track structure modeling in liquid water: A review of the geant4-dna very low energy extension of the geant4 monte carlo simulation toolkit. *Physica Medica 31*(8), 861–874.

Dodd, B. and R. J. Vetter (2009). Replacement of 137cs irradiators with x-ray irradiators. *Health physics 96*(2), S27–S30.

Hansen, J. and K. Olsen (1989). Predicting decay in free-radical concentration in l-α-alanine following high-let radiation exposures. *International Journal of Radiation Applications and Instrumentation. Part A. Applied Radiation and Isotopes 40*(10-12), 935–939.

Hansen, J., K. Olsen, and M. Wille (1987). The alanine radiation detector for high and low-let dosimetry. *Radiation protection dosimetry 19*(1), 43–47.

Hjørringgaard, J. G., C. Ankjærgaard, M. Bailey, and A. Miller (2020). Alanine pellet dosimeter efficiency in a 40 k v x-ray beam relative to cobalt-60. *Radiation Measurements*, 106374.

IAEA (2001). *Absorbed Dose Determination in External Beam Radiotherapy*. Number 398 in Technical Reports Series. Vienna: INTERNATIONAL ATOMIC ENERGY AGENCY.

Incerti, S. et al. (2010a). Comparison of geant4 very low energy cross section models with experimental data in water. *Medical physics 37*(9), 4692–4708.

Incerti, S. et al. (2010b). The geant4-dna project. *International Journal of Modeling, Simulation, and Scientific Computing 1*(02), 157–178.

Incerti, S., I. Kyriakou, M. Bernal, M. Bordage, Z. Francis, S. Guatelli, V. Ivanchenko, M. Karamitros, N. Lampe, S. B. Lee, et al. (2018). Geant4-dna example applications for track structure simulations in liquid water: A report from the geant4-dna project. *Medical physics 45*(8), e722–e739.

Kellerer, A. M. (1987). Models of cellular radiation.

Kellerer, A. M. et al. (1985). Fundamentals of microdosimetry. *The dosimetry of ionizing radiation 1*, 77–162.

Kellerer, A. M. and D. Chmelevsky (1975). Concepts of microdosimetry. *Radiation and environmental biophysics 12*(4), 321–335.

Khoury, H., E. da Silva Jr, K. Mehta, V. de Barros, V. Asfora, P. Guzzo, and A. Parker (2015). Alanine-epr as a transfer standard dosimetry system for low energy x radiation. *Radiation Physics and Chemistry 116*, 147–150.

Ma, C.-M., C. Coffey, L. DeWerd, C. Liu, R. Nath, S. Seltzer, and J. Seuntjens (2001). Aapm protocol for 40–300 kv x-ray beam dosimetry in radiotherapy and radiobiology. *Medical physics 28*(6), 868–893.

Malinen, E., M. Z. Heydari, E. Sagstuen, and E. O. Hole (2003). Alanine radicals, part 3: Properties of the components contributing to the epr spectrum of x-irradiated alanine dosimeters. *Radiation research 159*(1), 23–32.

Olko, P. (1999). Calculation of the relative effectiveness of alanine detectors to x rays and heavy charged particles using microdosimetric one-hit detector model. *Radiation protection dosimetry 84*(1-4), 63–66.

Olko, P. (2002). The microdosimetric one-hit detector model for calculating the response of solid state detectors. *Radiation measurements 35*(3), 255–267.

Olko, P. (2006). Microdosimetric interpretation of photon energy response in tl systems. In *Microdosimetric Response of Physical and Biological Systems to Low-and High-LET Radiations*, pp. 203–251. Elsevier.

Olsen, K., J. Hansen, and M. Wille (1990). Response of the alanine radiation dosemeter to high-energy photon and electron beams. *Physics in Medicine & Biology 35*(1), 43.

598 Poludniowski, G. G. (2007). Calculation of x-ray spectra emerging from an x-ray tube. part ii. x-ray production and filtration in x-ray targets. *Medical physics 34*(6Part1), 2175–2186.

600 Poludniowski, G. G. and P. M. Evans (2007). Calculation of x-ray spectra emerging from an x-ray tube. part i. electron penetration characteristics in x-ray targets. *Medical physics 34*(6Part1), 2164–
602 2174.

Rossi, H. H. and M. Zaider (1996). *Microdosimetry and its Applications*. Springer.

604 Sechopoulos, I., D. W. O. Rogers, M. Bazalova-Carter, W. E. Bolch, E. C. Heath, M. F. McNitt-Gray, J. Sempau, and J. F. Williamson (2018). Records: improved reporting of monte carlo radiation
606 transport studies: Report of the aapm research committee task group 268. *Medical Physics 45*(1), e1–e5.

608 Sharpe, P. and S. Duane (2003). Progress report on radiation dosimetry at npl. *Report CCRI (I)/99-20*.

Sleptchonok, O. F., V. Nagy, and M. F. Desrosiers (2000). Advancements in accuracy of the alanine
610 dosimetry system. part 1. the effects of environmental humidity. *Radiation Physics and Chemistry 57*(2), 115–133.

612 Waldeland, E., E. O. Hole, E. Sagstuen, and E. Malinen (2010). The energy dependence of lithium formate and alanine epr dosimeters for medium energy x rays. *Medical physics 37*(7Part1), 3569–
614 3575.

Waligórski, M. P. R. (1988). A model of heavy ion detection in physical and biological systems.
616 Technical report, Institute of Nuclear Physics.

Wieser, A. and R. Girzikowsky (1996). A unique calibration curve for alanine epr dosimetry systems.
618 *Applied radiation and isotopes 47*(11-12), 1269–1275.

Zaider, M. (1990). Microdosimetry and katz's track structure theory: I. one-hit detectors. *Radiation*
620 *research 124*(1s), S16–S22.

Zeng, G. and J. McCaffrey (2005). The response of alanine to a 150 kev x-ray beam. *Radiation physics*
622 *and chemistry 72*(5), 537–540.

Zeng, G., M. McEwen, D. Rogers, and N. Klassen (2004). An experimental and monte carlo inves-
624 tigation of the energy dependence of alanine/epr dosimetry: I. clinical x-ray beams. *Physics in Medicine & Biology 49*(2), 257.

DTU Health Tech
Department of Health Technology
Technical University of Denmark
Risø Campus, Frederiksborgvej 399
DK-4000, Roskilde, Denmark

https://www.healthtech.dtu.dk/english